STUDIES OF SATELLITE SUPPORT TO WEATHER MODIFICATION IN THE WESTERN U.S. REGION

Co-Principal Investigators: W. R. Cotton
L. O. Grant
T. H. Vonder Haar

Final Report

Grant NSG-5011

June 15, 1974 to January 17, 1978

DEPARTMENT OF ATMOSPHERIC SCIENCE
COLORADO STATE UNIVERSITY
FORT COLLINS, COLORADO

Final Report

for

Grant NSG - 5011

"STUDIES OF SATELLITE SUPPORT TO WEATHER MODIFICATION IN THE WESTERN U. S. REGION"

6/15/74 - 1/17/78

by

W. R. Cotton

L. O. Grant

T. H. Vonder Haar

Co - Principal Investigators

Department of Atmospheric Sciences
Colorado State University
Fort Collins, Colorado 80523

for

National Aeronautics and Space Administration

Grant Officer: G. Wiseman

Technical Monitor: Robert Adler

ABSTRACT

This report summarizes the results of studies performed under NASA Grant NSG-5011 and entitled Satellite Support to Weather Modification in the Western U. S. Region. These studies were completed during the period 1 April, 1974 to the present. The applications of meteorological satellite data to both summer and winter weather modification programs were addressed in this research. These studies included the appraisal of the capability of satellites to assess seedability, to provide real-time operational support, and to assist in the post-experiment analysis of a seeding experiment. This research has led to the incorporation of satellite observing systems as a major component in the Bureau of Reclamations weather modification activities.

Satellite observations acquired under this grant are an integral part of the South Park Area Cumulus Experiment (SPACE). The objective of the SPACE research program is to formulate a quantitative hypothesis for enhancing precipitation from orographically induced summertime mesoscale convective systems (orogenic mesoscale systems). Satellite observations assist in classifying the important mesoscale systems, defining their frequency and coverage, defining a potential area of effect. Satellite studies of severe storms were investigated under this grant. This document addresses the progress of those studies.

TABLE OF CONTENTS

FINAL REPORT: Studies of Satellite Support to Weather Modification in the Western U. S. Region
NASA/GLAS/Severe Storms Research Program
Grant NSG-5011

1.0 INTRODUCTION

This report summarizes the results of studies of satellite support to weather modification in the Western U. S. region for the period 1 April 1974 to the present. The early stages of this research were focused on the collection and analysis of satellite data for four major weather modification programs:

1) Meso/Synoptic Storm Modifications (National Oceanic and Atmospheric Administration)

2) National Hail Research Experiment (NCAR/NSF, RANN)

3) High Plains Precipitation Enhancement (HIPLEX; U. S. Dept. of Interior, Bureau of Reclamation)

4) Wintertime Orographic Cloud Modification (U. S. Dept. of Interior, CSU/Extra-Area Effect (NSF/RANN)).

During the period of this research, the first program never materialized, and the second program was rapidly phased out, while the HIPLEX program and wintertime orographic cloud modification studies have become increasingly functional. The Bureau of Reclamations weather modification programs have become increasingly dependent upon satellite support to the extent that they have provided funding for investigations of satellite support to both their summer and winter programs under Contract 6-07-DR-20020. The results of this research are described in section 2.0. The CSU/Extra Area Effect Experiment has relied on satellite data for important input.

Colorado State University has operated a series of field experiments in the Colorado Mountains (the South Park Area Cumulus Experiment - (SPACE) which are designed to investigate the relationship between

mountain-generated cumulus convection and precipitating mesoscale systems over the High Plains. This experiment provided an excellent opportunity for testing satellite analysis techniques because of the extensive ground truth data collected during experiments. Therefore the later stages of the research covered by this grant emphasized the SPACE experiment. The ultimate objective of this research is to formulate a quantitative hypothesis for the modification of precipitating mesoscale systems over the High Plains via modification of orogenic cumuli. The role of satellite meteorology in these investigations is described in section 3.0.

The intimate relationship between severe storm research and convective cloud modification is also pointed out in section 3.0. In section 4.0 recent progress in severe storm analysis using satellite-derived data is discussed.

2.0 SUMMARY OF SCIENTIFIC PROGRESS DURING THE PERIOD 1 APRIL 1974 TO 14 NOVEMBER 1976.

A thorough summary of the results of this research is given by Reynolds, VonderHaar and Grant (1978; Appendix A1). This paper surveys the applications of meteorological satellite data to both summer and winter weather modification programs. Included in the discussion is the appraisal of the capability of satellites to assess the potential for precipitation enhancement (seedability), to provide real-time operational support, and to assist in the post-experiment analysis of a seeding experiment. This paper demonstrates that present satellite observing systems have become an essential component in weather modification programs. Moreover, anticipated future advances in satellite observing systems will make the weather modification community increasingly dependent upon satellite technology.

3.0 THE SOUTH PARK AREA CUMULUS EXPERIMENT (SPACE)

The SPACE has been an evolving program whose ultimate objective is to develop a capability of precipitation enhancement from summertime convection over the Colorado Mountains and High Plains. Since the bulk of precipitation from summertime convection occurs in organized mesoscale systems, the experiment has naturally evolved into investigations into the factors contributing to the organization and intensity of such systems.

Initial satellite studies concentrated on the determination of satellite-derived cloud climatology (Stodt and Grant (1976); A2, Stodt (1978)) the determination of satellite 'ground truth' regarding cloud brightness (Reynolds, McKee and Danielson (1976, 1978); A3, A4) and the factors contributing to initial convection (Breed (1975); A5). Cotton, George and Pielke (1976; A6) demonstrated the analogy between sea-breeze generated mesoscale convective systems and mountain-generated or orogenic mesoscale convective systems.

SPACE-1977 was a major experiment which utilized a host of observation systems including triple-Doppler radar, convectional radar, cloud physics and turbulence equipped aircraft, Lidar, rawinsondes, micromet towers, boundary layer profilers, an acoustic sounder, recording mesomet stations, the NCAR PAM system, stereo photography and satellite observations. A complete description of the SPACE-77 is given in SPACE LOG (Danielson and Cotton (1977)). The SPACE-77 data set provides comprehensive observations of a wide variety of cumulus-scale and convective mesoscale meteorological events ranging from locally suppressed cumulus convection, heavy precipitating and hail-producing cumulonimbus systems exhibiting little motion relative to the mountain source region, and heavy

precipitating, tornado-producing, eastward propagating mesoscale systems.

July 19, 1977 has been selected as the first day for comprehensive case study analysis. George and Cotton (1978; A7) have described the characteristics of the evolving mesoscale system on that day. The day was characterized by locally heavily precipating cumulonimbi and several hail falls. Since the clouds exhibited little motion relative too the observational system, this day provides an excellent opportunity to test out the analysis techniques and to perform three-dimensional model simulations of storm-scale and mesoscale events. Knupp, Danielson and Cotton (1978; A8) have described the morphological characteristics of the radar observations of several cumulonimbus cells that developed on that day. The analyses performed on this day will provide a number of opportunities for ground truth-interpretation of satellite-derived data. This is especially enhanced by the use of 3D model simulations as a part of the overall analysis. Because of the relative spatial stationarity of the mesoscale systems that formed on July 19, it provides a contrasting observational model to the days characterized by eastward propagating systems.

August 4, August 8 and August 10, 1977 represent three days in which convection first occurred over the mountains and then propagated eastward as a major mesoscale convective system. These are not the only such events that occurred during the observational period but are the most active in terms of precipitation, and severe weather events. August 4 has been selected as a day for comprehensive case study analysis. It is intended that the analysis of this day should serve as a descriptive model of eastward propagating orogenic mesoscale systems. The detailed

observations over South Park are complemented by 3 minute-interval satellite data on this particular day. Figure 3.1 illustrates the scenario of events observed by satellite on August 4, 1977. Deep convection first formed over the mountains. By 02Z (August 5) a line of very deep cells extended along the entire Colorado eastern border into the Texas panhandle with the most intense cells east of South Park. By 18Z the entire complex had migrated well into western Missouri. This system produced a tornado near Kiowa, Colorado and produced in excess of 50mm of precipitation over widespread areas of northeast and Central Kansas. That amount of precipitation represents roughly 15% of the total annual precipitation in that region.

While a thorough climatic study has not been performed, it appears that eastward propagating orogenic mesoscale systems contribute about 75% of the annual precipitation over eastern Colorado and the Kansas High Plains. Thus, a major portion of the weather modification potential over the High Plains must be tied to the modification of such systems. Because of the scale of these systems (a north-south dimension of several hundred kilometers) and the total extent of propagation (greater than 1500 km), satellites are an excellent platform for defining the characteristics of such systems and the potential "area of effect" of any implemented mesoscale modification hypotheses. As can be seen in Figure 3.1, the potential area of effect of a modification capability is a large one.

Another factor of serious concern is that the same systems that are dominant contributors to precipitation are also sporadic generators of tornadoes and hail. These systems do not produce major outbreaks of severe weather but instead often a few small tornadoes or moderate hail

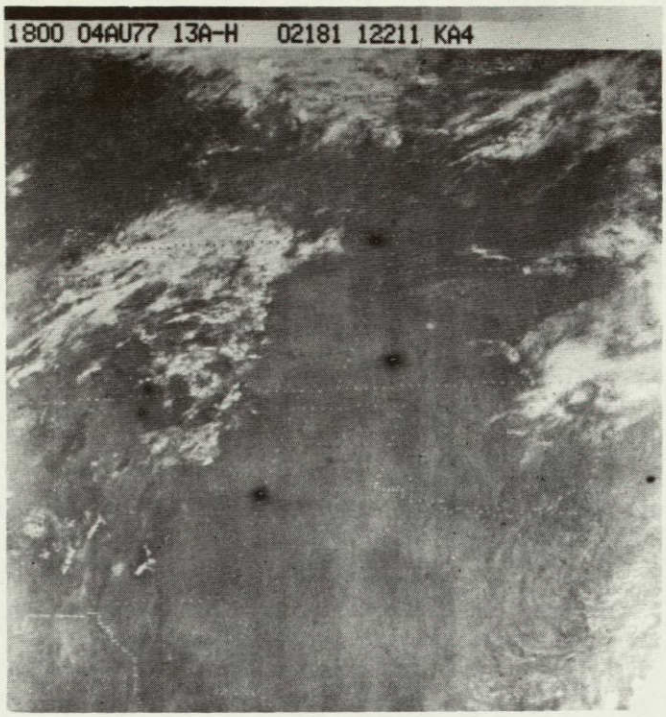

a

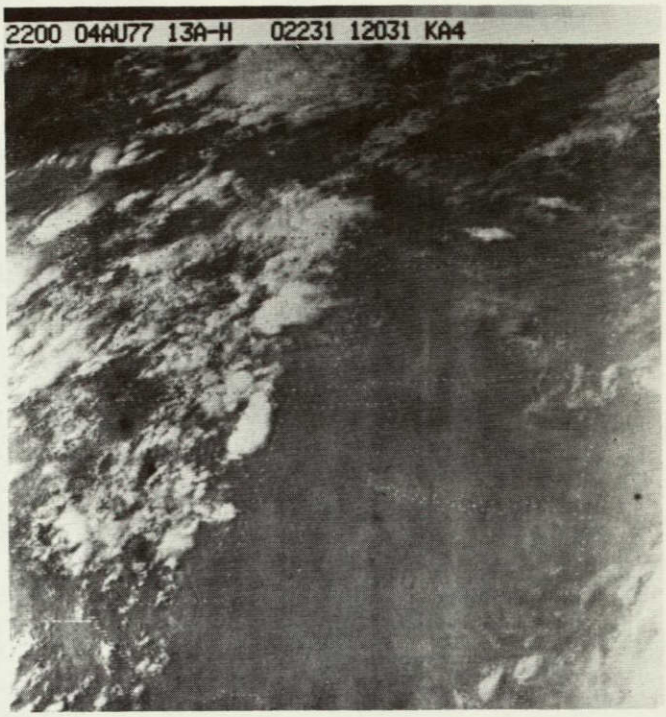

b

c

d

Figure 3.1. GOES-1 visible and infrared satellite imagery on August 4, 1977 for the period 1800 GMT to 1100 GMT (August 5, 1977).

e

f

g

h

Figure 3.1 Continued.

events such as the Kiowa tornado. Thus any methodology for enhancing precipitation from mesoscale convective systems must also include the capability for recognizing severe weather potential and defining immediate response strategies. Thus satellite support is essential to the definition of local severe weather indices. In addition, the implementation and testing of a convective mesoscale modification hypothesis will require active satellite support for the routine evaluations of these severe weather indices and for the activation of such response strategies as immediate shutdown of seeding operations, avoidance of a potential severe weather zone or implementation of alternate modification techniques.

Thus satellite-support is essential to the development of a quantitative mesoscale modification hypothesis and to the actual implementation and testing of such a hypothesis. Moreover one can see that the formulation and implementation of such a hypothesis is intimately tied to severe storm research.

4.0 SEVERE STORMS RESEARCH IN THE CENTRAL PLAINS USING SATELLITE DATA

Funding from NSG-5011 also supported a variety of severe convective storm research efforts that utilized satellite data. The particular day studied was April 24, 1975; a day when a number of severe storms occurred over the Central Plains and Central Mississippi Valley (see Fig. 4.1). A destructive tornado, spawned by an isolated supercell thunderstorm, struck Neosho, Missouri, just before sunset. An unusually comprehensive set of conventional and special satellite data were available for this particular day.

An upper-air sounding taken at Monett, Missouri, (approximately

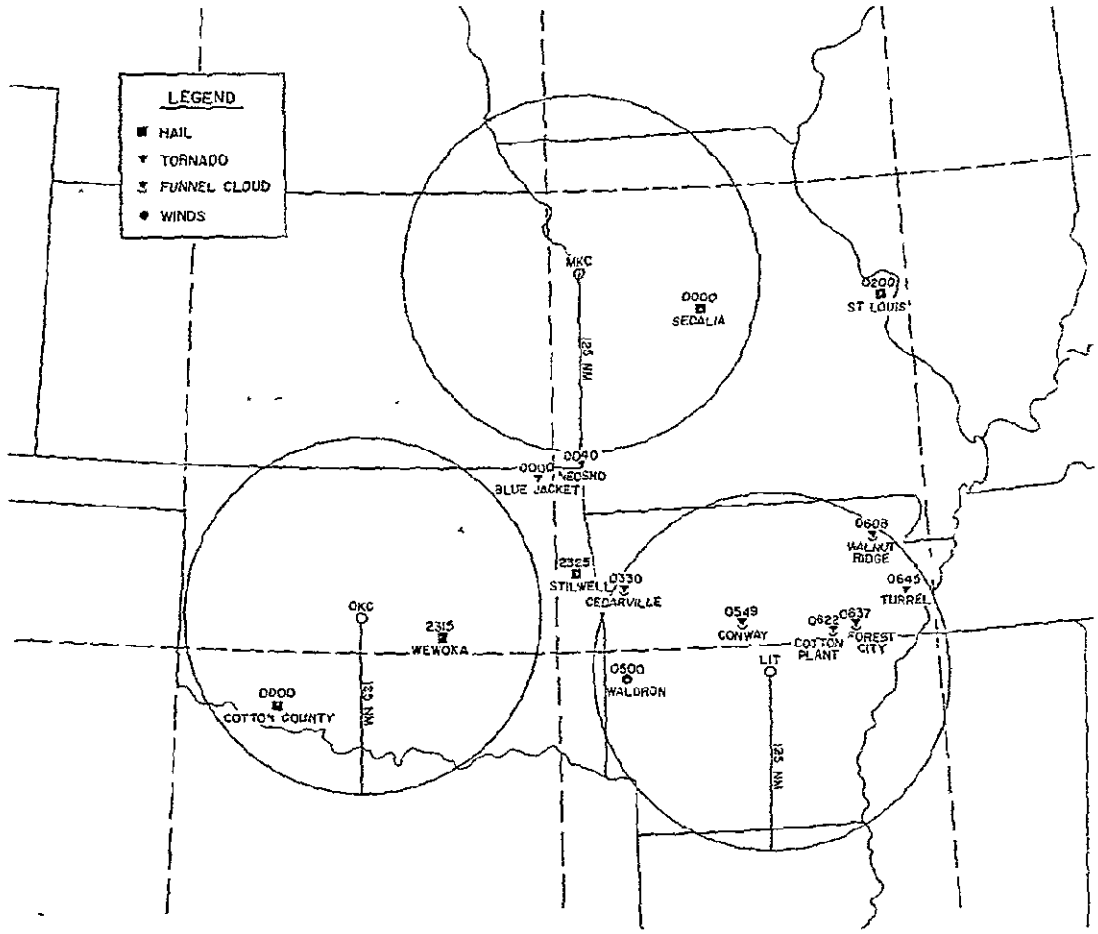

Figure 4.1. Severe storm reports for 24-25 April 1975.

25 nm east-southeast of Neosho) less than 4 h prior to the tornado indicated that significant lifting and/or air mass modification would be required to initiate deep convection. This sounding is shown in Fig. 4.2. Note the deep layer of negative buoyancy between the LCL (lifted condensation level) and LFC (level of free convection). Wilson (1976) computed large scale vertical motion fields using 2100 GMT soundings and his 700 mb ω field is shown in Fig. 4.3 with regions in which storms developed during the following several hours indicated. Since the storms developed in regions of weak upward motion, or in areas of subsidence, mesoscale features and forcing mechanisms must have played a dominant role in triggering storm development. Indeed, during late afternoon and evening when the storms were most intense they were relatively unorganized (e.g. no distinct squall or line orientation) and isolated.

Surface analyses (Fig. 4.4) for 18, 21, 00, and 03 GMT indicate that a sub-synoptic scale low (see Tegtmeir, 1974) and an attendant narrow zone of dry air moved eastward along the Kansas/Oklahoma border. An intense supercell storm developed just ahead of the dryline and moved eastward - becoming tornadic when it interacted with an old thunderstorm produced thermal boundary in extreme northeast Oklahoma and southwest Missouri.

Analyses of the 500 mb level (Fig. 4.5) indicate that the mesoscale surface low and the intense afternoon and evening severe storms were likely associated with a weak short-wave trough. This feature was moving rapidly eastward and weakening as a stronger short-wave had taken over as the dominant feature and helped to organize the storm activity into a well defined squall-line.

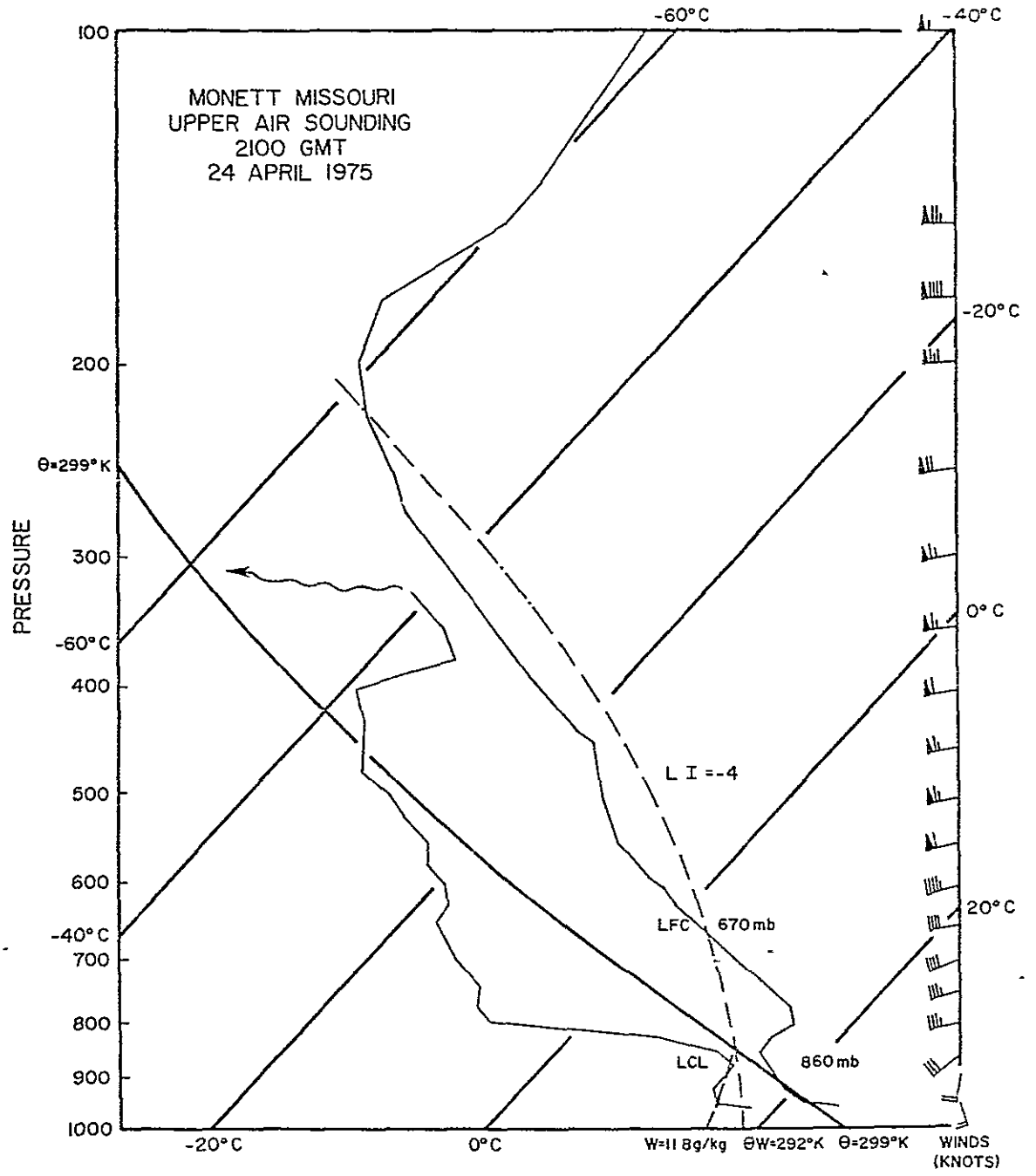

Figure 4.2. Monett, Mo. upper-air sounding for 24 April 1975, 2100 GMT.

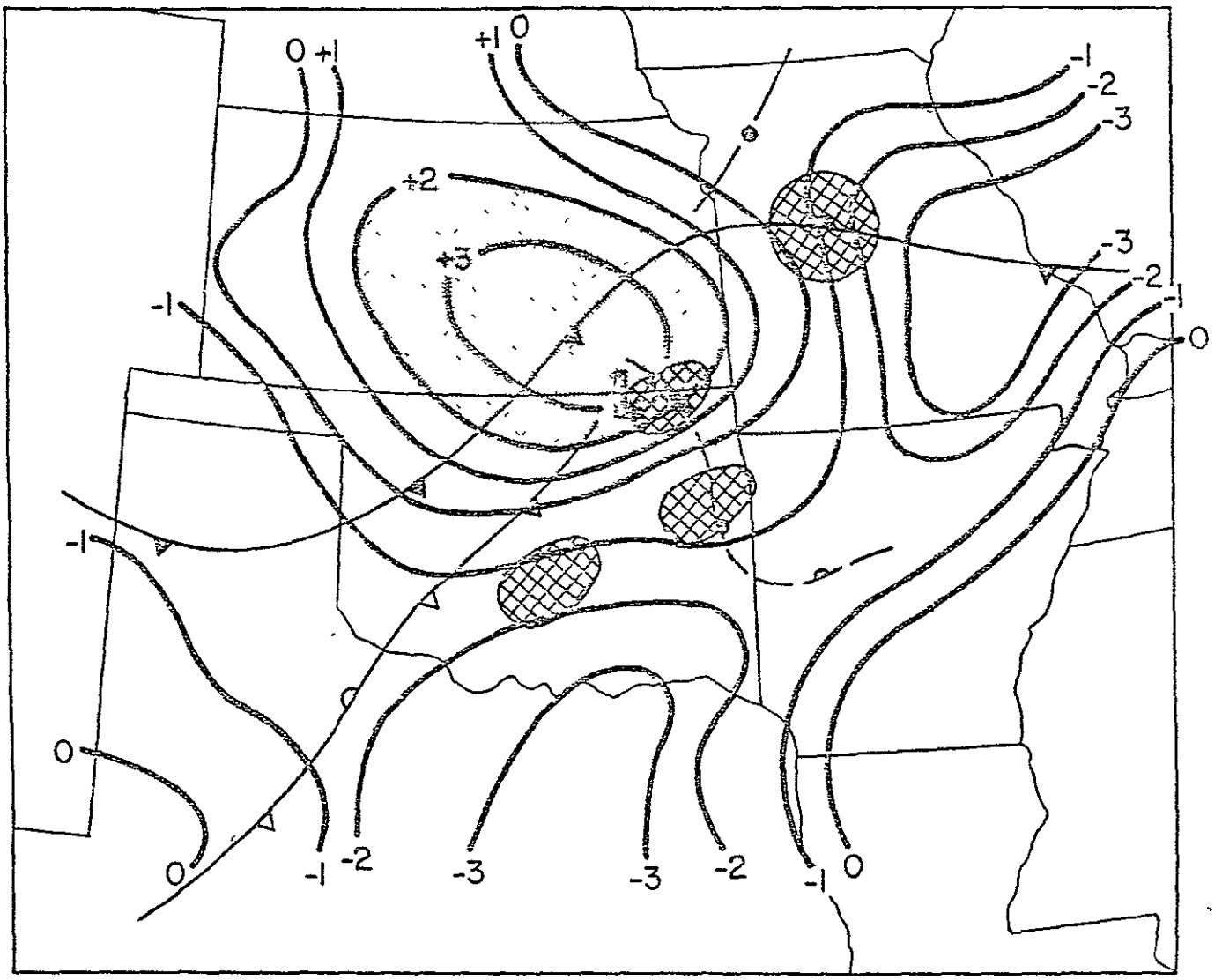

Figure 4.3. 700 mb ω field (u bars s^{-1}, from Wilson, 1977) for 2100 GMT, 24 April 1975, regions where severe thunderstorms developed are cross-hatched.

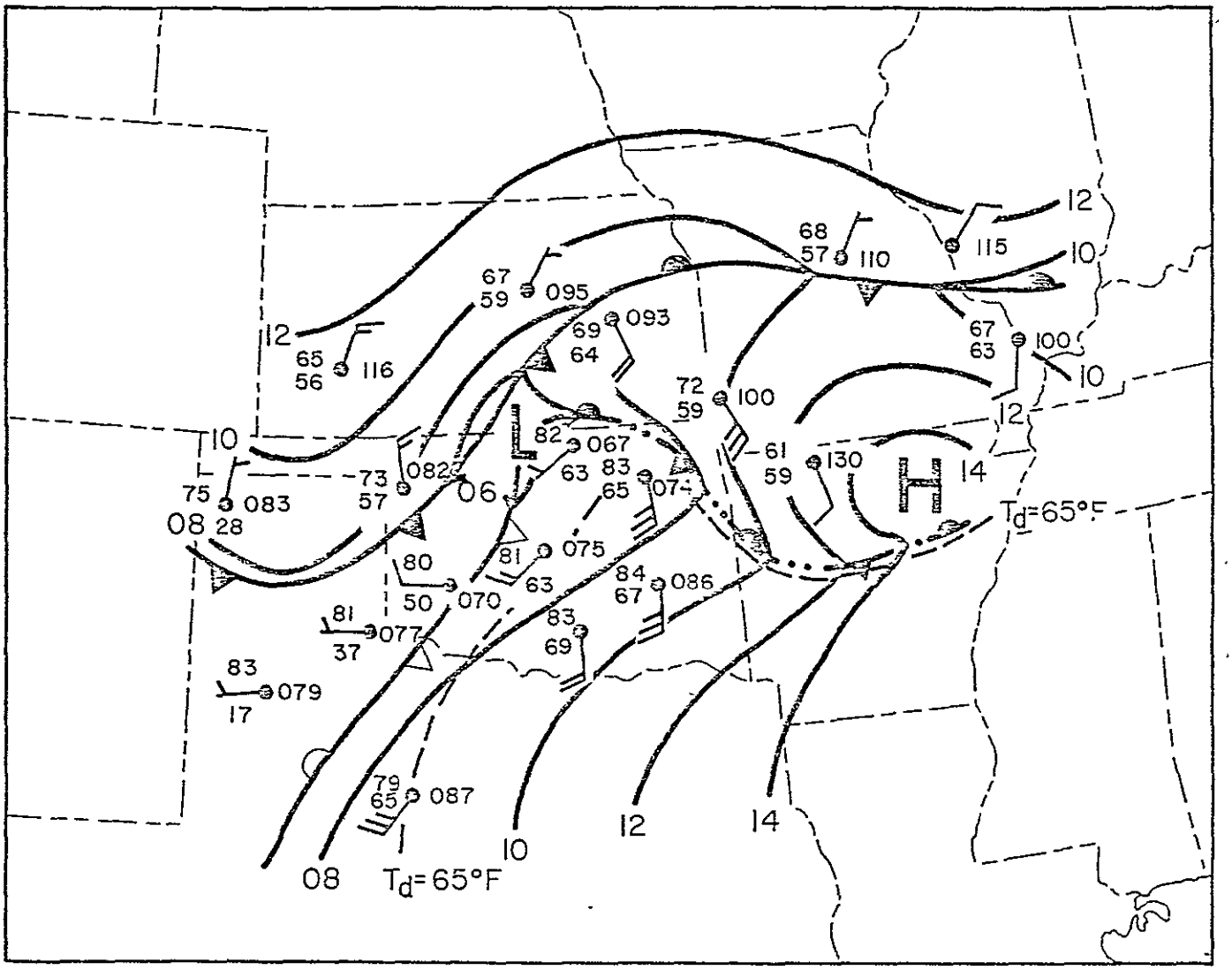

Figure 4.4a. Surface Analysis for 24 April 1975, 1800 GMT. Winds are in knots with full barb equal to 10 kt. Temperatures are in °F and 10 = 1010 mb. Surface dryline is shown with open frontal barbs. Thunderstorm outflow boundary is shown as squall line with frontal barbs added to indicate direction of movement.

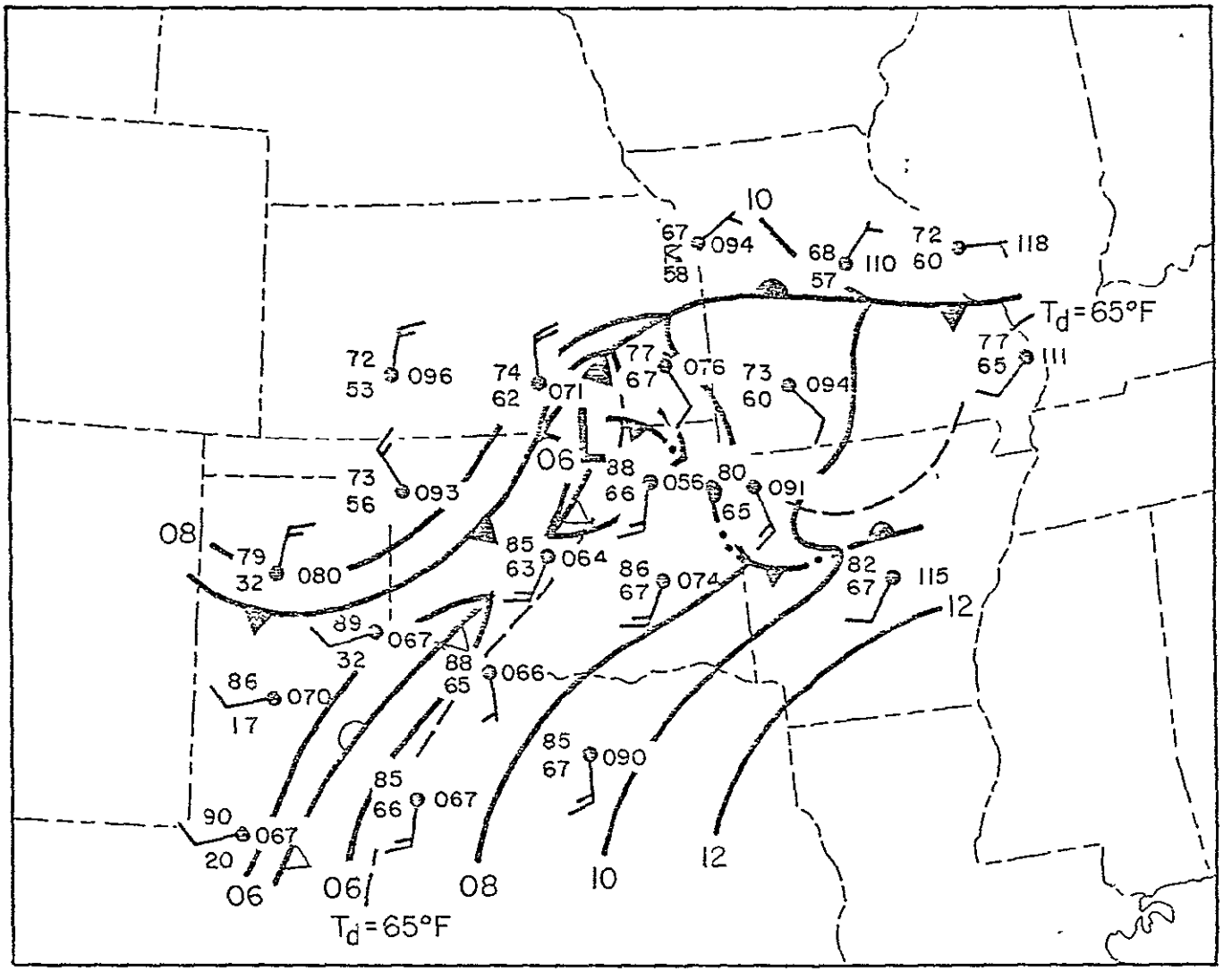

Figure 4.4b. Same as 4.4a except for 2100 GMT.

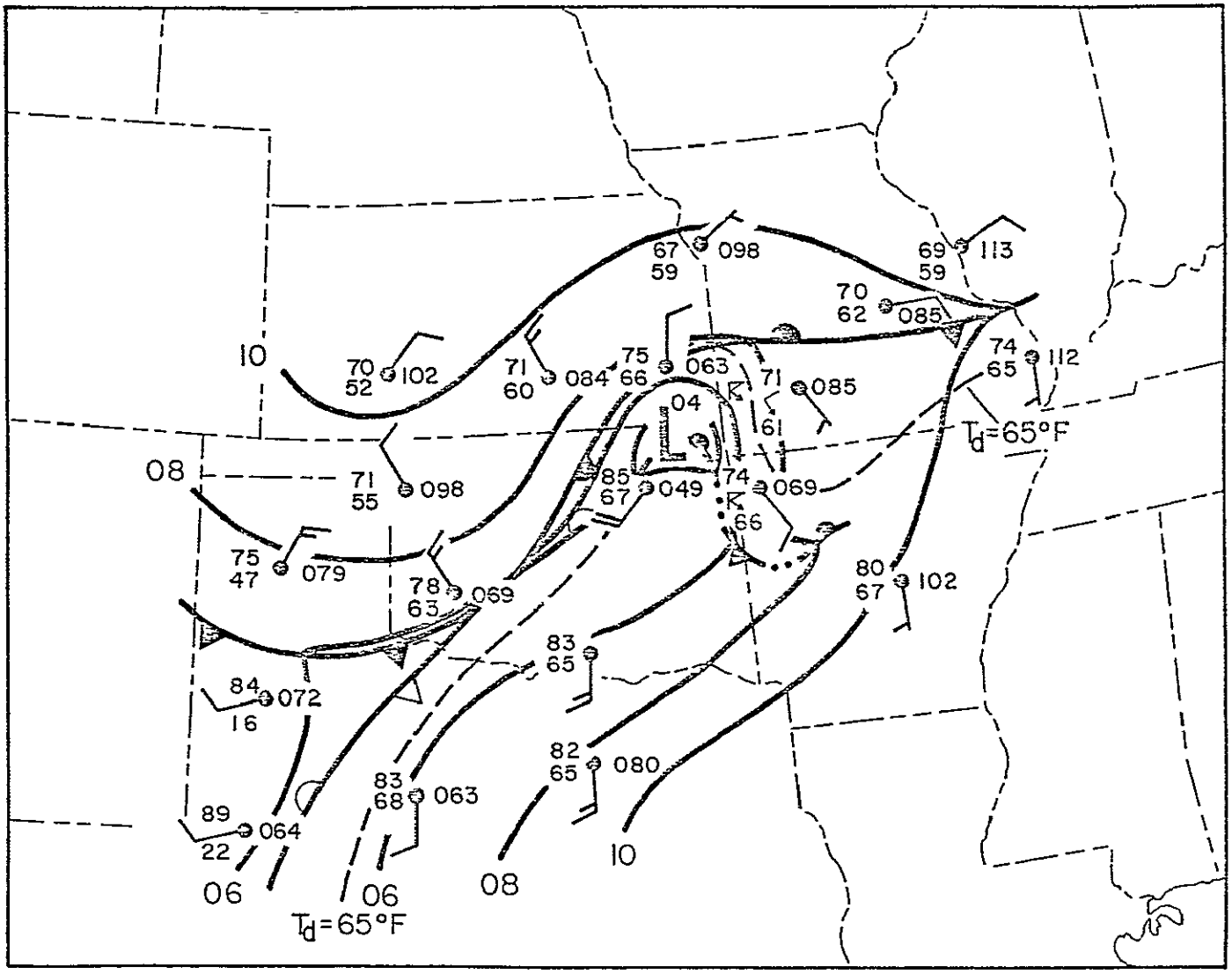

Figure 4.4c. Same as 4.4a except for 25 April 1975, 0000 GMT.

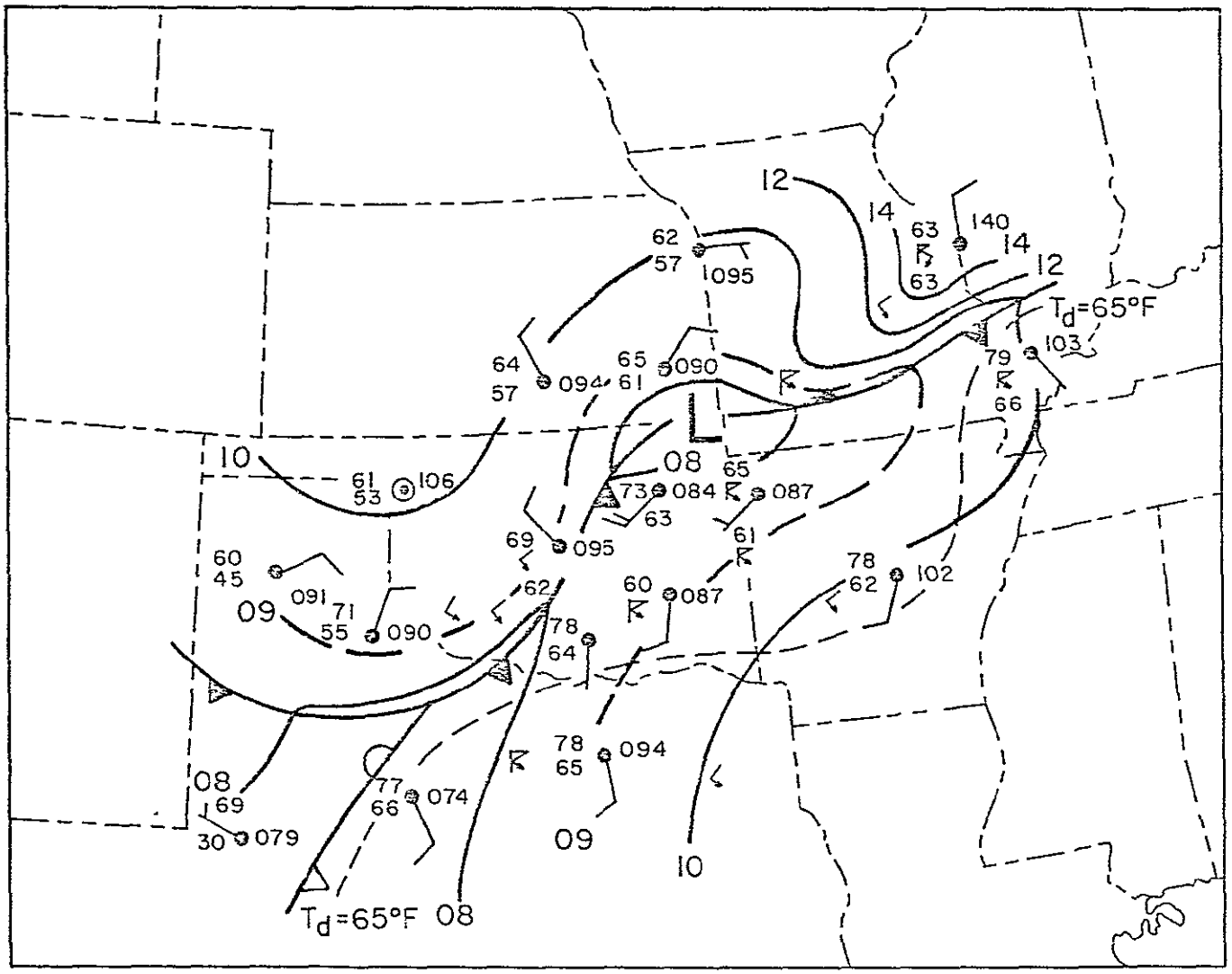

Figure 4.4d. Same as 4.4a except for 25 April 1975, 0300 GMT.

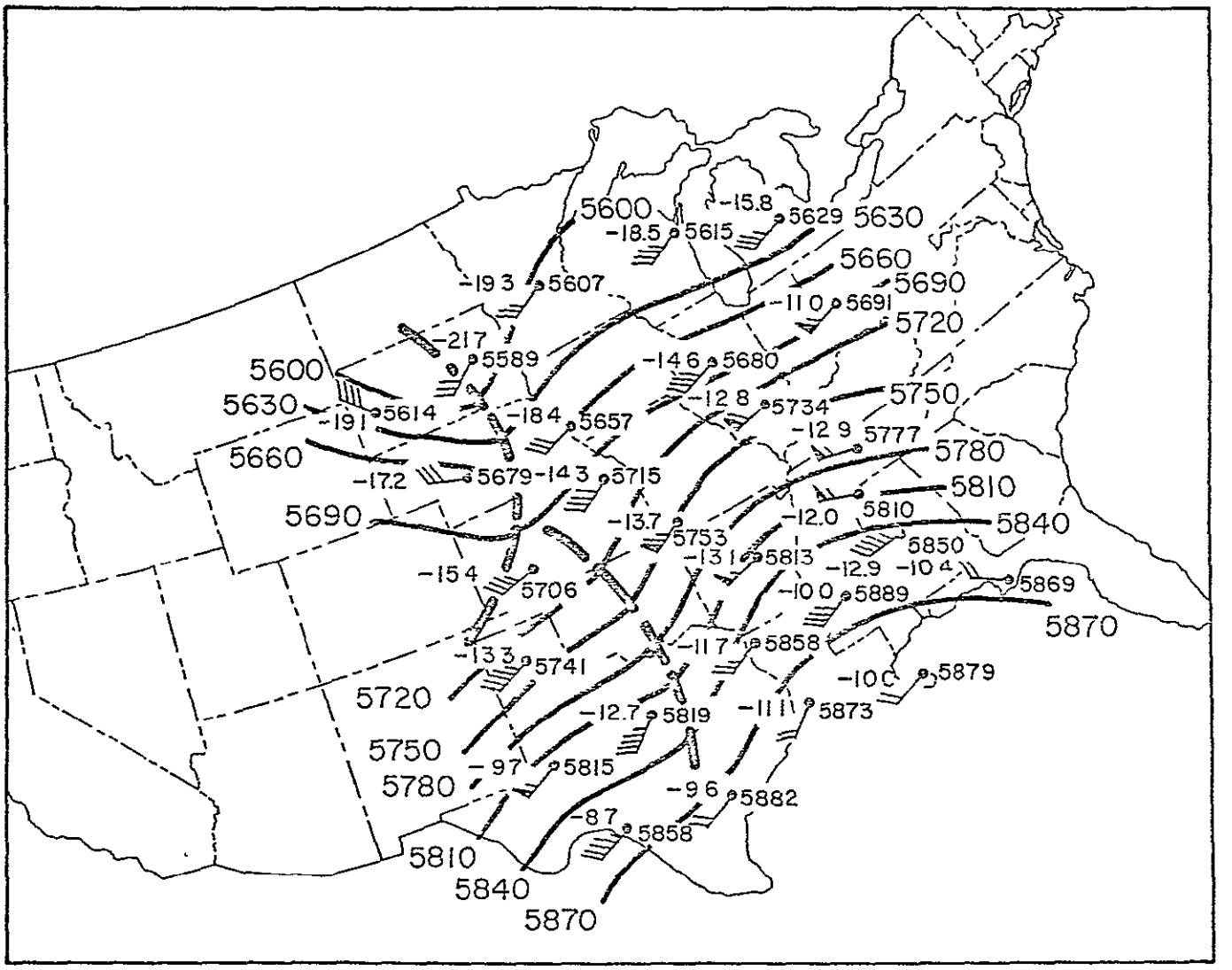

Figure 4.5a. 500 mb analysis for 24 April 1975, 2100 GMT. Short-wave troughs are indicated by heavy dashed lines and winds are in kt (flag = 50 kt.).

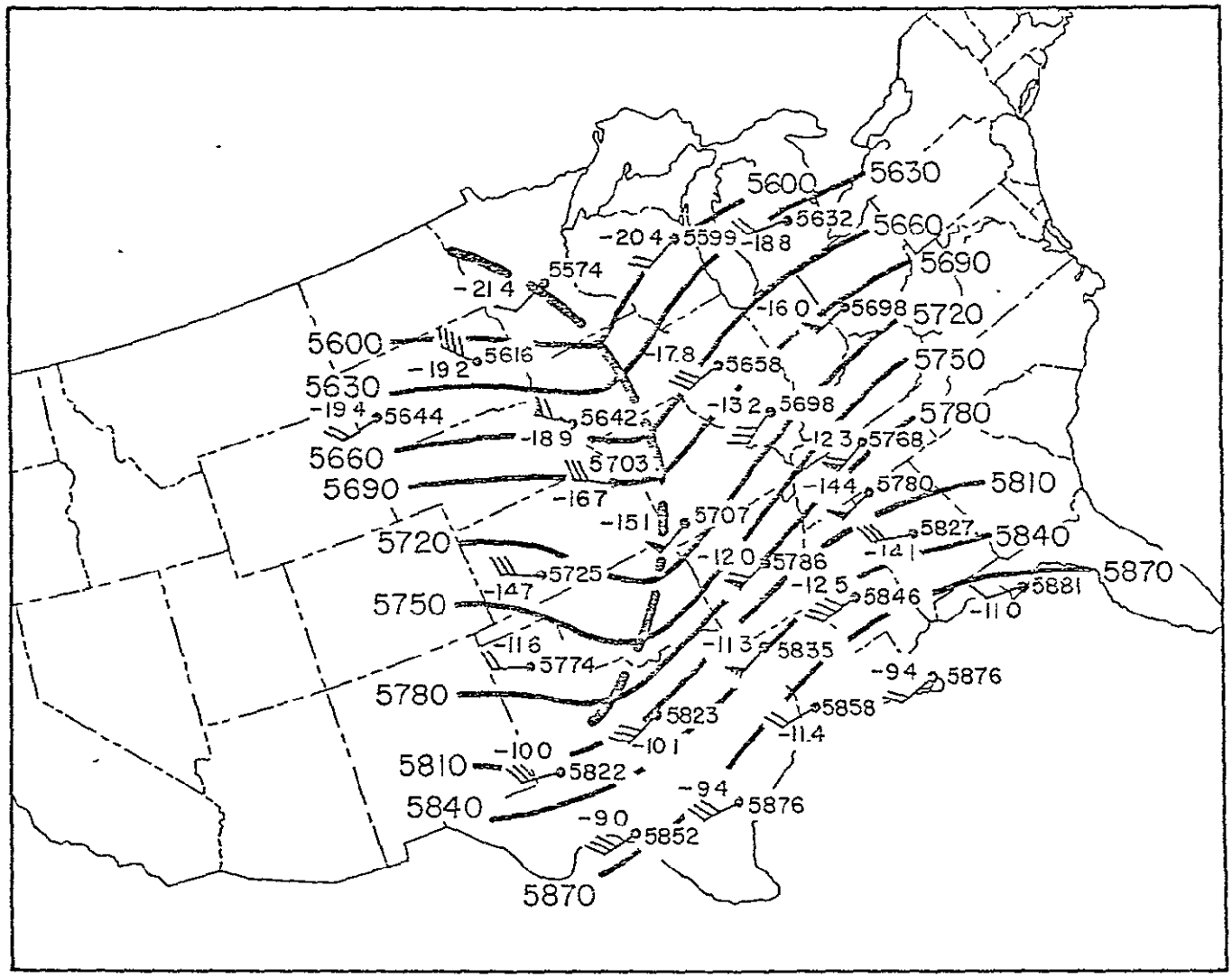

Figure 4.5b. Same as 4.5a except for 25 April 1975, 0600 GMT.

Many interesting and significant interactions between features on different scales appeared to occur on this particular day. Some of the more important effects seem to be upscale energy inputs from storm and mesoscale convective features that acted to alter the larger scale jetstream level feature and magnitudes. Jetstream charts (maximum winds aloft are plotted in ms^{-1} at each station) are shown in Fig. 4.6. Satellite imagery indicated thunderstorm areas are also shown. At 25/0000 GMT (Fig. 4.6a) several severe thunderstorms had developed in the diffluence zone between the strong subtropical jetstream (∿ 130 kt maximum) and a moderate polar jet (∿ 110 kt maximum). Only 6 h later dramatic changes were evident in the large scale flow. The subtropical jet had weakened to about 110 kt while the polar jet had reformed northward over the plains and undergone remarkable intensification over the lower Great Lakes region. A jet maximum of about 140 kt was now present. The concurrent satellite photo indicated an extensive canopy of thunderstorm generated cirrus spanned the region between the two jetstream maxima (note that radar data indicated that the active storms at 0600 GMT were oriented along the southern third of the cirrus region). These changes were undoubtedly due in part to the approaching second short-wave trough, but it certainly appears that convective scale feedbacks also played a role in the modification of the large scale jet structure.

The satellite data used in the various studies undertaken were in digital format on magnetic tape. A number of cloud growth rate computations and radar/satellite cloud top height comparisons were made. Low-level winds were generated by tracking clouds on the NASA AOIPS system. Dynamic parameters were calculated for these wind

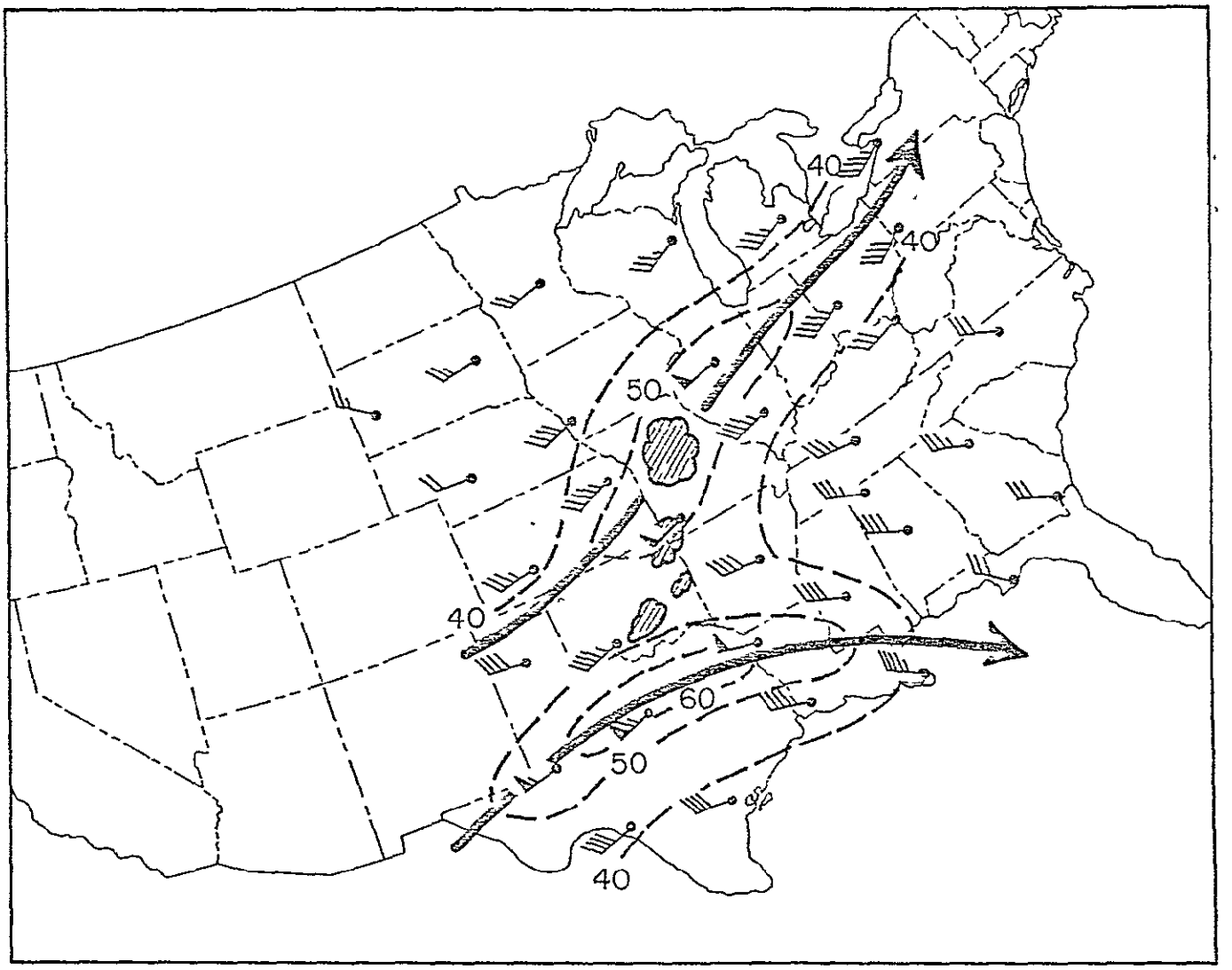

Figure 4-6a. Maximum winds aloft for 25 April 1975, 0000 GMT. Winds are in ms^{-1} with flag = 50 ms^{-1}. Satellite indicated thunderstorm regions are hatched.

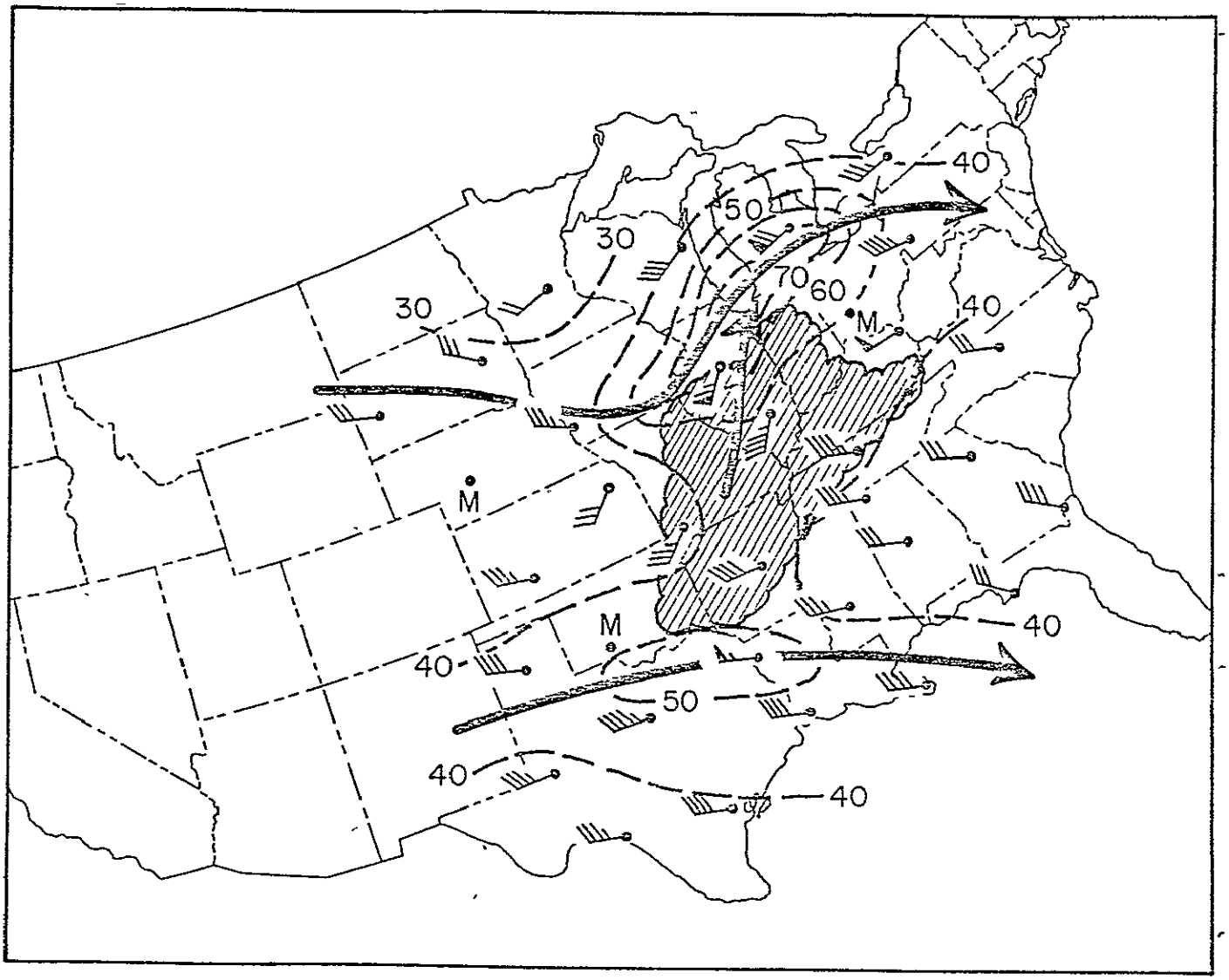

Figure 4.6b. Same as 4.6a except for 25 April 1975, 0600 GMT.

fields. The most significant results indicated that satellite wind fields might be combined with a moisture analysis (either conventionally or remotely sensed) to enable computation of moisture divergence fields. Several such fields were generated, and it was shown that regions characterized by high values of moisture convergence at 2100 GMT were generally the areas of subsequent severe storm development. Real time computation of such fields could provide valuable input to forecast and warning systems.

Papers detailing the specific research completed under NSG-5011 are included as appendices to this report.

5.0 CONCLUDING REMARKS

This research has elucidated a variety of satellite applications to weather modification programs in the Western U. S. Region. Several of these satellite applications have become a routine part of the decision making process and analysis procedures of the Bureau of Reclamation's weather modification programs.

In addition, satellite support has been an integral part of the CSU/SPACE program; a program operating on the frontiers of weather modification research. Satellite observations have also become an integral part of severe storm analysis.

REFERENCES NOT APPENDICIZED

Danielson, K. S. and W. R. Cotton: SPACE LOG 1977, Department of Atmospheric Sciences Report, Colorado State University, Fort Collins, Colorado, 399 pages.

Tegtmeier, S. A., 1974: The role of the surface, sub-synoptic, low pressure system in severe weather forecasting. M. S. Thesis, The University of Oklahoma, Norman, OK, 66 pages.

Wilson, G. S., 1976: Large-scale motion calculations in the AVE IV experiment. Geophysical Research Letters, 3, 735-738.

PAPERS, PRESENTATIONS AND THESES SUPPORTED BY NSG - 5011 FUNDING

Breed, D.W., 1976: Initial convection during SPACE-75, Unpublished manuscript, Department of Atmospheric Science, Colorado State University, Fort Collins, Colorado.

Maddox, R.A., A.J. Negri, and T.H. VonderHaar, 1976: Comparison of severe storm cloud top heights derived from satellite and radar observations. Presented at 1976 Fall Meeting,. American Geophysical Union, San Francisco, CA, by Maddox.

Reynolds, D.W., T.B. McKee and K.S. Danielson, 1976: Effects of cloud size and cloud particles on satellite observed reflected brightness. Peprints of International Conference on Cloud Physics, Boulder, Colorado, July 26-30, 413-416.

Reynolds, D.W., T.H. VonderHaar and L.O. Grant, 1976: Overview of satellite support to weather modification. Preprints of Second WMO Scientific Conference on Weather Modification, Boulder, Colorado, August 2-6, p.483-489.

Sheetz, V.R., and L.O. Grant, 1976: Satellite observations of seedable upslope cloud systems. Preprints of Second WMO Scientific Conference on Weather Modification, Boulder, Colorado, August 2-6, 491-496.

Stodt, R.W., and L.O. Grant, 1976: Satellite cloud climatology of summertime cumulus research areas. Preprints of the International Conference on Cloud Physics, July 26-30, Boulder Colorado, 423-426.

Danielson, K.S., and W.R. Cotton, 1977: SPACE Log. Edited by K.S. Danielson and W.R. Cotton, Atmospheric Science Department, Colorado State University, Fort Collins, Colorado.

Maddox, R.A., A.J. Negri and T.H. VonderHarr, 1977: Analysis of satellite derived winds for April 24, 1975. Preprints Tenth Conference on Severe Local Storms, AMS, Omaha, NE 54-60 pp., presented by Maddox.

Negri, A.J., 1977: Satellite observations of the onset and growth of severe local storms. M.S. Thesis, Colorado State University. and C.S.U. Atmospheric Science Paper No. 278.

Negri, A.J., D.W. Hillger, and T.H. VonderHarr, 1977: Moisture convergence from a combined mesoscale moisture analysis and wind field for 24 April 1975. Preprints Tenth Conference on Severe Local Storms, AMS, Omaha, NE 48-53 pp., presented by Negri.

George, R.L. and W.R. Cotton, 1978: The characteristics of evolving mesoscale systems over mountainous terrain as revealed by radar and PAM. Proceeding of the Conference on Cloud Physics and Atmospheric Electricity, July 31-Aug. 4, Issaquah, Washington.

Reynolds, D.W., T.B. McKee and K.S. Danielson, 1978: Effects of cloud size and cloud particles on satellite observed refelcted brightness. JAS, 35, p 160-164.

PAPERS, PRESENTATIONS AND THESES SUPPORTED BY NSG -5011 FUNDING (CONT)

Stodt, R.W., 1978: Summertime satellite cloud climatology, M.S. Thesis, Department of Atmospheric Science, Colorado State University, Fort Collins, Colorado.

APPENDIX A

[Reprinted from BULLETIN OF THE AMERICAN METEOROLOGICAL SOCIETY, Vol. 59, No. 3, March 1978]
Printed in U. S. A.

Meteorological Satellites in Support of Weather Modification

David W. Reynolds, Thomas H. Vonder Haar, and Lewis O. Grant
Department of Atmospheric Science
Colorado State University
Ft. Collins, Colo. 80523

Abstract

During the past several years, many weather modification programs have been incorporating meteorological satellite data into both the operations and the analysis phase of these projects. This has occurred because of the advancement of the satellite as a mesoscale measurement platform, both temporally and spatially, and as the availability of high quality data has increased. This paper surveys the applications of meteorological satellite data to both summer and winter weather modification programs. A description of the types of observations needed by the programs is given, and an assessment of how accurately satellites can determine these necessary parameters is made.

1. Introduction

The advancement in meteorological satellite technology has been rapid over the past decade. In the 1960s we saw the development of sun synchronous polar orbiter satellites with both visible and IR wavelength sensors that could monitor "weather" twice daily. These were very useful in monitoring synoptic scale disturbances but lacked the temporal frequency necessary to monitor short-term weather features. In 1966 the first geosynchronous meteorological satellite was launched; it provided visible imagery (4 km resolution at satellite subpoint) twice hourly and opened completely new avenues for satellite applications (Suomi and Vonder Haar, 1969). The time domain allowed such measurements as wind from cloud motion, cloud growth rates, identification of mesoscale disturbances causing short-term weather phenomena, and many others. In the 1970s the NOAA and DMSP (Defense Meteorological Satellite Program) series of polar orbiter satellites were developed, carrying sophisticated visible and IR radiometers and achieving very high resolution visible and IR imagery (1 km with the NOAA VHRR (Very High Resolution Radiometer) and 0.6 km with the DMSP VHR (very high resolution) sensor). The satellites also carried the first vertical temperature sounders, which allowed remote sensing of the temperature structure of the environment. NASA's Nimbus satellites also provided sounding capabilities including the microwave region and increased both the vertical and the horizontal resolution of the temperature and moisture measurements. The second generation geosynchronous satellites called the SMS-GOES (Synchronous Meteorological Satellite–Geosynchronous Operational Environmental Satellite) (Fordyce *et al.*, 1974) have been developed and are providing both visible (1 km resolution) and IR (8 km resolution) data twice hourly. The IR capability allows 24 h a day coverage of weather features for the first time. There are two GOES satellites presently in operation, GOES-E (east) positioned at 75°W and GOES-W (west) positioned at 135°W. During the First GARP Global Experiment (FGGE), the world will be girdled by such satellites (two from the United States, one from Europe, and one from Japan).

With the ATS satellites came a data dissemination network called the Satellite Field Service Station (SFSS). These were expanded and received more emphasis once the SMS-GOES satellites were launched. There are six of these SFSSs, which act as hubs or distribution points for photographic data users. Thus, near real-time imagery (20 min after scan) is now available from the GOES satellites to anyone tied into this distribution network. The quantitative digital data from the GOES satellites can be even more valuable both in research analysis and in operations if a suitable system is available to process the data. This paper will discuss how the digital satellite data can be used for weather modification applications and will describe some interactive time domain image-processing systems that have been and are being developed for applications use.

Dennis *et al.* (1973) investigated the usefulness of meteorological satellites in weather modification programs. They concluded that, with the observational requirements needed in a weather modification program, presently available satellite information (as of 1973) could not by itself satisfy these requirements. Their strongest recommendation was that imagery from a geosynchronous satellite with improved spatial resolution and the capability of accurately measuring cloud top temperature (CTT) be provided in real time to the field users. As we have stated, the SMS-GOES satellite systems have satisfied these major requirements and have provided even more in the way of support. We will discuss these present capabilities, as well as point out what satellites may offer in the next decade.

2. Application of satellite information to weather modification programs

a. Summertime cumulus modification experiments

1) Cloud climatologies

One of the first objectives in beginning a summer cumulus weather modification program in a given area is determining whether enough convective clouds are present naturally for seeding to take place and what

0003-0007/78/0269–0281$06.50

their natural characteristics are, i.e., isolated cells, well-developed squall lines, etc. The next objective is to determine whether these cumulus clouds are developing with the proper microphysical characteristics so that seeding would change their natural growth pattern in such a way as to increase precipitation.

There are several ways in which one could try to determine the first objective. One would be to take a long history of surface cloud observations to determine how many days convective clouds were observed and the degree of intensity of the day's activity. This is appropriate when a limited area is to be chosen or where a number of surface weather stations are available in a given area to allow complete coverage. This has been attempted by the authors and others and constitutes a very lengthy undertaking. Limited visibility due to rain, low clouds, etc., will severely limit the quality of these types of observations. Also, surface observations could not accurately provide numbers and sizes of convective clouds observed. Another procedure would be to use radar plan position indicator (PPI) data to determine the number of precipitating convective cells, sizes, intensity, rate of growth, and lifetimes (Bark, 1975). Unfortunately, for many of the areas that are being considered for summer weather modification programs, no radar data are available, or the data have not been archived in a format that could be easily processed. Use of radar data is, by its very nature, limited to precipitating clouds. Satellite visible data can sense all convective type clouds above a certain size threshold both before and after they reach the precipitation stage or even if they never precipitate. A comparative study between radar and satellite climatology performed simultaneously may show the ratio of the number of clouds observed (satellite) versus the number of precipitating clouds, which may indicate the potential of a locality for cloud seeding.

The third alternative in determining the seeding potential of a given area is through the use of satellite data. The most useful satellite data in such a study would be geosynchronous satellite data, preferably with both visible and IR measuring capabilities. This type of information has only been available since 1975 when SMS-1 was first positioned at 75°W with the VISSR (Visible and Spin Scan Radiometer) on board, providing high-resolution (1 km visible, 8 km IR) data on a half-hour basis. This type of data is the best source of information since the geosynchronous data provide the *temporal* frequency of the convective activity. The high-resolution visible data allow detection and measurement of very small cumulus clouds, and the IR data allow measurement of CTTs for the larger size clouds. The latter is needed to determine if the cloud has reached a temperature level where supercooled water may be present and seeding can be preformed.[1] Work is now beginning in the archiving of this information in digital form so that a true cloud climatology can be developed

[1] This technique would obviously not be applicable to tropical cumulus undergoing the warm rain precipitation process.

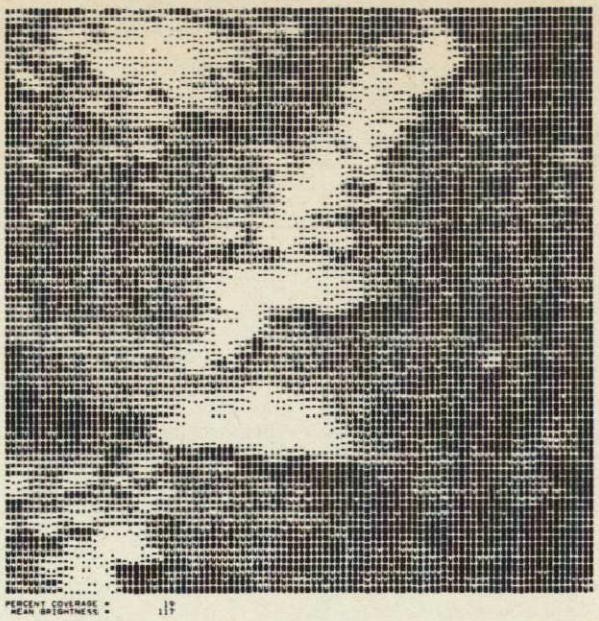

CLOUD	SIZE	MEAN BRIGHTNESS	VARIANCE	STANDARD DEVIATION
1	4	124	0.00	0.00
2	269	147	284.66	16.87
3	2	130	4.00	2.00
4	2	126	4.00	2.00
5	2	128	0.00	0.00
6	661	136	594.00	24.39
7	4	132	24.00	4.90
8	2	124	0.00	0.00
9	11	136	96.00	9.80
10	1	124	0.00	0.00
11	1	126	4.00	2.00
12	6	129	35.56	5.96
13	1	124	0.00	0.00
14	9	130	35.95	6.00
15	3	128	10.67	3.27
16	3	131	46.22	6.80
17	2	128	0.00	0.00
18	1	124	0.00	0.00
19	1	124	0.00	0.00
20	1	124	0.00	0.00
21	2	128	0.00	0.00
22	6	127	23.56	4.85
23	1	128	0.00	0.00
24	1	124	0.00	0.00
25	1	124	0.00	0.00
26	4	126	4.00	2.00
27	1	124	0.00	0.00
28	1	124	0.00	0.00
29	6	124	0.00	0.00
30	2	124	0.00	0.00
31	4	125	3.00	1.73
32	2	124	0.00	0.00
33	1	124	0.00	0.00
34	1	124	0.00	0.00
35	2	124	0.00	0.00
36	5	125	2.56	1.60
37	1	124	0.00	0.00
38	1	124	0.00	0.00
39	269	164	814.70	28.54
40	1	124	0.00	0.00
41	21	137	243.23	15.60
42	2	128	30.41	5.51
43	18	137	85.33	9.24
44	3	125	3.56	1.89
45	1	124	0.00	0.00
46	5	138	55.04	7.42
47	1	128	0.00	0.00
48	181	149	472.39	21.73
49	1	124	0.00	0.00
50	1	124	0.00	0.00
51	1	124	0.00	0.00
52	1	124	0.00	0.00
53	3	127	14.22	3.77

FIG. 1. (Top) Gray shade display of a small sector of SMS visible data showing the clouds as the white areas. (Bottom) Computer output giving statistics on the clouds observed in top photo. The size is in satellite element numbers.

(Reynolds and Vonder Haar, 1976). Figure 1 is an example of a computer-derived cloud count using SMS data. The image is reproduced in a gray shade format, and the number and size of each cloud are given.

Prior to the launch of SMS-GOES, the ATS series of satellites provided geosynchronous visible satellite data (4 km resolution at subpoint) on a half-hour basis, so that at least cloud sizes, numbers, locations, and temporal variations could be determined during daylight hours. Several years of ATS data have been used to determine cloud populations and active areas of convection for the three High Plains Cooperative Proj-

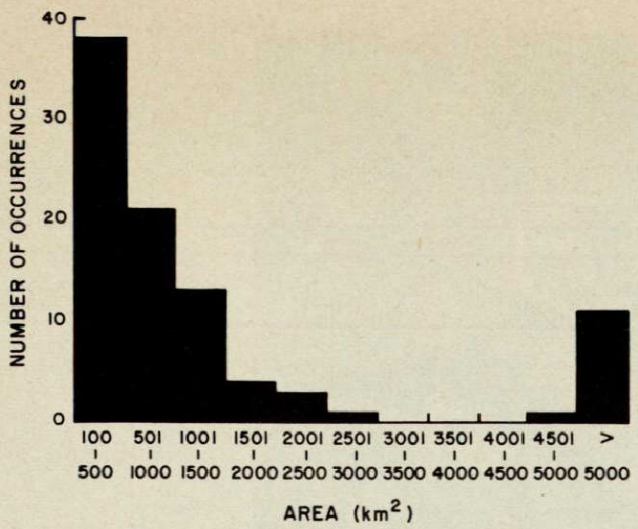

FIG. 2. Cloud size distribution histograms for Miles City, Mont., area as observed from the ATS-3 satellite. The satellite resolution is 113 km².

ect (HIPLEX) field sites (Miles City, Mont.; Goodland, Kans.; and Big Spring, Tex.) being used by the Bureau of Reclamation (see Reynolds and Vonder Haar, 1975). Not only can information be derived about the seeding potential of the sites, but decisions on the optimum location of rain gage networks can also be aided by having this type of information. Figure 2 shows results from a cloud population study done over Miles City, Mont., using ATS-3 data.

Other types of satellite data have also been used for these types of studies. Stodt and Grant (1976) have used data from the low-orbiting, very high resolution (0.6 km) DMSP satellite to obtain cloud numbers and sizes for weather modification sites over the western United States. Although this information provides only a snapshot of the clouds at local noon, even the very small cumulus can be detected with these data (see Table 1).

Another aspect of using satellite information for determining cloud climatologies is that the general numbers, sizes, growth patterns, and also cirrus extent will be known for both the target site and areas downwind. This will aid in determining to what extent seeding may affect the normal convective activity both at the site and downwind of the site. This will be discussed in more detail in a later section.

There are problems in using satellite data for developing cloud climatologies as there are with other techniques. Cirrus clouds can obscure lower clouds, and ground resolution problems may cause the smaller clouds to be missed. Computational time is extensive in processing the digital satellite data. Determination of cloud thresholds is also difficult. A man-computer interactive processing system is necessary for this type of study for accurate results to be obtained. However, we believe that the satellite provides a valuable tool to help assess the seeding possibilities in a given area.

2) Real-time operational support

As was mentioned earlier, near real-time high-resolution SMS-GOES satellite photo imagery is available to operational field sites at half-hour intervals. This allows qualitative analysis of both synoptic scale cloud features, as well as smaller mesoscale convective cloud developments to aid in the "nowcasting" of target site conditions for deploying aircraft or starting seeding operations. Reynolds and Matthews (1976) and Reynolds and Vonder Haar (1976) have described how geosynchronous satellite information has aided in supporting operations for HIPLEX (Bureau of Reclamation). It was noted that such convective triggering mechanisms as dry lines, vorticity centers, and fronts could be defined using the imagery and used for making the day's forecast of convective activity (Fig. 3; see also Purdom (1974)). Since all of the HIPLEX sites are located east of mountainous terrain, some of the convection passing over the sites is generated over the mountains. The generation and movement of these cells and whether or not they are increasing or decreasing in intensity can easily be monitored using the satellite imagery. Enhanced IR imagery can provide this type of information by monitoring CTTs to see if they are increasing or decreasing. Figure 4 is an example of this type of imagery, and the change in CTTs can be noted by the change in gray level of the tops (see Corbell *et al.* (1976) for details).

3) Use of digital and image satellite data in postexperiment analysis

Operations debriefing and evaluation. Much of the postanalysis work to date has been in using imagery to help locate certain synoptic or mesoscale features that may have influenced an experimental day's activities and to monitor their time histories. Reynolds and

TABLE 1. Mean values for days with convective clouds, July 1974

	Miles City, Mont.	Goodland, Kans.	Big Spring, Tex.	NE Colorado*	Palmer Lake Divide	South Park	Upper Arkansas River Valley†
Average cloud cover, %	4.9	10.1	8.3	4.4	11.1	20.3	27.0
Average number of clouds per 10^4 km²	4	6	9	8	7	18	19
Average size of cloud, km²	144.1	172.1	87.3	54.7	158.1	115.2	140.5

* National Hail Research Experiment.
† Leadville and Buena Vista.

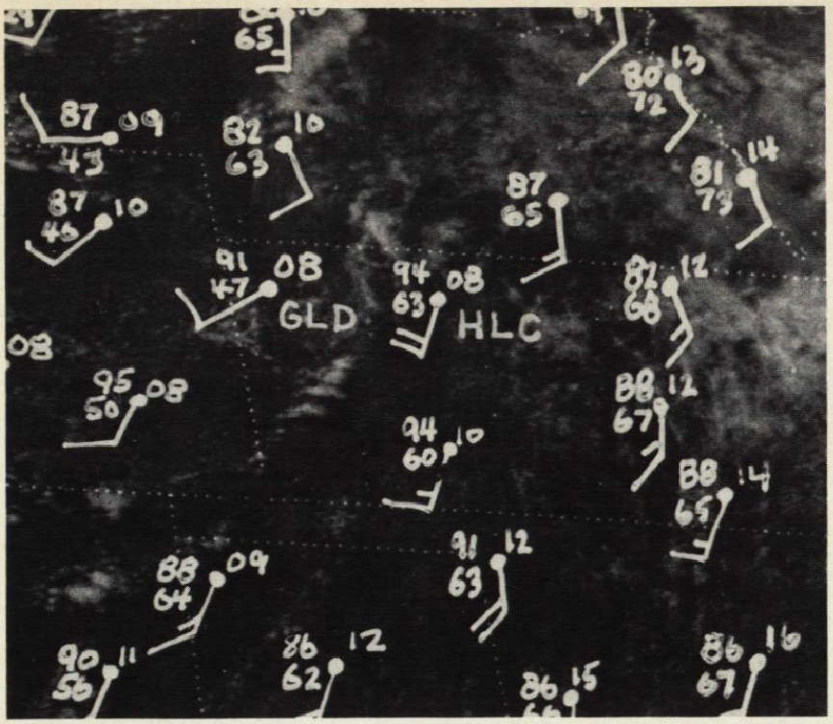

FIG. 3. SMS-2 2 km visible sector image taken at 2045 GMT on 28 August 1975 showing a line of thunderstorms developing between Goodland (GLD) and Hill City (HLC), Kans., extending to the southwest. The 2100 GMT surface observations are plotted. Note the dew point gradient across the thunderstorm activity.

Matthews (1976) and Reynolds and Vonder Haar (1976) have discussed these types of techniques in detail. This type of research analysis allows stratification of a given day's events into certain categories, which may be filed for later reference, regarding the time when a seed/no-seed decision must be made. One of the most important features that must be defined by this study is determining those days when organized rather than isolated convection will be present. With the use of conventional meteorological data, those days when organized convection was observed with imagery to develop may be studied and classified. It is felt that ultimately, to generate meaningful increases in precipitation, generation by seeding of organized, long-lived convective systems is needed. Satellite information may aid in developing the technology for identifying these situations.

A very important observation that the satellite is capable of making, and one that is critical to the evaluation of any weather modification program, is a comparison of the convective clouds behavior on seed versus no-seed days. This specifically addresses the problem of *relative* differences between cloud characteristics on the randomized seed/no-seed days. The visible digital satellite imagery can quantify such cloud characteristics as size, number of clouds, reflected brightness, anvil extent, cloud duration, movement (both speed and direction with respect to the environmental winds), cloud organization (line cluster, etc.), cloud separation distances, etc. The IR data can monitor CTT (height) variations of clouds on the seed/no-seed days to determine both temporal and spatial growth patterns on the different days. This may be important in assessing whether a dynamic seeding approach is modifying the growth patterns of these clouds. The IR data will also be important for they will be the only data available after sunset. This technique will require several seasons of data before an evaluation can be made, but from present experience it should offer an important evaluation mechanism.

The satellite data may also provide information on exactly how random a seeding program might be. This would concern itself with whether the "equality of the draw" was really equal. A comparison can be made of the general surrounding cloudiness (areal visible extent, vertical development (IR)) to determine if on the seed days more generalized convective development was apparent than on the no-seed days and vice versa. Thus in the evaluation of the seeding results, if a bias did exist, it could be eliminated before the final statistics were tabulated. This method might also lend itself to the determination of covariates for objective decision making of the day's events. For example, if more well developed cloudiness is observed, a look at the synoptic-mesoscale weather analysis may show a particular feature that could then be classified for future use.

Cloud parameter determinations. With use of digital satellite data, certain quantitative measurements can be made of individual clouds and cloud systems, and these results can be compared to other ground and aircraft observations. Emphasis must be placed on collection of

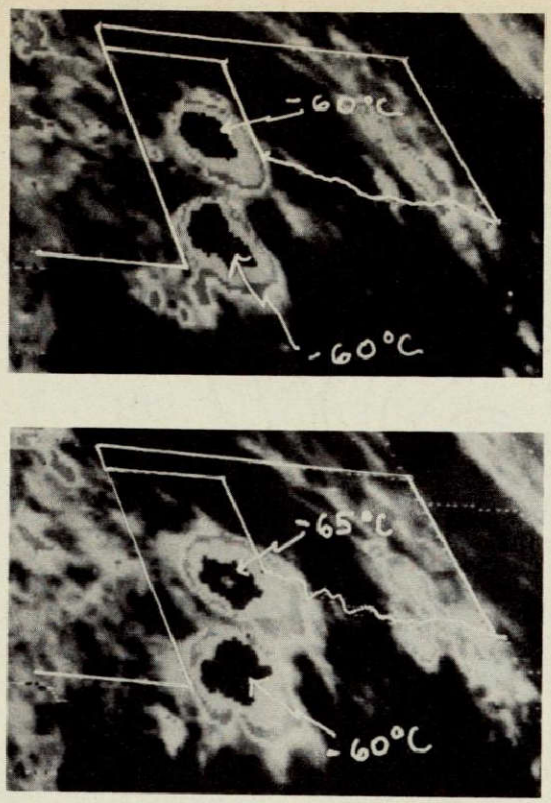

FIG. 4. (Top) The 0115 GMT, 22 June 1976, enhanced IR image showing two large thunderstorms located in the Texas panhandle. (Bottom) The 0215 GMT, 22 June 1976, enhanced IR image showing that the northern storm has increased in height while the southern storm appears to have remained constant.

digital rather than photo image data for these quantitative studies. There are several reasons for this:

1) Digital data can be earth located, "navigated," accurately for proper location of target sites and colocation with other data (Smith and Phillips, 1972).
2) Data can be normalized for sun angle changes and viewing angles using bidirectional reflectance models (Sikula and Vonder Haar, 1972).
3) Data can be directly input into digital processing systems (see Section 4) for analysis, and this allows computer mixing of several different types of data as well as time-sequencing capabilities.

Probably the most important parameter that must be measured in any weather modification program is precipitation. Given an area as large as the High Plains region of the United States, it is very difficult to have enough rain gages available to obtain good estimates of rainfall. Radar coverage is very limited in these regions but is the next most accurate tool for use in rainfall measurements. However, recent studies in HIPLEX show a single *Z-R* relationship is very difficult to obtain. Over the past several years, work has been done in attempting to estimate rainfall from visible and IR satellite data (Griffith *et al.*, 1976; Follansbee and Oliver, 1975; and Scofield and Oliver, 1977). In an attempt to extend some of this work, we compared digital SMS satellite data (available every 7.5 min) to digital radar data over the Goodland/Colby HIPLEX sites (Negri *et al.*, 1976) for 28 August 1975 during weak convective activity. The main conclusions from this study were that:

1) with use of a reflected brightness thresholding technique, precipitating versus nonprecipitating clouds may be defined;
2) a lag of as much as 20 min may elapse between the time this brightness threshold is reached and a radar echo is noted;
3) brightness does not seem to correlate well with any radar echo parameters such as area, volume, or intensity, but it does seem to be related to cloud size, and the center of maximum brightness locates well with the maximum radar reflectivity during the growth stage of the storm;
4) the areal growth rate of a cloud may relate to storm severity and to determine these growth rates, rapid scan data are necessary (5–15 min interval data).

These studies are in their very formative stages, and much work is needed to test the possibility of this procedure.

In relating cloud visible brightness to cloud parameters of interest, a separate study was needed to determine the relationship between changes in cloud brightness and simple changes in the cloud's vertical or horizontal extent (Reynolds *et al.*, 1978). This is a very important problem if we are going to use satellite brightness data to quantitatively measure changes in intensity of precipitation. Preliminary results seem to indicate that geometric factors outweigh change in cloud microphysical characteristics in influencing cloud brightness changes. McKee and Cox (1974, 1976) have discussed this problem in detail on a more theoretical basis, and the question must be studied further.

One other aspect of using quantitative satellite data is for input to and verification of cumulus cloud models (Kreitzberg, 1976). One-, two-, and even three-dimensional cloud models are being used in many weather modification programs. Ideal input to these models requires a closely spaced rawinsonde network for determining the atmospheric temperature and moisture structure and the vertical and horizontal wind components. With the advent of vertical temperature sounders on NOAA polar-orbiting satellites, high horizontal resolution (approximately every 70 km) temperature and moisture measurements became available for use in these types of models. Hillger and Vonder Haar (1977) have used VTPR (Vertical Temperature Profile Radiometer) data in conjunction with the conventional rawinsonde network to obtain mesoscale temperature and moisture fields over the High Plains. Figure 5 is an example of the use of VTPR data to derive mesoscale fields of temperature and precipitable water. (Although vertical resolution from satellite data is poor, having gradients in these parameters over short horizontal distances provides much information at the mesoscale.)

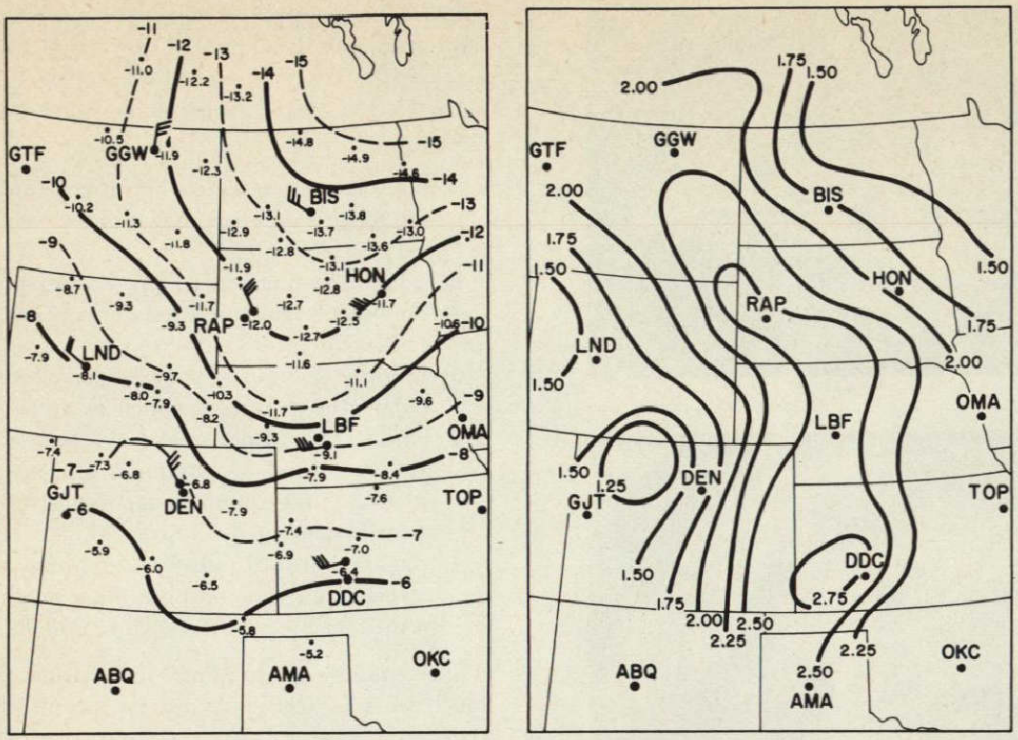

FIG. 5. (Left) Combined NWS and VTPR 500 mb temperature (in degrees Celsius) field for 9 August 1973. The thermal winds for the 700–300 mb layer are shown as derived from the VTPR data. (Right) VTPR-derived total precipitable water field (in centimeters) for 9 August 1973 at 1700 GMT.

This type of information is now being integrated into HIPLEX so that it will be available in real time for input into cloud models or for analysis of mesoscale features likely to cause convective activity. When GOES-D is launched in the 1980s, it will provide the first geosynchronous vertical temperature sounder data, allowing soundings to be made at rapid intervals over small areas where convective activity is likely to occur.

4) SPECIALIZED APPLICATION AREAS

Tropical cumulus modification study. Two general areas can be specified when discussing tropical weather modification activities. The first includes such activities as the Florida Area Cumulus Experiment (FACE) (Woodley *et al.,* 1976), which is involved in the seeding of tropical cumuli to increase rainfall. The seeding hypothesis of the FACE program is to increase the organization of the convective activity by seeding certain elements of a cloud line increasing the dynamics of the system so that it may precipitate for a longer period of time. As was mentioned earlier, Griffith *et al.* (1976) have been using satellite data to determine rainfall over the target area for a limited data sample. Other uses of satellite data are to simply pinpoint areas of existing cloud lines or clusters so that seeding aircraft can be deployed to these areas in time for seeding to occur. With the IR data now avilable from SMS-GOES it is possible to monitor these cloud lines and note any changes in CTT during seeding or the extent of cirrus for the seeded versus non-seeded storms. These IR data will also allow comparison to radar data to further explore satellite-rainfall relationships.

The other specific application area that is immediately thought of is that of hurricane modification. Satellite data allow the only consistently available monitoring system for determining storm strength, motion, and the changes in these parameters. A more direct verification method to evaluate hurricane modification can be accomplished by using geosynchronous satellite data to determine wind speeds from cloud motions within the storm system. With a clear view of the eye, measurements can be made of cloud motions along the eye wall (Gentry *et al.,* 1976). Dvorak (1975) has developed a technique for determining the intensity of tropical disturbances that can be used as a type of climatology when seeding occurs to determine if any radical effects have taken place. Project Stormfury, which is to begin again in 1978, will rely heavily on the SMS-GOES satellites for the monitoring of these storms as well as for the evaluation of the experiment.

Extra-area effects (downwind, etc.). The question of whether seeding effects are limited to the local area in which they are applied has been discussed as a political and scientific issue since weather modification activities began. There are several ways in which summertime cumulus activity and the modification of this activity can affect other areas outside the proposed target site. One method is that the cirrus outflow from the seeded storms could be more extensive than in non-seeded

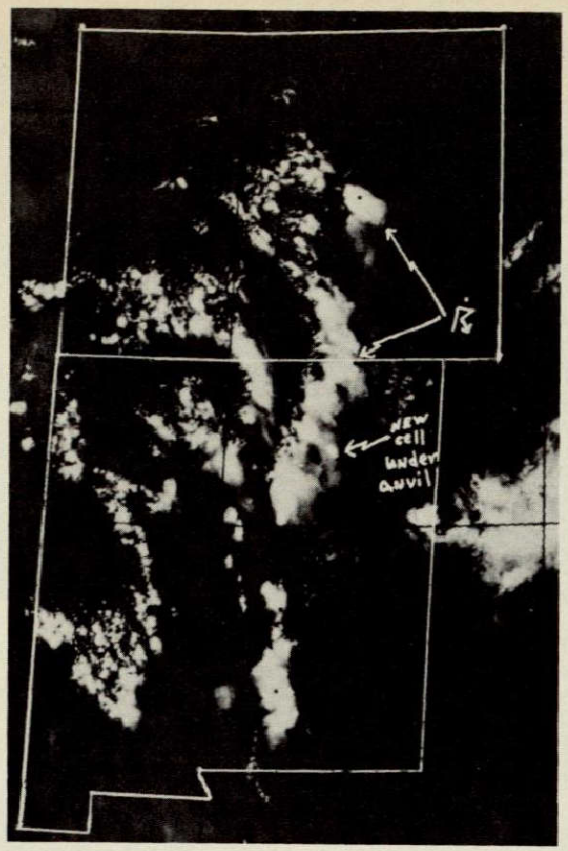

FIG. 6. DMSP 0.6 km visible image showing thunderstorm development along the front ranges and mountains of Colorado and New Mexico. Note the cirrus blow-off and the new cell under cirrus.

cases; this could decrease the local heating under this cirrus canopy, thus reducing convection. Satellites provide a complete view of all areas both in and out of the target areas and can easily monitor the cirrus outflow of both the seeded and non-seeded cells to determine any differences in cirrus extent and whether convection is growing through the cirrus canopy or suppressed in areas where the canopies existed. It may also be that the cirrus can act as a natural seeding device by injecting large amounts of ice crystals into developing cumulus clouds to increase cloud growth. Figure 6 is an example of a DMSP 0.6 km visible image showing convection along the continental divide and front range areas of Colorado and New Mexico. Note the extent of cirrus outflow of these naturally forming clouds and also the new cell development under the cirrus outflow of an earlier cloud. It is this type of monitoring that can aid in the analysis of extra-area effects of seeding programs.

b. Wintertime cloud modification experiments

1) COLD OROGRAPHIC AND PACIFIC FRONTAL RAINBAND CLOUD MODIFICATION

The potential for increased precipitation from supercooled orographic stratiform and frontal rainband precipitation clouds is well established (Grant and Mielke, 1967; Elliott *et al.*, 1971; Chappell *et al.*, 1971; Grant and Elliott, 1974; Gagin and Neuman, 1977). In fact it may be that these types of clouds offer the best possibility for seeding and for increasing precipitation over those areas where they exist. Some of the research experiments that have dealt with this type of cloud seeding are:

Group	Area for Field Studies
EG&G Inc.	San Juan Mountains of southern Colorado
Colorado State University	Central Colorado (Climax)
CSIRO	Tasmania
Desert Research Institute	Sierra Nevada
E. Bollay Assoc.	Park Range in northwest Colorado
Fresno State University	Sierra Nevada
Montana State University	Bridger Range in Montana
New Mexico State University	Jemez Mountains of New Mexico
North American Weather Consultants	Mountains near Santa Barbara, Calif.
Utah State University	Wasatch Mountains of northern Utah
University of Washington	Cascade Mountains in Washington
University of Wyoming	Elk Mountain and Wind River Mountains in Wyoming

Grant and Elliott (1974) have summarized the results from many of these studies and others to show that seeding effectiveness is highly dependent upon CTT (see Table 2.) Their studies show that increases in precipitation can be expected when seeding is performed on clouds with CTTs in the range of −10°C to −25°C. For clouds colder than −28°C, decreases in precipitation can actually occur after seeding. During many of these pro-

TABLE 2. Santa Barbara 2 (1967–70) average precipitation as a function of estimated CTTs for seeded and non-seeded cases.*

CTT, °C	Seeded		Non-Seeded		Precipitation Ratio Seed/ No-Seed
	Precipitation, mm/band	No. of Cases	Precipitation, mm/band	No. of Cases	
−17	10.7	13	5.1	22	2.10
−18	18.8	12	6.4	23	2.96
−19	16.5	24	6.4	21	2.60
−20	12.5	22	6.6	17	1.88
−21	9.9	21	6.4	14	1.56
−22	10.4	21	7.6	11	1.36
−23.5	8.6	10	7.1	8	1.21
−24.5	10.2	10	8.9	8	1.14
−26	11.4	10	9.7	10	1.18
−27.5	15.8	9	12.5	7	1.26
−28.5	15.0	7	8.9	5	1.40
−31	9.4	6	5.6	4	†
−33.5	7.4	3	5.1	2	†

* Values of precipitation for moving means of two temperature steps of 2.5°–3°C are centered on the indicated CTT. (Reproduced from Grant and Elliott, 1974).

† Sample too small to be significant.

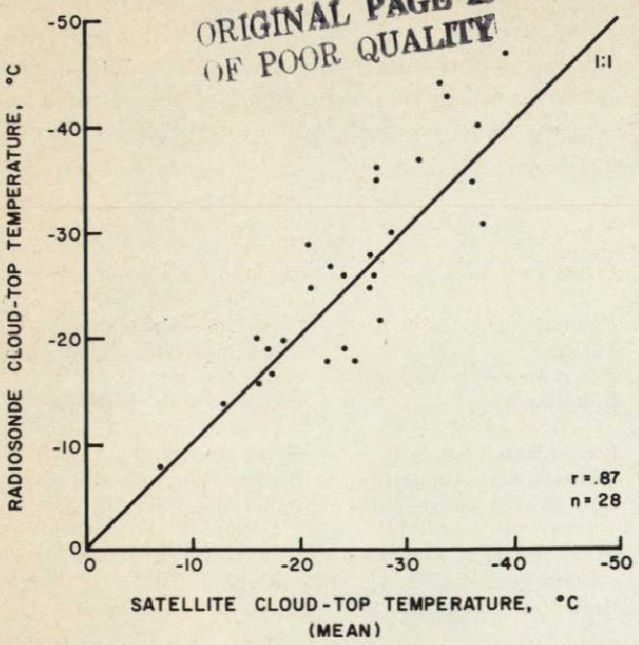

FIG. 7. Relationship between mean satellite-observed CTTs and radiosonde-determined CTTs for the entire data set of 1973–74 for the San Juan Mountain area.

FIG. 8. Enhanced GOES-W IR image from a digital display for 1745 GMT, 15 March 1977, showing a Pacific storm entering the California coastal region. Darker gray represents CTTs from −43° to −47°C; medium gray, from −39° to −43°C; and white, from −31° to −39°C.

grams, estimates of CTT were derived from either rawinsonde data or interpolated 500 mb temperatures. These have frequently proved to be inadequate in that only 3–5 rawinsondes can be launched per day and cloud tops cannot always be adequately deduced from the soundings alone. In addition, the 500 mb temperatures do not represent CTTs in many instances. As was stated earlier, Dennis *et al.* (1973) noted that one of the most beneficial uses of satellite data would be in monitoring CTTs from a geosynchronous satellite to provide half-hour information on CTT and its changes.

Real-time operational support. The term "opportunity recognition" has been used in the field of weather modification to designate those environmental conditions in which it has been determined that seeding will have positive effects. As we have pointed out, the CTT is a very important parameter when discussing these types of cloud systems. Another important question of "opportunity recognition" concerns the spatial and temporal location of seedable clouds. The inhomogeneities of actual clouds and their seedability are so great that considerable variability generally exists over even moderately sized weather modification targets. The ability of IR satellite data to provide CTT information has been demonstrated by Dumont *et al.* (1974) in a preliminary study using NOAA polar orbiter satellite data. Using the IR portion (10–12 μm) of the scanning radiometer (SR) on the NOAA satellite, they were able to measure CTTs for clouds over the San Juan Mountain area of Colorado during the Bureau of Reclamation's Colorado River Basin Pilot Project. Figure 7 is a comparison of satellite-determined CTT and radiosonde-determined CTT for all cases available. The results show that on the mean, the satellite observes a warmer cloud top (+1.8°C) than does the radiosonde. Although such problems as time differences between satellite and radiosonde observations, cirrus clouds overlying the orographic cloud, and cloud emissivity problems affect these comparisons, this preliminary study demonstrated the general feasibility of using satellites for this type of measurement. A second season (1974–75) of data is now being processed; NOAA polar orbiter data, again for the San Juan Mountain region, are being used. During this season, the first geosynchronous IR data became available from SMS-1 positioned at 75°W. Digital data from this satellite are available, and maps of CTT over the San Juan Mountains can be generated on a half-hour basis for a 24 h period.

To provide the real-time support necessary for field operations there are several methods in which the cloud top information could be provided. The first is using the enhanced IR imagery data where a specific gray scale would denote clouds with temperatures in the seeding window. These images would be available to the forecaster on a half-hour basis so that he could decide not only in what locations out of the entire storm complex seeding should take place but also when to begin and end the seeding operations. This is particularly important since several studies have strongly indicated that the main seeding effect is an increase in the duration of precipitation (Chappell *et al.*, 1971; Gagin and Neuman, 1977).

A second method would be to strip out the specific area of interest for the seeding activities from the digital data taken directly at the satellite ground station and either to map this information with a computer printer or to display the data on a CRT using a video recording

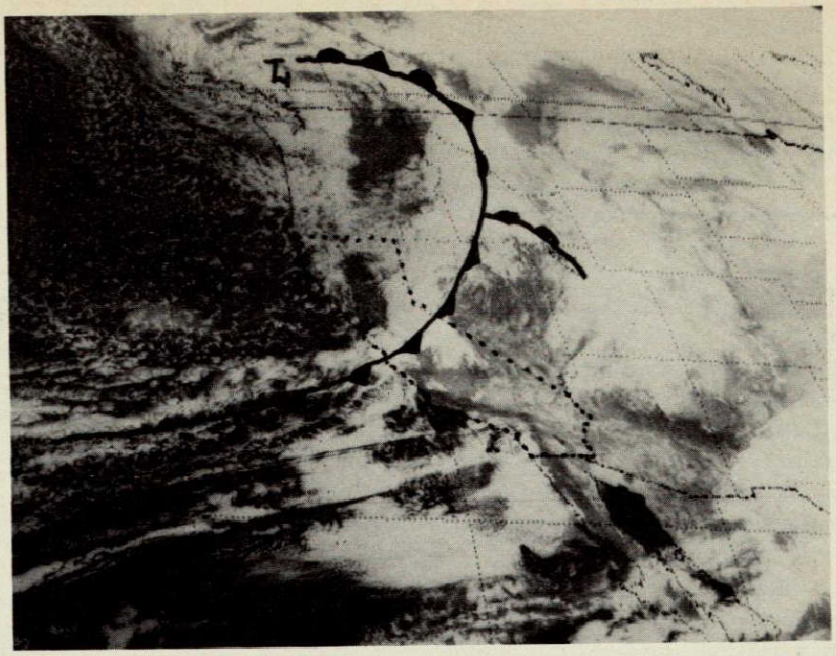

FIG. 9. SMS-2 2 km visible image for 1645 GMT, 9 March 1977, showing a Pacific frontal system situated over the Sierra Nevada.

system. These types of data could be transmitted to a field site by phone line to give the forecaster a constant update of CTTs. More on this video-digital display capability will be given in Section 3.b.

Use of digital satellite data in postexperimental analysis. During the postexperiment phase of the seeding program the digital SMS-GOES imagery collected can be used to stratify each day's seeding event into CTT categories. This is being done for the 1974–75 Colorado River Basin Pilot Project experiment using NOAA and SMS data and will be done for the Bureau of Reclamation's Sierra Cooperative Pilot Project, which began during the 1976–77 winter season over the central Sierra Nevada of California. The Bureau of Reclamation is now involved in a preliminary investigation of the characteristics and natural variability of convective rainbands as they impinge on the Sierra Nevada of California. In cooperation with the Bureau of Reclamation, Colorado State University has recorded digital SMS full resolution visible and IR data continuously from the time the bands are just off the coast of California to their passage through the Sierra Navada. We hope to obtain information on the capability of the satellite to determine the accuracy to which the top temperatures of these rainbands can be measured, how these temperatures vary with time, and the effects topography has on these bands (see Fig. 8). As verification, a cloud top aircraft is being flown over these bands to estimate their height and temperature. Photographs will be taken, and the presence of clouds, such as cirrus, that may overcast these bands will be noted. As was done for the summertime projects, radar-satellite comparisons will be made to determine if any relationships exist and whether the satellite data can be used to quantitatively determine precipitation amounts.

Not only can CTTs be determined, but an assessment of the types of synoptic situations that give rise to seedable clouds can also be determined through the use of satellite imagery and conventional meteorological data. The satellite allows an overall view of the synoptic situation (Fig. 9), which can allow categorization of optimum seeding situations and can be used as a forecasting aid for future events.

The same application of the satellite data can be made in the wintertime program as was made in the summertime programs. This relates to the relative difference in cloud characteristics of the seed/no-seed events as well as determining any biases in the randomized seeding events ("equality of draw"). For the wintertime clouds, such observable cloud features as stratiform layers versus presence of imbedded convection, CTT variation and magnitude, and visible cloud appearance (i.e., fuzzy (ice present?) versus distinct cloud edges (possibly only supercooled water clouds), etc.) could be analyzed for these different days. Chappell *et al.* (1971) have found that for the Climax Experiment, seeding tended to increase the duration of precipitation rather then the intensity of the precipitation event. It may be that by either monitoring the CTT (height) fluctuation through a storm period or determining the duration of the orographic clouds' fuzzy appearance, the satellite data might be used to decide if the precipitation event is of longer duration or more intense in nature.

For determining whether a true random sample has been chosen for a given experimental period, the satellite information can provide measurements of overall cloud extent both in and out of the target region. The

mean CTTs for the entire storm complex can be determined, and the direction and speed of cloud motions over the mountain barriers and indications of band structures (associated with either fronts or mesoscale features) can be observed for all seeding events. If any biases are present on the seed or no-seed days, then they can be removed before final analysis. Again, these same measurements might aid greatly in a covariate determination technique.

2) Specialized wintertime applications

As was mentioned with the summertime program, there has been concern with the effects downwind from the wintertime seeding programs. Brier *et al.* (1974) review much of the work carried out to date in determining the downwind effects from seeding cold orographic clouds. Many of the results to date show varying degrees of effect, from large increases to slight decreases. Brown *et al.* (1976) have recently summarized the results of the seeding program over Santa Barbara, Calif., where Pacific frontal rainbands were seeded over a 7-year period. Their conclusions stated that the primary cause of extra-area effects is probably a dynamic intensification of organized convective activity that produces increases in precipitation ~150 km downwind from the seeding source and ~30° to the right of the 700 mb wind flows. With satellite data it should be a fairly straightforward problem to monitor this area in an effort to determine whether the activity is more intense or continues for a longer period of time.

Mulvey and Grant (1976) have proposed a separate mechanism for extra-area effects downwind from the Climax Experiment in Colorado. Their hypothesis is that seeding material carried up into the orographic cloud is not entirely used and is transported downwind along with unused ice crystals. The seeding materials and ice crystals that survive the downwind transport can seed lower upslope cloudiness along the Front Range of the Rockies, which are warmer and deficient of the proper number of ice nuclei for efficient precipitation. This inadvertent seeding then should supply the cloud with an increased number of nuclei for increased precipitation. Scheetz and Grant (1976) have prepared a climatic estimate of the frequency with which High Plains upslope clouds are seedable. With both visible and IR satellite data it is possible to monitor the ice blow-off from the orographic cloud. In the area where this intersects the upslope cloudiness, a change in both the visible appearance of the cloud and in top temperature can be monitored to see if this seeding has any effect. Without aircraft data this is the only way to monitor this type of extra-area effect directly.

3. Present and developing technology in satellite observation systems and data processing

a. Present and near future capabilities

We have discussed many of the present capabilities of meteorological satellites as they relate to existing weather modification activities. However, we have certainly not discussed all the widely varying activities and uses of the data. There is one important area that should be discussed as it relates to the World Meteorological Organization (WMO) Precipitation Enhancement Experiment (PEP) (List, 1976). Site selection is one of the first priorities of the WMO. Although there are many political, social, and economical influences on these decisions, one overwhelming factor must be the requirement for "seedable" clouds to exist at the site frequently enough that seeding can be done. The satellite data can observe the presence of clouds and their appearance, i.e., stratified (stable) versus convective (unstable) over a particular site, aiding in the decision of whether to use a static (microphysical) seeding approach or a dynamic seeding approach. As was mentioned earlier, satellite data can provide this type of information on a worldwide basis. There exist many years of polar orbiter data with afternoon cross-over times that can and have been used to monitor convective activity. Also, on board many of the satellites are IR sensors allowing the measurement of CTTs of clouds large enough to fill the field of view of the sensor, so that it can be determined whether the clouds are cold enough for seeding materials to be effective.

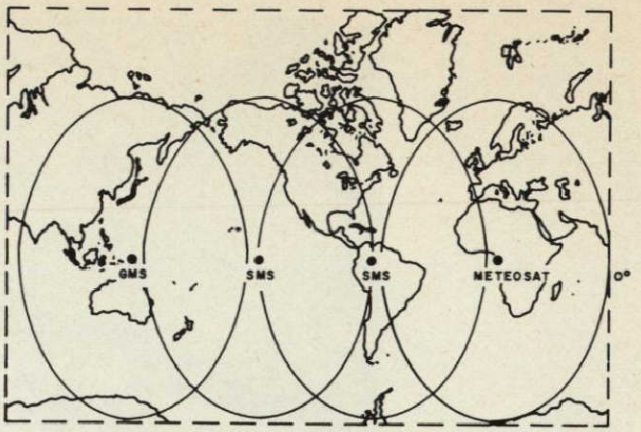

Fig. 10. Proposed geosynchronous satellite coverage for the late 1970s showing that all proposed WMO Precipitation Enhancement Experiment sites will be in view during all local times.

By 1979, in cooperation with FGGE there will be four, possibly five, geosynchronous satellites girdling the globe, (Fig. 10), allowing for the first time high spatial and temporal frequency satellite data continuously for the whole globe. These types of data will prove invaluable in assessing future weather modification sites both for summer and for winter programs.

We should mention here that there is one other important use of the SMS/GOES satellite that can be a real-time source of information besides providing satellite visible and IR data. This involves the communications channels on board the satellite that can interrogate, every half-hour, the transmitters of ground-based data collection platforms (DCPs). Such observations as temperature, humidity, and wind can be obtained and transmitted down to the ground station and displayed

on the aforementioned remote terminal Also, rain gage data or stream gage data can be monitored, especially for analysis of seeding effects or for flash flood alerts and snowpack conditions, to see if additional seeding or suspension of seeding is necessary in a given area This capability of SMS should be integrated with the digital imagery to provide extremely useful and timely information to all aspects of field operations and forecasting

b Real-time satellite data analysis and display systems

As has been mentioned in the previous discussions, of equal importance to the gathering of new data from new systems is the development of quantitative digital data analysis methods These digital data allow the monitoring of cloud brightness, CTTs, and cloud motions In addition, accurate navigation of the data can be performed through the recording of the line documentation being sent by the satellite (Smith and Phillips, 1972) This includes the housekeeping information of the satellite such as the geometry of the earth, sun, and satellite and time marks for each scan line This information can then be input to an analytic model for navigation of each visible image to ±1 (1 km) satellite element (relative picture to picture) Knowing the earth, sun, and satellite locations also allows brightness normalization to be made, which can account for changing sun angle effects and can try to compensate for cloud anisotropy

Generally, satellite data, to be of maximum usefulness, must be available in real time. Over the past several years, development of digital data-processing systems with man-computer interactive capabilities and CRT display have been developed The following is a list of several of these systems now in use throughout the United States

1) AOIPS—Atmospheric and Oceanographic Information Processing System (NASA Goodard Space Flight Center),
2) LARS—Laboratory for Applications of Remote Sensing (Purdue University),
3) McIDAS—Man Computer Interactive Data Access System (University of Wisconsin, Space Science and Engineering Center),
4) MMIPS—Man-Machine Interactive Processing System (NOAA/NESS),
5) ADVISAR—All Digital Video Imaging System for Atmospheric Research (Colorado State University),
6) ESIAC—Electronic Satellite Imaging Analysis Console (Stanford Research Institute)

These systems, when located with the satellite ground station, can provide real-time processing and analysis of cloud growth rates, cloud motions, change in top height, etc, that can be useful to field operation. (Real-time navigation is now in use at the Direct Readout Ground Station at the Space Science and Engineering Center in Wisconsin) These systems operate through input of digital satellite data, which can be stored on digital systems and displayed sequentially through rapid refresh of a CRT monitor Thus, 2–3 h of satellite data can be "looped" through, allowing cloud motions to be determined and thus providing information on mesoscale divergence, convergence, etc Also, the operator can interact directly with the data to enhance through color or black and white shading methods, he can zoom in on small features or rotate or translate the image and can determine, through use of a joystick and cursor, CTT or brightness of any cloud he so desires Through recent and ongoing advances in solid state electronics, these types of systems can be remotely placed in the field away from ground stations with just a telephone hook-up to a keyboard and CRT necessary for data access and manipulation. At the present time, work is under way in developing such a system that can meet the needs of not only weather modification programs but also severe storm forecasters and many other satellite data users, including industrial meteorologists (Bristor and Raynore, 1977)

4. Future advances in satellite observing systems

Future advances in satellite technology should be as impressive and as rapid as those that took place during the last 10 years One important new development that could provide dramatic technological advances will be the Space Shuttle The Space Shuttle will put much larger sensor payloads into orbit either by constructing them in space or by launching them on the Shuttle and then boosting them into geosynchronous orbit by space taxis Thus, large microwave (passive and active) antenna systems can be launched allowing direct measurements of precipitation over land and oceans and also allowing measurements of water vapor profiles at very high horizontal resolution (~10 km) and having 2–5 km resolution in the vertical Shenk and Kreins (1975) discuss some of these future breakthroughs that will come about in the 1980s

Not all of the advances will have to wait for the Space Shuttle Planned for launch around 1981 will be the GOES-D satellite equipped with VAS (VISSR Atmospheric Sounder) This will be the first sounder placed into geosynchronous orbit and will provide soundings at ~30 km spacing every half hour for a 750 km north-south latitude band and entire earth width The VAS will have nine channels, sensing temperatures (resolution to ±2 5°C) below the 100 mb level (thus temperature every 100 mb) and two water vapor channels for determining precipitable water

The next generation of satellites being considered will be Stormsat (Shenk and Kreins, 1975), which will improve both the imaging and the sounding capabilities of the GOES series of satellites This will be a three-axis stabilized spacecraft, which means it will always be pointing toward the earth and will be mechanically stepped both in the east-west and in the north-south direction Thus, very rapid scan information over a 750 km² area will be available Also, soundings using microwave channels can be made in overcast regions with 2°–3°C

temperature resolution at a 50 km interval every 30 min, and these microwave channels will allow moisture determination (10–15% accuracy in relative humidity) for 30 km intervals every 30 min This type of information can be used directly in two- and three-dimensional numerical cloud models for both initialization and verification

There are now even plans to fly radiometers that will determine something about a cloud's physical properties, i e, cloud top pressure level, the density and phase (i e, ice versus water) of condensed water in the clouds, a drop-size parameter, and the cloud thickness, both optical and geometrical

5 Summary

We believe that satellite information has the greatest utility for weather modification application when it is incorporated into a research operation along with other data sets Over the past several years, satellite technology and analysis technology have improved greatly The last section of this paper was designed to show the projected advances that may take place in the next decade, even though they may be overly optimistic Satellite sounder systems offer one of the highest potentials for application to weather modification programs, and it is hoped that, through the use of multispectral instruments, a high degree of vertical (albeit still crude compared to radiosonde) and horizontal resolution can be obtained, both in temperature and in moisture Continued research is needed on quantifying observed features from the satellite image, quantification must be such that the numbers can be incorporated into numerical models to help predict cloud development, seeding potential, and possible extra-area effects

Acknowledgments This research was sponsored by NASA under contract NSG-5011 and by the Bureau of Reclamation under contract 6-07-DR-20020

References

Bark, D. L, 1975 A survey of the radar echo population over the western Kansas High Plains Vols 1 and 2, Dept of Physics, Kansas Agric Exper Station, Kansas State Univ, Manhattan, Kans

Brier, G W, L O Grant, and P W Mielke, 1974 The evidence for extra-area effects from purposeful weather modification projects *Preprints, Fourth Conference on Weather Modification (Ft Lauderdale)*, AMS, Boston, pp 510–515

Bristor, C L, and W. L Raynore, 1977 Digital satellite imagery in industrial meteorology *Bull Amer Meteor Soc*, 58, 480–487

Brown, K J, R D. Elliott, and J R Thompson, 1976 Seeding convective bands in winter storms and the observed large scale effects *Proceedings of the Second WMO Conference on Weather Modification, 2–6 August, Boulder, Colo*, WMO, Geneva, pp 465–472

Chappell, C F, L O Grant, and P. W Mielke, Jr, 1971 Cloud seeding effects on precipitation intensity and duration of wintertime orographic clouds *J Appl. Meteor*, 10, 1006–1010

Corbell, R P, C J Callahan, and W J Kotsch, 1976 *The GOES/SMS User's Guide* NOAA/NESS, Washington, D C

Dennis, A S, P L Smith, and K R Biswas, 1973 Use of meteorological satellite observations in weather modification programs Rep 73-6, Inst of Atmos Sci, South Dakota School of Mines and Technology, Rapid City, S Dak (NTIS #N73-22583)

Dumont, R J, D W Reynolds, L O Grant, and T. H Vonder Haar, 1974 Determining the seedability of winter orographic clouds from satellite observations *Preprints, Fourth Conference on Weather Modification (Ft Lauderdale)*, AMS, Boston, pp 454–461

Dvorak, V F, 1975 Tropical cyclone intensity analysis and forecasting from satellite imagery *Mon Wea Rev*, 103(5), 420–430

Elliott, R D, P. St Amand, and J R Thompson, 1971: Santa Barbara pyrotechnic cloud seeding test results, 1964–1970 *J. Appl Meteor*, 10, 785–795

Follansbee, W A, and V J Oliver, 1975 A comparison of infrared imagery and video pictures in the estimation of daily rainfall from satellite data NOAA Tech Memo, NESS 62, Washington, D C, 14 pp

Fordyce, D. V, R J Wirth, and W E Shenk, 1974 The synchronous meteorological satellite (SMS) system *Preprints, Sixth Conference on Aerospace and Aeronautical Meteorology (El Paso)*, AMS, Boston, pp 158–164

Gagin, A, and J Neuman, 1977 The second Israeli cloud seeding experiment—The effects of seeding on varying cloud populations Dept of Atmos Phys, Hebrew Univ, Jerusalem, 10 pp

Gentry, R C, E Rodgers, W E Shenk, and V Oliver, 1976 Deriving winds for hurricanes using short interval satellite imagery *Preprints, Seventh Conference on Aerospace and Aeronautical Meteorology and Symposium on Remote Sensing from Satellites (Melbourne, Fla)*, AMS, Boston, pp 115–118

Grant, L O, and R D Elliott, 1974 The cloud seeding temperature window *J Appl Meteor*, 13, 355–363

——, and P W. Mielke, 1967 A randomized cloud-seeding experiment at Climax, Colo, 1960–65. *Proceedings of the Fifth Berkeley Symposium on Mathematical Statistics and Probability*, Vol 5, University of California Press, Berkeley, pp 115–132

Griffith, D, W L Woodley, S Browner, J Teijero, M Maier, D. W Martin, J Stout, and D Sikdar, 1976 Rainfall estimation from geosynchronous satellite imagery during daylight hours NOAA Tech Rept, ERL 356-WMPO 7, 106 pp (NTIS #PB-254 652/1GI)

Hillger, D W, and T H Vonder Haar, 1977. Deriving mesoscale temperature and moisture fields from satellite radiance measurements over the United States *J Appl Meteor*, 16(7), 715–726

Kreitzberg, C W, 1976 Interactive applications of satellite observation and mesoscale numerical models *Bull Amer Meteor. Soc*, 57(6), 679–685

List, R, 1976. Objectives and status of the WMO precipitation enhancement project (PEP) *Proceedings of the Second WMO Scientific Conference on Weather Modification*, WMO, Geneva, pp 445–453

McKee, T B, and S K Cox, 1974 Scattering of visible radiation by finite clouds *J Atmos Sci*, 31, 1885–1892

——, and ——, 1976. Simulated radiance patterns for finite and cubic clouds *J Atmos Sci*, 33(10), 2014–2020

Mulvey, G J, and L O Grant, 1976. A physical mechanism of extra-area effects from the Climax orographic cold cloud seeding experiment *Proceedings of the Second WMO Scientific Conference on Weather Modification*, WMO, Geneva, pp 477–479

Negri, A J, D W Reynolds, and R A Maddox, 1976 Measurements of cumulonimbus clouds using quantitative satellite and radar data *Preprints, Seventh Conference on Aerospace and Aeronautical Meteorology and Symposium on Remote Sensing from Satellites (Melbourne, Fla.)*, AMS, Boston, pp 119–124.

Purdom, J F, 1974 Satellite imagery applied to the mesoscale analysis and forecast *Preprints, Fifth Conference on Weather Forecasting and Analysis (St Louis)*, AMS, Boston, pp 63–68

Reynolds, D W, and D A Matthews, 1976 Real time satellite support for the High Plains cooperative experiment *Proceedings of the Second WMO Scientific Conference on Weather Modification*, WMO, Geneva, pp 497–502

——, and T H Vonder Haar, 1975 Satellite support to the HIPLEX activities for 1975 Final report to the Bureau of Reclamation, contract no 14-06-D-7630 (NTIS #PB-250 563/4GI)

——, and ——, 1976 Satellite support to the HIPLEX activities for 1976 Annual report to the Bureau of Reclamation, contract no 6-07-DR-20020, Denver Federal Center, Denver, Colo

——, T B McKee, and K S Danielson, 1978 Effects of cloud size and cloud particles on satellite observed reflected brightness *J Atmos Sci*, **35**, 160–164

Scheetz, V R, and L O Grant, 1976 Satellite observation of seedable upslope cloud systems *Proceedings of the Second WMO Scientific Conference on Weather Modification*, WMO, Geneva, pp 491–496

Scofield, R A, and V J Oliver, 1977 A scheme for estimating convective rainfall from satellite imagery NOAA Tech Memo, NESS 86, Washington, D C

Shenk, W E, and E R Kreins, 1975 The NASA severe storm program *Preprints, Ninth Conference on Severe Local Storms (Norman, Okla.)*, AMS, Boston, pp 468–473

Sikula, G J, and T H Vonder Haar, 1972 Very short-range local area weather forecasting using measurements from geosynchronous meteorological satellites Atmos Sci Pap no 185, Colorado State Univ, Ft Collins, 73 pp

Smith, E A, and D R Phillips, 1972 Automated cloud tracking using precisely aligned digital ATS pictures *IEEE Trans Comp*, C-21(1), 715–729

Stodt, R W, and L O Grant, 1976 Satellite cloud climatology of summertime cumulus research areas *Proceedings, International Conference on Cloud Physics (Boulder)*, AMS, Boston, pp 423–427

Suomi, V E, and T H Vonder Haar, 1969 Geosynchronous meteorological satellite *J Spacecraft Rockets*, **6**, 342–344

Woodley, W L, J Simpson, R Biondini, and G Sambataro, 1976 On NOAA's Florida Area Cumulus Experiment (FACE) main rainfall results, 1970–1975 *Proceedings of the Second WMO Scientific Conference on Weather Modification*, WMO, Geneva, pp 151–158

SATELLITE CLOUD CLIMATOLOGY OF SUMMERTIME CUMULUS RESEARCH AREAS

Richard W. Stodt and Lewis O. Grant
Department of Atmospheric Science
Colorado State University
Fort Collins, Colorado

1. INTRODUCTION

Satellite imagery produced by the Defense Meteorological Satellite Program (DMSP) has provided very high resolution visual images of the western United States once daily during daylight hours from each satellite. This study utilizes DMSP data available for the summer of 1974 to construct a cloud climatology of areas where weather modification or cloud physics experiments are currently being conducted or planned. These areas include the three High Plains Experiment (HIPLEX) sites at Colby, Kansas (CBY), Big Springs, Texas (BGS), and Miles City, Montana (MLS); South Park, Colorado (SPK), where the South Park Area Cumulus Experiment (SPACE) is being conducted; and the National Hail Research Experiment (NHRE) area in northeastern Colorado. The Palmer Lake Divide region (PLD) located between Denver and Colorado Springs, Colorado, and the upper Arkansas River Valley (ARK) between Buena Vista and Leadville, Colorado, were chosen for their proximity to current weather modification projects and their potential as sites for new weather modification studies.

The satellite used in this study is sun-synchronous polar orbiter passing over the study areas at approximately 1200 local time. Digital data tapes were produced from the transparencies and a computer analysis was accomplished, producing areas and numbers of clouds for each area and day as well as providing data for cumulative averages over selected time periods for each study area. Cloud locations and sizes were stratified with respect to a subjective cloud classification scheme as well as with respect to synoptic weather conditions. The relationship between cloudiness and topographic features was also examined.

2. DELINEATION OF STUDY AREAS

Figure 1 shows the location and shape of each of the areas analyzed in this study. The three HIPLEX sites are circles with a 112 km (60 n.m) radius from MLS, CBY, and BGS. These sites are included even though a similar study has already been performed for the summers of 1972-74 using data from the ATS-III satellite (Reynolds and Vonder Haar, 1975) since the DMSP satellite data has better resolution. The NHRE area was described for analysis purposes by using the 1973 borders of the NHRE study area (NCAR, 1974). The PLD area was chosen with the western border at the edge of the Front Range of the Colorado Rockies. The eastern border is the most easterly extent of the divide itself, about 130 km (70 n.m) east of the mountains. The north-south extent of the study area is equal to the width of the divide, from the south edge of Denver to the north edge of Colorado Springs, a distance of about 90 km (50 n.m). The western boundary of this area was determined to have "hot spots" that favored thunderstorm formation (Henz, 1973). The South Park study area (SPK) was chosen to provide satellite data coverage of the geographical area of interest in the South Park Area Cumulus Experiment (SPACE) presently being conducted by Colorado State University. The area was designed to include all of the topographical features known as South Park as well as to have a rectangular shape for ease in computer processing of data. The area for which satellite data is analyzed is bounded by the crest of the Mosquito Range to the west, the Kenosha and Tarryall Ranges to the east, a latitude line through Buena Vista on the south, and the Continental Divide to the north. The area is approximately 45 km (23 n.m) east-west and 65 km (35 n.m) north-south. The seventh area encompasses the upper

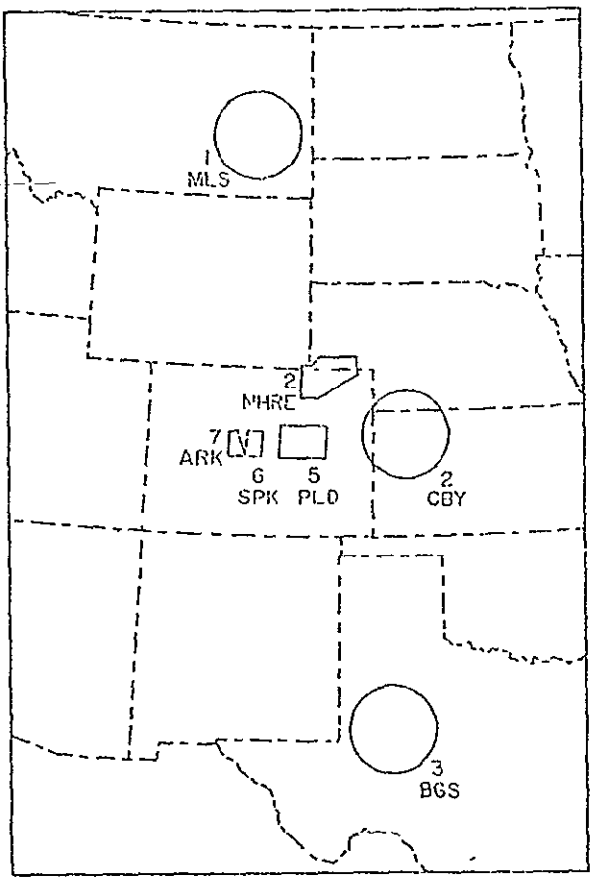

Figure 1. Study and analysis areas.

Arkansas River valley bounded roughly by the Continental Divide north of Leadville, on the north, the latitude of Buena Vista on the South, the Sawatch range to the west and the Mosquito range to the east. The area of study becomes narrower to the north as the river valley narrows. The approximate size is 65 km (35 n.m) north-south and averages 30 km (16 n.m) east-west. This area was chosen for study because of its proximity to SPACE.

3. SATELLITE SENSOR DATA

The DMSP satellite that produced the data used in this study is a polar orbiter with an average spacecraft height of 833 km (450 n.m). The orbit is circular with an angle of inclination of 98.7°. This inclination angle was selected to insure the satellite orbit would be sun-synchronous at this altitude. (Dickinson et al, 1974) The nodal period of this sun-synchronous orbit is 101.56. Since the earth revolves under the orbit to the east, and the orbit processes slightly to the east, each nodal crossing is approximately 25.4 degrees west of the previous crossing. The sensor scans 76.6 degrees of latitude across the subtrack. The very high resolution visual radiometer that provided the data for this study has a spectral range of 0.4 to 1.1 micrometers. The resolution of the imagery is nominally 0.6 km (.33 n.m) at the satellite subtrack. This degrades slowly to about 3.7 km (2 n.m) at the edge of the data due to foreshortening. It is interesting to note that while each nodal crossing is 25.4 degrees west of the previous crossing, the width of the scan track is 26.6 degrees of latitude. This causes a 1.2 degree overlap at the equator between successive passes which becomes progressively larger as the satellite approaches either pole. Although the resolution at the edge of the scan is degraded by foreshortening, if the area of interest falls near the edge of two successive passes, data can be obtained on cloud movement and cloud growth occurring during the 101.56 minute orbital period. The satellite used for this study (DSMP 8531) has a noontime sun-synchronous orbit. For the area of interest in this paper, a latitude range from 32 degrees to 47 degrees north, the longitude of the ascending node of the satellite is about 7 to 13 degrees east of the longitude of the satellite subtrack. Since best resolution is obtained when the satellite subtrack passes over or very close to the area of interest, the local solar time of satellite passover varies from about 20 minutes before local noon at BGS to about 35 minutes before local noon at HLS.

4. SITE IDENTIFICATION

The method chosen for accurately locating the study areas on the satellite imagery involved producing an overlay containing several properly located geographical reference points large enough to be easily visible on the imagery. The study areas were then accurately positioned on the overlay with respect to these landmarks. Since most days during the summer had large areas of clear skies, the method worked well. On days when landmarks were obscured by cloud, the study area overlay was accurately positioned using the grid supplied with the satellite imagery. It has been estimated that land or cloud features can be located to within 2.8 km (1.5 n.m) across track and 5.6 km (3.0 n.m) on the center line using the grid (Dickinson et al, 1974). The landmark method appeared to work equally well.

5. SYNOPTIC WEATHER PATTERN

In order to provide a better background for the cloud climatology data, a brief summary of significant weather patterns for Summer 1974 is included here. The weather of June 1974 was characterized by a well developed broad ridge over the western states which was accompanied by persistent clear skies, warmer than normal maximum temperatures, and generally below normal precipitation except for portions of western Kansas and eastern Colorado. The first week of June was cool and wet with snow falling in the Colorado mountains June 8 and 9. The warm and dry pattern became established the second week of June and maintained itself for the rest of the month (Taubensee, 1974). The mean 700 mb ridge migrated slightly eastward during July and became established over the Central Plains. The HIPLEX areas were warmer and drier than normal with the greatest precipitation deficiency being observed in the CBY and BGS areas. The Colorado mountain and plains areas generally reported near normal temperatures in the mountains (Wagner, 1974). There were marked circulation changes from July to August over the western states and Great Plains area. Troughing at 700 mb replaced the mean ridge over the central plains resulting in cooler than normal temperatures over the entire region. Precipitation was generally above normal in the southern and central plains, near normal in eastern Montana, with all the areas in Colorado involved in this study receiving less than normal precipitation (Dickson, 1974).

In Colorado during the summer months, storms typically form over the mountains, translate and propagate eastward onto the High Plains during the afternoon and evening. The mechanism for storm formation is a combination of diurnal heating and local mountain-valley breeze circulation. The propagation seems to be controlled by low level fluxes of heat and moisture, the stability, and the atmospheric wind structure (Tibes, 1976). Since this study is a climatology representing only one point in time during the day, this effect is reflected in the size and number of clouds observed in the areas.

6. DATA ACQUISITION

Very high resolution visual data for the months of June, July and August, 1974 were obtained from DMSP archives maintained by the University of Wisconsin, in the form of transparencies produced from original satellite analog data. Eighty-eight days of very high resolution (0.6 km) data were available and four days of high resolution (3.7 km) data making a complete set of 92 days of satellite imagery near local noon available for analysis. The scale of the 0.6 km data is 1:7,500,000 and the scale of the 3.7 km is 1:15,000,000. Two data reduction methods were employed. The first involved subjective classifications of clouds in

Table 1

This table shows the percentage of days of each type of major synoptic classification. Figures in parentheses indicate the percentage of occurrence of each cloud category within the mesoscale classification.

	EXPERIMENT 1 SITES						
CLOUD CLASSIFICATION	1 MLS	2 CBY	3 BGS	4 NHRE	5 PLD	6 SPK	7 ARK
COLD FRONT (Synoptic Scale)	19%	18%	7%	4%	2%	3%	3%
UPSLOPE	5%	5%	0	7%	6%	1%	1%
MESOSCALE	76%	77%	93%	89%	92%	96%	96%
SMALL CUMULUS < 2 km dia.	(31%)	(41%)	(36%)	(52%)	(25%)	(27%)	(29%)
ISOLATED CB	(33%)	(41%)	(27%)	(34%)	(65%)	(49%)	(44%)
CLOUD CLUSTER	(4%)	(14%)	(24%)	(2%)	(6%)	(20%)	(25%)
CLOUD LINE	(23%)	(2%)	(4%)	(10%)	(2%)	(2%)	(2%)
EMBEDDED CB	(9%)	(2%)	(9%)	(2%)	(2%)	(2%)	(2%)
TOTAL SAMPLE SIZE (days)	92	92	92	92	92	92	92
NO. OF DAYS WITH CLOUDS	59	61	59	46	65	76	75
% DAYS WITH CLOUDS	64%	66%	64%	50%	71%	83%	82%

the project areas by cloud type and cloud amount. The second method involved digitizing the images of project areas on the Optical Data Digitizer and Display System (OD^3) at Colorado State University. The components of the OD^3 system are a videcon camera, a television screen, a small computer, and a typewriter for transmitting instructions to the system. The computer was programmed to sense brightness levels from the screen and convert these into digital data. The data is stored on magnetic tape for later processing. For the digitizing process, one pixel or one data bit was equated to the resolution of the imagery such that the area represented by one pixel was equal to the highest resolution of the sensor.

7. DATA CLASSIFICATION

Subjective classification of the data with respect to synoptic and mesoscale influences was performed by inspection of the satellite imagery. Table 1 shows the categories used and the percentage of days during the summer that each of these cloud types and weather types was present. Three major categories , cold front, upslope, and mesoscale, were considered. Mesoscale systems were further divided and values in parentheses show the percentage of mesoscale days affected by the respective cloud types. These divisions were patterned after a cloud study of the HIPLEX areas by Reynolds and Vonder Haar (1975). The small cumulus category was added because of the increased resolving power available from the DMSP sensor. Mesoscale processes dominated the weather pattern over the region for most of the summer. The two most common mesoscale cloud types observed on the noontime imagery at all areas were the small cumulus, and the isolated cumulonimbus. From Table 1 it is seen that imbedded cumulonimbi account for 9% of the mesoscale occurrences at MLS, 2% at CBY, and 9% BGS. If the small cumulus category is removed to make the data more comparible with the Reynolds and Vonder Haar study and the mesoscale percentages are recalculated, imbedded cumulonimbi then account for 13% of the mesoscale weather occurrences at MLS, 3% at CBY, and 14% at BGS. These percentages are larger than those determined by the previously mentioned study, no doubt due in part to the better resolution of the DMSP data. Frontal activity was more apparent at MLS and CBY than at any of the other areas. In both cases, most of this activity was observed during the month of August. Surface frontal systems did not appear to penetrate as far south as BGS until the last few days of August. A large number of days when no clouds could be seen occurred at every area except SPK and ARK. The fewer number of clear days at these stations can be considered an indication of the effectiveness of the surface heating, mountain-valley circulation regime in producing cumulus clouds. These statistics, though in similar format to Reynolds and Vonder Haar (1975), are not directly comparible due to the inclusion of 1972 and 1973 data in the previous study.

8. DATA ANALYSIS

The digitized data discussed in Section 6 has been subjected to a number of tests. The first involved determining cloud sizes and cloud numbers for each of the areas for the summer of 1974. This is done by selecting a brightness threshold for the cloud border and summing all of the pixels within that border to determine the total area of the clouds.

The cloud brightness threshold was chosen by comparison of printouts of cloud pictures with printouts of actual digitized brightness values for each file. The computer senses each closed threshold brightness value contour as a cloud. The total number of clouds per site, the total cloud coverage for the day studied, and the average size of the clouds within the site area were calculated. Table 2 presents a summary of this output for the month of July 1974. Three tabulations are presented, the average percent of cloud cover, the average number of clouds normalized to an area of 10,000 km^2, and the average size of the cloud in km^2 for each study area. At both MLS and CBY the average cloud size was relatively large but the number of clouds per 10,000 km^2 was low. These data would seem to indicate that when convective activity was present at noon it was already well developed. The data for BGS in conjunction with Table 1, showed that large numbers of small cumulus clouds predominated at noon but that the few cases when larger cumulonimbi were present increased the average individual cloud area. NHRE, PLD, SPK, and ARK, when considered together, corroborate the description of a typical weather day over the mountains and high plains of Colorado. Since SPK and ARK are both located in the mountains, a noontime climatology should show a relatively high amount of clouds in these areas. This was, in fact, the case with SPK and ARK having an average cloud cover of 20.3% and 27% respectively. There were a large number of clouds present with individual clouds having relatively large sizes. PLD, located adjacent to a "hot spot" for thunderstorm development had less average cloud cover than the mountain areas and fewer clouds. Since all of the activity analyzed at PLD for this month was convective, the clouds that were present at this time were already well developed and they tended to be positioned at the western edge of the area. NHRE, being further away from the mountains had a low average percent cloud cover, few clouds, and a small average cloud size. On most days during the month the mountain thunderstorm cycle did not begin early enough for large cells to reach NHRE by pass time. Although not applicable to these data sets, cloudiness should have increased in the NHRE, MLS, CBY, BGS, and PLD areas later in the afternoon due to eastward translation and propagation of mountain induced thunderstorms, with a corresponding decrease in mountain cloudiness.

9. SUMMARY

Mesoscale processes dominated the weather pattern over the entire study region, more so over the mountains than over the plains areas. The smallest and least developed clouds were observed at NHRE. More developed, larger clouds were observed at the three HIPLEX sites, more so in the northern and central plains, probably due to a greater frequency of synoptic scale effects. PLD, SPK, and ARK were all similar in cloud size. The least number of clouds present were on the central northern plains averaging 4 to 6 per 10,000 km^2. More clouds were present at BGS and PLD, but, by far, the greatest number of clouds were present over the mountain areas. Average coverage was sparse everywhere east of the mountains, at this time with the greatest percent cloud cover over the mountain sites. This compares well with the typical diurnal summertime cloud regime over Colorado. These satellite data are a valuable tool for determining cloud population and with the advent of geosynchronous satellite data. Cloud systems can be followed from development to dissipation at half hour time increments.

10. ACKNOWLEDGEMENTS

This research was supported in part by the National Aeronautics and Space Administration under Grant NSG-5011 and by the National Science Foundation under Grant ENV 71-01885-A03.

11. REFERENCES

Dickinson, L.G., S.E. Boselly, III, and W.F. Burgmann, 1974: Defense Meteorological Satellite Program (DMSP) User's Guide AWS-Tech. Report 74-250, 98 pp.

Dickson, R. R., 1974: Weather and Circulation of August 1974 - Relief from Heat and Drought in the Central United States. Mon. Wea. Rev., 102., 807-811

Erbes, R. E., and I.O. Grant, 1976: A Kinematic Description of some Colorado Thunderstorms. Preprints of Int'l Cloud Physics Conf., Boulder, Colorado.

Henz, J. F., 1973: Characteristics of Severe Convective Storms on Colorado's High Plains. Proc. 8th Conf. on Severe Local Storms, Amer. Meteor. Soc., 96-103.

NCAR, 1974: Calendar of Events During 1973 Field Operations of the National Hail Research Experiment. NHRE Data Report No. 73/1, 62 pp.

Reynolds, D.W., and T. H. Vonder Haar, 1975. Satellite Support to the HIPLEX Activities for 1974. Final Report to Bureau of Reclamation, Contract No. 14-06-D-7630, 137 pp.

Taubensee, R. E., 1974. Weather and Circulation of June 1974 - Increasing Drought in the Northwest. Mon. Wea. Rev., 102, 662-666.

Wagner, A.J., 1974. Weather and Circulation of July 1974 - Heat Wave and Drought Over the Middle Third of the Country. Mon. Wea. Rev., 102, 736-742.

Table 2

Mean values for days with clouds, July 1974

	MLS	CBY	BGS	NHRE	PID	SPK	AKK
Average Cloud Cover (Percent)	4.9	10.1	8.3	4.4	11.1	20.3	27.0
Average Number of Clouds/10,000 km^2	4	6	9	8	7	18	19
Average Size of Cloud km^2	144.1	172.1	87.3	54.7	158.1	115.2	140.5

5.1.3

EFFECTS OF CLOUD SIZE AND CLOUD PARTICLES ON SATELLITE OBSERVED REFLECTED BRIGHTNESS

David W. Reynolds, T B. McKee and K. S. Danielson

Department of Atmospheric Science
Colorado State University
Fort Collins, Colorado

1. INTRODUCTION

Modeling of the visible radiation scattered from semi-infinite to finite size clouds has been attempted for several years. Hansen (1969) and Twomey, Jacobowitz and Howell (1967) resolved that for a plane parallel atmosphere with semi-infinite clouds having optical depths near 100 (cloud 1 - 1.5 km deep and having liquid water contents of 2 gm/m^3) that these clouds would be at their maximum brightness. These results showed that remote sensing of clouds in the mid-visible wavelengths would be of little value for clouds of any real vertical extent, and it would be impossible to determine anything about the clouds microphysical properties. However, observational measurements from satellites of convective clouds of significant vertical extent, (>>2 km), have shown increasing brightness with increasing height, Griffith & Woodley (1973), Reynolds & Vonder Haar, (1973), Griffith et. al., (1976). Recent work by Busygin et. al., (1973) and McKee and Cox (1973, 1975) have shown that the finite cloud poses a particular problem for monitoring its brightness due to energy passing through the vertical sides of the cloud. Thus their reasoning for this observed brightness-height change is related to the fact that as the cloud grows it becomes wider as well as thicker making side effects less important and allowing more light to be reflected off the top. However, even this theory does not account for some of the observed change in brightness for semi-infinite clouds which will be reported in this article.

During this past summer, a unique data set was obtained during the South Park Cumulus Experiement (SPACE). Data on cloud dimensions and cloud position were collected through the use of two cameras which simultaneously photographed the experimental area. Since these stereo photographs were taken in a time lapse mode, the growth characteristics of the clouds could also be deduced Cloud microphysical data for the experiment were collected by aircraft, radar, and surface observations. Three aircraft were used to penetrate the cumulus clouds The CSU Areocommander and the University of Wyoming Queenaire both are instrumented to study cloud microphysical processes Emphasis is placed on collecting data pertaining to cloud particle distributions, IN and CCN concentrations, and liquid water contents as well as the state parameters The NOAA/NCAR Explorer sailplane, because of its ability to remain in the clouds for extended periods of time while collecting microphysical data, was a particularly unique data gathering system which was utilized extensively in SPACE. The Limon WSR-57 10 cm radar and the CSU M-33 10 cm radar provides data on position, intensity and motions of clouds with precipitation sized particles. The CHILL dual 10 cm and 3 cm wavelength radar with doppler capabilities was used to determine position and intensity of natural clouds and was also used in radar chaff tracer experiments which have yielded substantial data on cumulus cloud microphysical processes and on cloud morphology. A surface meso-net collected data on low level fluxes of heat and moisture A surface chase vehicle provided data on precipitation type and size distribution. Several daily air mass soundings were taken to provide data on the changes experienced by the non-cloud air mass and provided a reference for satellite derived cloud-top temperatures. All these data complement, support, and strengthen observations made by the satellites of the South Park region

Along with this data, digital SMS-2 (Synchronous Meteorological Satellite) visible (.5 - .7 μm) (.9 km resolution at SSP) and infrared (10 5 - 12.5 μm) (9 km resolution at SSP) radiance data were received for this area through the Direct Readout Ground Station at White Sands Missile Range This allowed us to observe reflectance patterns of the clouds as well as estimate their top heights.

Using the Monte Carlo cloud model for finite clouds developed by McKee and Cox, (1973) we used different distributions of drop sizes and numbers (Deirmendjian, 1969) along with varying cloud depths and widths to determine how theory would predict what the satellite would view from its given location in space Results of these runs along with satellite observed reflectance will be presented in the following sections

2. MODEL CALCULATIONS

Fig. 1 shows the two drop size distributions used in the model (C.1, C 3), along with the average distribution observed during the last 3 days of SPACE. Note that the two distributions used bounded that observed during this period so that C.2 results would fall between the curves shown in Fig. 2 From Deirmendjian (1969), we obtained the 2 phase functions and volume scattering coefficients for a water cloud at a wavelength of 7 μm The phase function labeled C.1 is characterized by a very strong forward scattering peak while C.3 is not nearly as strongly peaked. Accuracy of the computations depends on the number of photons processed through the computer program

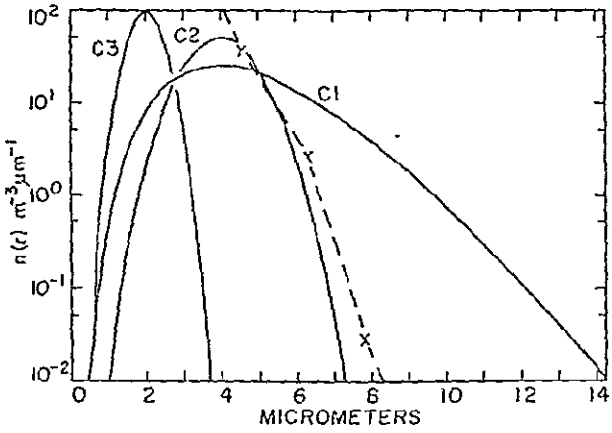

Fig. 1. Particle size and number distributions available for model input (Deirmendjian, 1969) South Park observed distributions are shown as the dashed line Note curve continues upward showing large number of small particles.

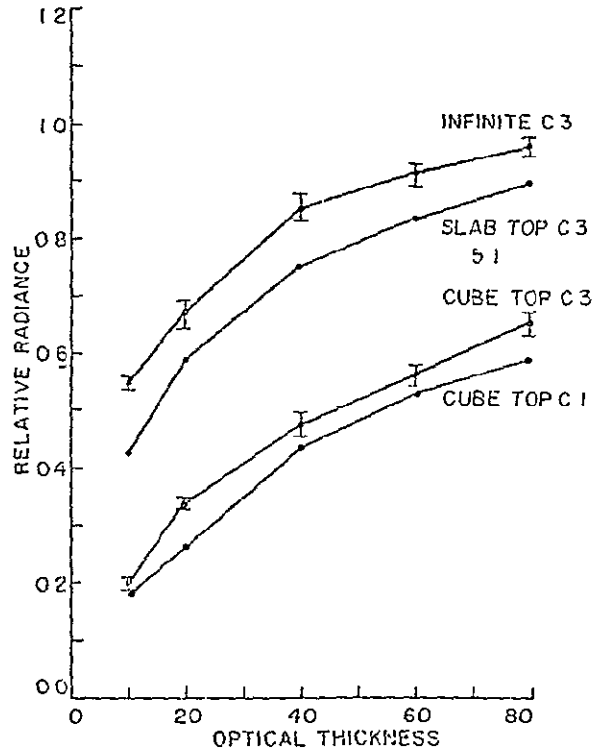

Fig 2. Model results showing small variation in relative radiance for C.1, C.3 drop size distributions over the optical depths shown Note also that a cloud slab having a width to depth ratio of 5·1 by optical depth 80 is very nearly equal in brightness to an infinite layer.

The accuracy of the relative radiance for a semi-infinite cloud and the top of a cubic cloud is indicated by error bars.

Fig. 2 shows the results from this computational study. The first test was to determine what effect the two drop size distributions would have on the reflected brightness for the top of a cubic cloud. To orient the reader, for a cloud having a C.2 particle distribution and a $\tau = 80$, its' vertical depth would be 1 5 km and have a liquid water content of 15 gm/m^3. The two curves show that over a wide range of optical depths, there appears to be a small effect due to phase functions which were determined from the drop size distributions This confirms the early work by Twomey, Jacobowitz and Howell that remotely sensing clouds in the mid-visible wavelengths for determining their microphysical structure seems unlikely.

The second study carried out was to determine the differences in reflectance between infinite and cubic clouds Fig. 2 indicates the relative radiance for the semi-infinite cloud is about 50% greater than for the top of the cube at optical depth of 80 The relative difference increases for smaller optical depths. The semi-infinite cloud is near a theoretical limit for optically thick clouds as the slope of the curve is nearing horizontal. The cubic clouds have a theoretical limit identical to the semi-infinite cloud but require a much larger optical thickness to approach this limit. Consequently, the cubic cloud would continue to get brighter for increasing optical thickness.

A third feature is indicated by calculating the relative radiance for a cloud with a width to depth ratio of 5 to 1 while maintaining a square top. Theory indicates the radiances are closer to the semi-infinite layer than to the cube. Observations illustrated in Fig 4 indicate a ratio of 10 to 1 needed to approach a maximum brightness. Real clouds do not have flat tops as is the condition of the cube. Irregular structure is likely to slow the transition to a semi-infinite layer, since small irregularities will retain characteristics of smaller clouds.

3. SATELLITE OBSERVED REFLECTED BRIGHTNESS

Digital SMS-2 VISSIR (Visible and Infrared Spin Scan Radiometer) data was obtained for August 6, 7, and 8th during the initial stages of convection over South Park, Colorado. The SMS-2 satellite was positioned at 115°W during this period giving it a nadir angle of the South Park area of 46° and 17° west of a due south view This gives SMS a ground resolution in this area of 1.2 km in the visible. The infrared sensor on board allowed cloud top temperature/heights to be determined for clouds with horizontal dimensions greater than 12 km. Thus only large clouds could be viewed For those clouds where heights could be determined, the maximum heights ranged to 1 5 to 2 km Fig. 3 is an SMS-2 view of the South Park region showing the range of cloud sizes observed on August 6 which was fairly typical of the clouds observed on the following two days although this day may have been a little more active. A comparison was first made of satellite measured visible radiance versus satellite derived cloud top temperature for co-located SMS visible - IR digital sectors. Nine separate sectors were compared for the three days, all within 1 hour of local noon. Approximately 250 data points per picture were correlated From this, correlation coefficients ranged from -.3 to -.65 These were fairly low correlations and seemed to show that visible radiance was not well related to top temperature/height. The relationship between visible radiance and cloud horizontal dimensions was also

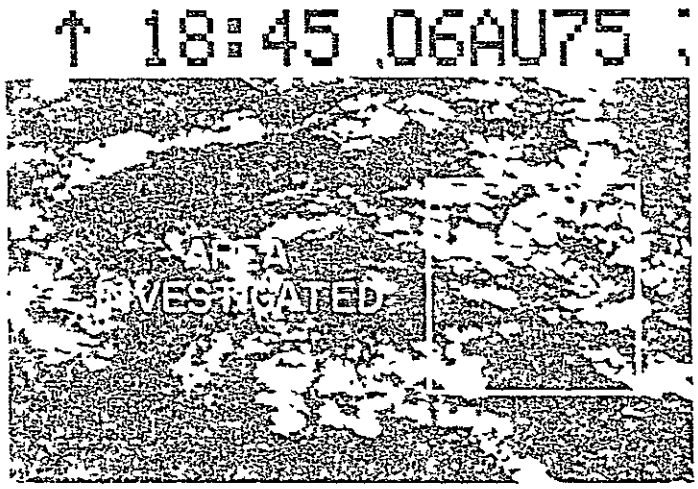

Fig. 3. SMS-2 .9 km visible image for 1845Z 6 August 1975. Area of interest is shown. Scale: 1mm = 6.2 km

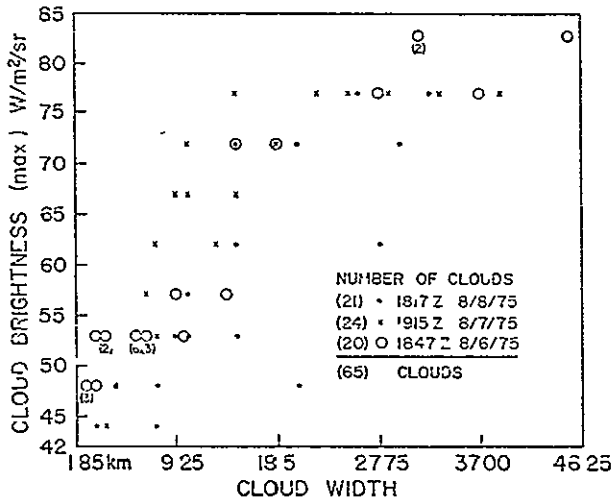

Fig. 4 Satellite derived maximum cloud brightness versus horizontal width for 65 clouds investigated during this three day period. Numbers under points represent multiple data points at this location

investigated Clouds were chosen from the three days at three different times around local noon and their horizontal dimension and maximum brightness were determined. Fig. 4 shows the results of this study which indicate that the brightness does not level off until the width approaches 20 km For clouds approaching the 2 km height the ratio of width to depth is 10 to 1. This is well past the 5 to 1 ratio suggested by McKee and Cox where the brightness changes should level off This curve may be demonstrating a lack in the model in its handling of the cloud top surface features. As was mentioned earlier, the model handles only flat tops of clouds, while we know that growing cumulus are distorted, rough turrets It is felt that due to this cloud top configuration, that a cloud may not approach the infinite stage until much further in its life cycle when the top begins to flatten and glaciate. We should add here that many of the larger clouds viewed were conglomerates of clouds spaced closer together than 1 2 km so were averaged by the sensor into a large cloud. There may be some interaction between the cloud sides that we see but this is assumed to be small compared to cloud top reflectance properties. Ranges of visible radiance measured for these clouds for the wavelength interval used agrees well with what theory predicts. The discrepancy occurs in the sizes of clouds over which this range should exist.

4. CONCLUSIONS

Several results have been obtained through looking at theoretical and observational cloud reflectance properties

1) Cannot remotely sense the microphysical structure and change taking place in cumulus clouds in the mid-visible spectral region for clouds greater than 1.5 km in depth.

2) Can predict that geometrical factors will strongly affect the cloud brightness and far outweigh microphysical changes but have not predicted these changes for clouds of width to depth ratios as large as that observed from satellites (10.1).

3) The theory used can predict the range of brightness that should be observed, but does specify the width to depth ratios in accord with observations.

4) Discrepencies from theory and observations may be due to theory not adequately representing the non-uniformity of the cloud top which we feel strongly controls the brightness observed from satellites.

Work is progressing on modifying this program to handle more of the shape factors involved with clouds as well as streamlining the computational scheme to reduce the noise problem It appears that some reflection is needed on previous work which has compared satellite brightness to cloud heights and rainfall rates and liquid water contents. We may better appreciate what these apparent brightness changes in observed clouds are actually telling us through both theoretical modeling and comparison from ground and aircraft observed cloud structure, as well as satellite observations.

5. REFERENCES

Busygin, V. P , N. A Yevstratov and Ye. M. Feygel'son (1973). Optical Properties of Cumulus Clouds and Radiant Fluxes for Cumulus Cloud Cover, Atmos. and Oceanic Physics, Vol. 9, No. 11, pp. 1142-1151.

Deirmendjian, D (1969) Electromagnetic Scattering on Spherical Polydispersion. The Rand Corp , Santa Monica, California, Published by American

Elsevier Publishing Co., Inc., New York, 290pp.

Griffith, C. G., and W. L. Woodley (1973): On the Variation with height of the top brightness of precipitating convective clouds. J. Appl. Meteor., 12, 1086-1089.

Griffith, C. G., W L. Woodley, S Browner, J. Teijero, M Maier, D. W. Martin, J. Stout, D. Sikdar (1976): Rainfall Estimation from Geosynchronous Satellite Imagery During the Daylight Hours. NOAA Tech. Rep. FRL 356-WMP07. U. S. Dept. of Commerce.

Hansen, J. E. (1969) Exact and Approximate Solutions for Multiple Scattering by Cloudy and Hazy Planetary Atmospheres J. Atmos. Sci., 26, No. 3, pp. 478-487.

McKee, T. B. and S. K. Cox, (1974): Scattering of Visible Radiation by Finite Clouds. J. Atmos. Sci., 31, No. 7, pp 1885-1892.

McKee, T. B. and S K. Cox (1975). Simulated Radiance Patterns for Finite Cubic Clouds. Submitted to J. Atmos. Sci.

Reynolds, D. W. and T. H. Vonder Haar, (1973): A Comparison of Radar Determined Cloud Height and Reflected Solar Radiance Measured from the Geosynchronous Satellite ATS-3. J. Appl. Meteor., 12, 1082-1084.

NOTES AND CORRESPONDENCE

Effects of Cloud Size and Cloud Particles on Satellite-Observed Reflected Brightness

DAVID W. REYNOLDS, THOMAS B MCKEE AND KELVIN S DANIELSON

Department of Atmospheric Science, Colorado State University, Fort Collins, Colo 80523

15 March 1977 and 30 August 1977

ABSTRACT

The relationship between a cumulus clouds' brightness, horizontal dimension and internal microphysical structure are investigated Cumulus clouds located over the South Park region of Colorado are observed by the SMS-2 satellite and their brightness and size are determined Aircraft observations were made in-cloud to obtain the drop size distributions and liquid water content (LWC) of the cloud A Monte Carlo cloud model is used to imitate the sun-satellite-cloud geometry in an effort to understand the role of cloud size and microphysical structure in affecting cloud brightness

Results show that for clouds of optical thickness between 20 and 60 (i e., LWC of 0 037 gm^{-3} and 0 11 gm^{-2} for a 2 km deep cloud), information about a cloud's LWC may be obtained through monitoring cloud brightness for clouds of uniform depth and variable width Theoretical results using this Monte Carlo method approximate very closely the relative brightness changes of clouds of the size and depth monitored by the SMS-2 satellite for these few days Theory and observation both conclude that a cloud having a width to depth ratio of approximately 10 1 (and constant optical thickness) is nearly reaching its maximum brightness Theory predicts that geometric factors affect cloud brightness more than microphysical changes.

It is also discussed that the previously reported work on the cloud height-cloud brightness relationship may indeed be seeing increasing brightness with increasing horizontal size changes (size being related to height) with finite small perturbations on top of the growing cloud slowing its approach to maximum brightness

1. Introduction

Modeling of the visible radiation scattered from semi-infinite to finite size clouds has been attempted for several years Hansen (1969) and Twomey *et al* (1967) found that for a plane-parallel atmosphere with semi-infinite clouds having optical thicknesses near 100 (cloud 1–1 5 km deep and having liquid water contents of 0 2 g m^{-3}) that these clouds are within 20% of their maximum brightness These results showed that remote sensing of clouds in the mid-visible wavelengths would be of little value for clouds of any real vertical extent, and it would be impossible to determine anything about the microphysical properties of the clouds However, observational measurements from satellites of convective clouds of significant vertical extent (≫2 km) have shown increasing brightness with increasing height (Griffith and Woodley, 1973, Reynolds and Vonder Haar, 1973) Recent work by Busygin *et al* (1973) and McKee and Cox (1974, 1976) has shown that the finite cloud poses a particular problem for monitoring its brightness due to energy passing through the vertical sides of the cloud Thus their reasoning for this observed brightness-height change is related to the fact that as the cloud grows it becomes wider as well as thicker, making side effects less important and allowing more light to be reflected off the top. To further understand cloud brightness changes, a small study was performed using measured satellite brightness data and comparing these to expected theoretical results

The South Park Area Cumulus Experiment (SPACE) collected microphysical data on cumulus clouds in South Park, Colo , during the summer of 1975 The data set included cloud drop size distributions made with an electrostatic disdrometer (Keily and Millen, 1960) mounted on the NCAR/NOAA *Explorer* sailplane This instrument measures cloud droplets from 4 to 16 μm in 1 5 μm increments and has a ninth channel for cloud droplets >19 μm Liquid water contents were simultaneously measured with a Johnson-Williams liquid water content meter mounted on the *Explorer*

Along with these data, digital SMS-2 (Synchronous Meteorological Satellite) visible (0 5–0 7 μm) (0 9 km resolution at SSP) data were received for this area

0022-4928/78/0160-0164S05 00

through the Direct Readout Ground Station at White Sands Missile Range. This allowed us to observe visible brightness of the clouds as well as estimate their top heights from the infrared readout using an appropriate temperature sounding.

A Monte Carlo cloud model for finite clouds developed by McKee and Cox (1974) was run using different distributions of drop sizes and numbers (Deirmendjian, 1969), while varying the cloud depth and width to determine how theory would predict what the satellite would view from its given location in space. Comparison of these results to the satellite observed reflectances will be presented in the following sections.

2. Model calculations

Fig. 1 graphically compares the two theoretical drop size distributions (C.1 and C 3) used in the numerical simulation of satellite measured visible brightness, with the average drop size distribution observed on 6–8 August of the 1975 SPACE field program. The specific values but not the shape of the depicted theoretical distributions are dependent on the liquid water content (LWC) of the clouds. C 1 and C 3 in Fig. 1 are adjusted to a LWC of 0.055 g m^{-3} which was the average observed LWC of the three days under study. The daily average LWC values ranged from 0.047 g m^{-3} on 8 August to 0.07 g m^{-3} on 7 August. This was lower then one might expect for cumulus clouds but we feel these numbers are representative.

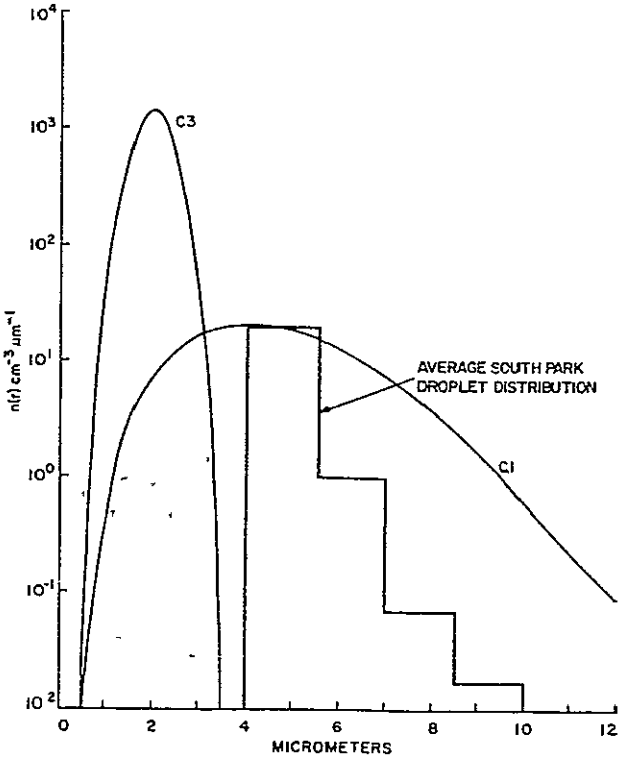

FIG. 1. Particle size and number distributions used for model input (Deirmendjian, 1969). Average South Park observed distributions for three case study days are also shown.

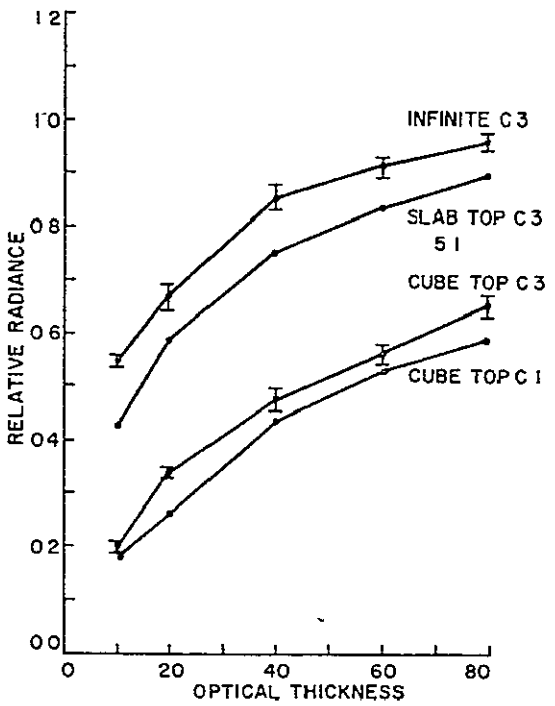

FIG. 2. Model results showing small variation in relative radiance for C 1 and C 3 drop size distributions over the optical thicknesses shown. Note also that a cloud slab having a width to depth ratio of 5 1 by optical thickness 80 is very nearly equal in brightness to an infinite layer.

The observed drop size distribution is also plotted on Fig. 1, primarily to allow a comparison of the shape of the observed distributions with the theoretical distributions utilized in the numerical simulation. The drop size distribution observed with the electrostatic disdrometer has several problems which are discussed by Dye (1976). One prominent difficulty is that the LWC integrated from the electrostatic disdrometer is typically half the LWC observed with a Johnson-Williams (J-W) liquid water content meter. The average LWC as observed by the J-W on 6–8 August was ~0.18 g m^{-3}. Second, the distributions are skewed toward smaller drops by the electrostatic disdrometer.

The observed distributions were measured along the *entire vertical extent of the clouds*. For the three days studied, the distributions were generally monomodal and showed good colloidal stability. The sailplane did observe ice particles in the clouds but ice particles are not considered in the calculations presented.

Evaluation of both theoretical distributions C 1 and C 3 were processed through the model because neither distribution exactly approximates the observed distribution and the sensitivity of the simulation may be sensitive to the shape of the distribution. The theoretical droplet distribution C 1 and C 3 and cor-

responding phase functions and volume scattering coefficients (at 0.7 μm wavelength) for a water cloud were obtained from Deirmendjian (1969). The phase function labeled C.1 is characterized by a very strong forwardscattering peak, while C.3 is not nearly as strongly peaked.

The relative radiance from the cloud top for the satellite geometry is shown in Fig. 2 for a cloud layer of specified thickness and of semi-infinite horizontal extent (C.3), a cloud with width 5 times the depth (C.3), and a cubic cloud with two different particle size distributions. Relative radiance is presented as a function of optical thickness defined by

$$\tau = -\int_0^s \beta ds, \qquad (1)$$

in which τ is optical thickness, s the distance and β the volume scattering coefficient. The volume scattering coefficient is determined by the drop size distribution and the liquid water content. For a given drop size distribution the scattering coefficient varies linearly with liquid water content. Consequently, the optical thickness varies with the three parameters of the drop size distribution, with liquid water content and with geometric distance. Accuracy of the computations depends on the number of photons processed through the computer program. The accuracy of the relative radiance for the semi-infinite cloud and the top of the cubic cloud are shown by error bars for one standard deviation. For reference, a cloud with a C.1 particle distribution, an optical thickness of 80 and a liquid water content of 0.15 g m^{-3} has a vertical depth of 2.0 km. The two curves for the cubic cloud indicate only a small change in relative radiance due to particle size distributions for a large range of optical thickness.

In contrast, the changes in relative radiance for the semi-infinite cloud is about 50% greater than for the top of the cube at an optical thickness of 80. The relative difference increases for smaller optical thickness. The semi-infinite cloud is approaching a theoretical limit for optically thick clouds as the slope of the curve is approaching zero. The cubic clouds have a theoretical limit identical to the semi-infinite cloud but require a much larger optical thickness to approach this limit. Consequently, the cubic cloud would continue to get brighter for increasing optical thickness.

Another feature of shape is indicated by calculating the relative radiance for a cloud with a width to depth ratio of 5:1 while maintaining a square top. Theory indicates the radiances are closer to the semi-infinite layer than to the cube.

3. Satellite observed reflected brightness

Digital SMS-2 VISSR (Visible and Infrared Spin Scan Radiometer) data were obtained for 6–8 August 1975 during the initial stages of convection over South Park, Colo. The SMS-2 satellite was positioned at 115°W during this period resulting in a satellite zenith angle for the South Park area of 46° and a relative azimuth angle of 17° west of a due south view. Since all observations were made within one hour of local noon a fixed solar zenith angle of 23° was used for model calculations along with the satellite viewing angles. The ground resolution of the SMS visible data in the South Park area is 1.2 km. The infrared sensor on board allowed cloud top temperature and heights to be determined for clouds with horizontal dimensions greater than 11 km. Thus only large clouds could be viewed in the IR. For those clouds where heights could be determined, the maximum heights ranged from 1.5 to 2 km above cloud base (cloud base determined by surface observations). Fig. 3 is an SMS-2 view of the South Park region showing the range of cloud sizes observed on 6 August which was fairly typical of the clouds observed on the following two days although this day may have been a little more active. A comparison was first made of satellite measured visible brightness versus satellite derived cloud top temperature for co-located SMS visible-IR digital sectors. Nine separate sectors were compared for the three days. Approximately 250 data points per section were correlated including some noncloudy regions. From these correlations the nine coefficients ranged from -0.3 to -0.65. These were fairly low correlations but for this sample size, still significant at the 1% level. Thus, although noisy, some relationship exists between visible brightness and cloud height. In an attempt to further explain this, we investigated the relationship between visible brightness and cloud horizontal dimensions. It is felt that as a cloud increases in height, it also increases in width with the width increase dominating the

FIG. 3. SMS-2 1.2 km resolution visible image for 1845 GMT 6 August 1975. The South Park area of Colorado and surrounding areas is shown in the outlined box. Scale: 1 mm = 6.2 km.

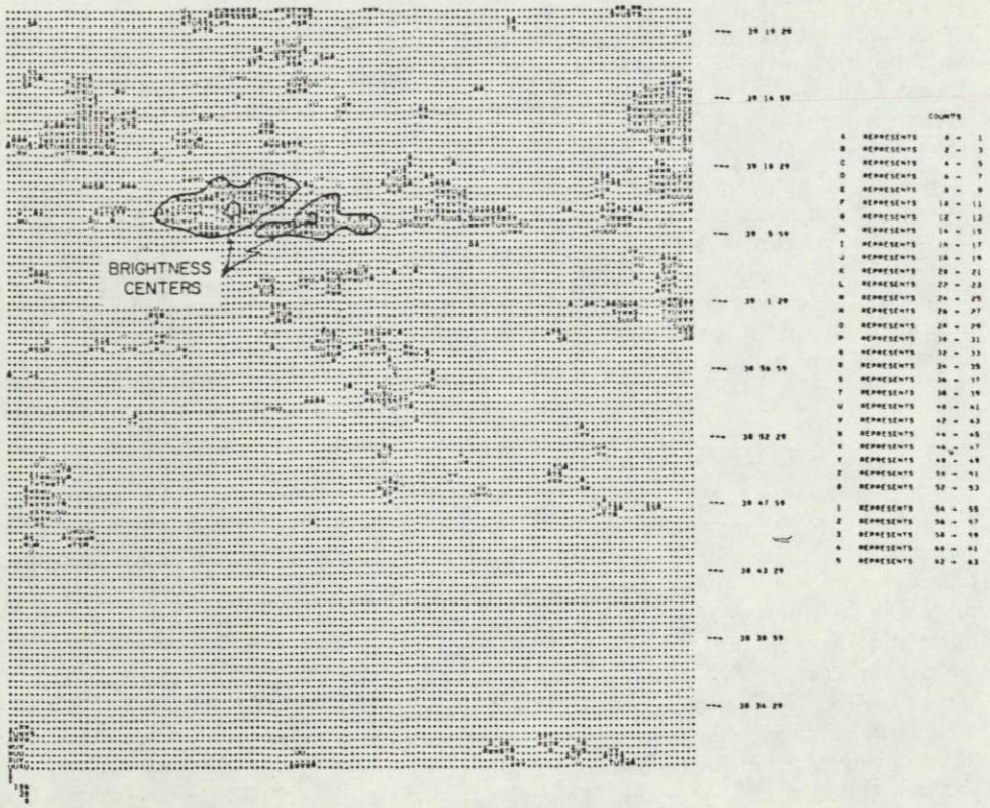

FIG. 4. Digital SMS-2 1.2 km resolution visible display of clouds over the South Park region of Colorado on 8 August at 1817 GMT. Using a thresholding technique only clouds are shown. The size and maximum brightness of the clouds chosen at random for this study were obtained off printouts such as this. Latitude in degrees, minutes, seconds is given on the right along with the character representation per count interval used.

brightness change. We hope to show this in the following results.

Clouds were chosen from the three days at three different times around local noon and their horizontal dimension and maximum brightness [here maximum brightness refers to the brightest pixel measured for each individual cloud as taken from the digital display (see Fig. 4)] were determined. Fig. 5 shows the results of this study which indicate that the brightness does not level off until the width approaches 20 km. For clouds approaching a height of 2 km, the ratio of width to depth is 10:1.

The solid lines in Fig. 5 are the theoretical relative radiances (brightnesses) from clouds with fixed thickness of 2 km and a variable width which ranges from a cube at width 2 km to a slab 40 km wide. Maximum radiance from theory has been scaled to coincide with the highest satellite maximum (count of 57) brightness so that relative changes could be compared with theory. (Note the convergence of the two lines at optical depth 40.) Two different liquid water contents are represented to illustrate the effect on cloud brightness. Optical thickness 60 is derived from a liquid water content of 0.11 g m^{-3} and optical thickness

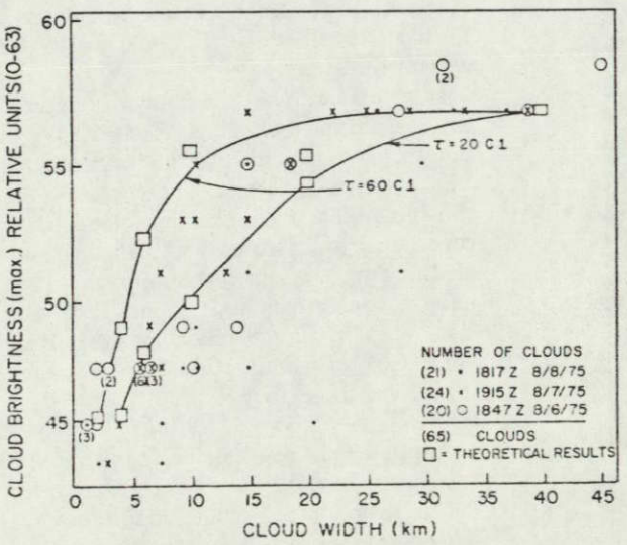

FIG. 5. Satellite derived maximum brightness versus horizontal width for 65 clouds investigated during the three-day period. Numbers under points represent multiple data points. Also shown are the theoretical results (for satellite geometry) using the C.1 distribution for a cloud of fixed depth (2 km) and variable width. The τ of 20 and 60 correspond to LWC's of 0.037 and 0.11 g m^{-3}, respectively.

20 from 0 037 g m^{-3} The theory predicts both the magnitude of the brightness change and the shape of the change rather well and indicates a sensitivity to the liquid water content The sensitivity to liquid water content is actually restricted to clouds with optical thickness $\lesssim 60$ Results of Fig. 5 indicate a distinct possibility of inferring liquid water content of cumulus clouds from satellite measurements. More work is needed to separate effects of particle size distribution and liquid water content on the scattered radiation.

4. Conclusions

Several results have been obtained through looking at theoretical and observational cloud reflectance properties·

1) For clouds of optical thickness between 20 and 60, information about a cloud's liquid water content may be obtained through monitoring cloud brightness changes for clouds of uniform depth and variable width. Beyond this point, geometrical factors dominate

2) Theoretical results using this Monte Carlo method approximate very closely the relative brightness changes of clouds of the size and depth monitored by the satellite for these few days.

3) Theory and observations both conclude that a cloud having a width to depth ratio of approximately 10 1 is nearly reaching its maximum brightness for a specified optical thickness

4) Theory predicts that *geometrical factors* will strongly affect the cloud brightness and far outweigh microphysical changes Thus, finite perturbations on top of a large cloud ($\gg$2 km in depth) may account for these types of clouds increasing in brightness past the theoretical limits shown here

Some initial work has been done in adding finite shapes onto semi-infinite clouds in the Monte Carlo program These show that the finite perturbations do decrease the rate at which a cloud will reach maximum brightness Thus theory lends evidence to our final conclusion that a cloud may continue to increase in brightness past previously indicated size limits if the top of the cloud has distorted finite shape factors, i e , growing cumulus clouds. As satellite resolution continues to increase, this finite cloud problem must be dealt with to a greater degree if satellite reflected brightnesses are to be interpreted correctly with respect to cloud heights, rainfall rates and liquid water contents A better appreciation of these apparent brightness changes in observed clouds will be revealed through both theoretical modeling and comparisons to ground, aircraft and satellite observations

Acknowledgments This work was sponsored by the Bureau of Reclamation under Contract 6-07-DR-20020, NASA under Contract NSG-5011 and NSF under Grant OCD75-13924. Computer time was made available through the National Center for Atmospheric Research which is supported by the National Science Foundation We would like to thank the Atmospheric Sciences Laboratory at White Sands Missile Range for allowing use of their Direct Readout Ground Station to obtain the digital satellite data. Thanks also to Mr. John Klehr for programming services.

REFERENCES

Busygin, V P , N. A Yevstratov and Ye. M. Feygel'son, 1973 Optical properties of cumulus clouds and radiant fluxes for cumulus cloud cover *Atmos Oceanic Phys* , 9, 1142–1151

Deirmendjian, D , 1969. *Electromagnetic Scattering on Spherical Polydispersion* American Elsevier, 290 pp

Dye, J E , 1975 Comparison of the electrostatic disdrometer with impactor slides *J Appl Meteor* , 15, 783–789

Griffith, C G , and W L Woodley, 1973 On the variation with height of the top brightness of precipitating convective clouds *J Appl Meteor* , 12, 1086–1089

Hansen, J E , 1969 Exact and approximate solutions for multiple scattering by cloudy and hazy planetary atmospheres *J Atmos Sci* , 26, 478–487

Keily, D P , and S G Millen, 1960 An airborne cloud-drop-size distribution meter *J Meteor* , 17, 349–356

McKee, T B , and S K Cox, 1974 Scattering of visible radiation by finite clouds *J Atmos Sci* , 31, 1885–1892.

——, and ——, 1976 Simulated radiance patterns for finite cubic clouds *J Atmos Sci* , 33, 2014–2020

Reynolds, D W , and T H Vonder Haar, 1973 A comparison of radar determined cloud height and reflected solar radiance measured from the geosynchronous satellite ATS-3 *J Appl Meteor* , 12 1082–1084

Twomey, S , H Jacobowitz and H B Howell, 1967 Light scattering by cloud layers *J Atmos Sci* , 24, 70–79.

INITIAL CONVECTION DURING SPACE[1], 1975

by
Daniel Breed

INTRODUCTION

The reason for locating a cloud physics experiment in South Park was that the early formation of small, isolated cumuli over the Mosquito Range and their subsequent growth and movement eastward over South Park created a natural laboratory for surface observations and aircraft operations. This study attempts to determine the time and location of initial convection ("first puff") in the South Park area using SMS-2 satellite photos for the 1975 season (July7-August 7). The formation of these cumuli are attributed to the differential heating of the mountains and to the adequate summer moisture supply in the park. Location of primary heat source areas are attempted, and one case study of thunderstorm organization and movement is presented as an introduction to various studies that are feasible using this data.

The data base for this study was SMS-2 visible photographs scanning a particular sector every half hour.[2] One mile resolution photos (one data point per square mile) for the KB8 sector (central North America) were available for the entire period and the visible pictures usually began by 14:45 GMT. For part of the period, one half mile resolution photos were used for

---

[1] South Park Area Cumulus Experiment

[2] There were a few SMS-1 pictures also.

more accurate location of first puffs when the scanned sector included South Park (e.g. 32N102W, printed as the last row of numbers on the upper right portion of the photo). Table 1 lists the days, times, and resolution of the available visible satellite photos that include the South Park area. A log book of field observations and first puff forecasts from the morning rawinsondes were used for verification and comparison of the satellite-determined initial times. The 07:00 MDT sounding was usually followed by an afternoon sounding between 12:00 and 14:00 MDT which would be useful in following the growth of these cumuli. Other data available for use with the satellite photos include cloud stereo-photography (terretrial photogrammetry), a doppler radar (with hail signal), a mesoscale network measuring pressure, temperature, relative humidity, and winds, and cloud physics aircraft penetrations. Development of precipitating cumuli, distinction between hail and non-hail convective systems, wind shear and flow fields are a few satellite projects that could use the surface observations as ground truth.

PROCEDURE

A. Set-up

The OD[3] was used to magnify the pictures so that visual analysis could be made more easily. The digitizer and computer were not used in this study, because the abundance of visual landmarks in South Park and the complications of setting up orientation overlays to account for the wobble of the SMS satellite justified the procedure of visual locations of first

DAYS	TIMES(GMT)	RESOLUTION
7/7	14:45-23:45	1 mile
7/8	14:45-23:45	1 mile
7/9	14:47-23:45	1 mile
"	20:45-21:15	½ mile
7/10	15:15-23:45	1 mile
7/11	14:45-23:45	1 mile
7/12	14:45-23:45	1 mile
7/13	14:45-23:45	1 mile
7/14	13:30-23:45	1 mile
"	13:30-00:00	½ mile
7/15	15:45-23:45	1 mile
"	13:00-23:30	½ mile
7/16	14:45-23:45	1 mile
"	17:30-23:31	½ mile
7/17	12:45,14:45-23:45	1 mile
7/18	14:45-23:45	1 mile
7/19	15:15-23:45	1 mile
7/20	14:45-23;45	1 mile
"	16:45-23;45	½ mile
7/21	14:45-23:45	1 mile
"	15:15-00:15	½ mile
7/22	14:45-23:45	1 mile
"	12:45,14:45-00:15	½ mile
7/23	14:45-23:45	1 mile
"	14:45-23:45	½ mile
7/24	14:46-23:45	1 mile
"	14:46-00:15	½ mile
7/25	14:00-23:45	1 mile
"	14:46-00:15	½ mile
7/26	14:45-23:45	1 mile
"	14:45-00:15	½ mile
7/27	15:15-23:45	1 mile
"	15:15-00:15	½ mile
7/28	14:45-23:45	1 mile
"	14:46-00:15	½ mile
7/29	13:30-23:45	1 mile
"	14:45-00:15	½ mile
7/30	14:46-23:15	1 mile
7/31	14:45-23:15	1 mile
8/1	—	1 mile
8/2	—	1 mile
8/3	14:45-23:15	1 mile
8/4	14:45-23:45	1 mile
8/5	14:46-23:45	1 mile
"	14:45-00:15	½ mile
8/6	15:15-21:45	1 mile
"	15:15-22:16	½ mile
8/7	14:45-21:46	1 mile
"	14:45-22:15	½ mile

TABLE 1

Available visible satellite photos that include South Park (1975).

Dave R is working with 8/1 and 8/2 -

puffs. The equipment could be used in determining cloud top brightness or other characteristics in a hail study. Extension tubes were tested to increase the magnification of the picture onto the TV screen. But, the contrast became so poor and the quality of the picture became so coarse that the trade-off between magnification and contrast resulted in the use of the camera lens with no extension tubes. The picture to be studied was put on the light table under the camera and flattened by the glass cover. It was then adjusted so that South Park was centered on the TV screen. The f-stop was adjusted for the best contrast and the focus was adjusted for the sharpest picture. This was the initial set-up for examining the satellite photos.

B. Initial Time

The time of the first puff was determined by examining the early morning photographs by eye or with a magnifying glass, and then choosing two pictures, one with the first visible convective element and one a half hour earlier. These two photos were examined on the OD-3, first checking to see if there was any trace of the cloud in the earlier one, and then using the photograph that contained the first visible cumulus to determine location. Accuracy of the initial cloud time is ± 15 minutes, using the average time of the two photos (no clouds and first puff). Also, since the resolution is ½ mile at best, this time would tend to be an overestimate because of the growth time necessary to develop a cumulus large enough to see on the satellite picture. There were a few days when high clouds and

mesoscale systems obscured the South Park area, and rough estimates were made when the first convective elements could be detected on the pictures.

C. Location

The first puff on any particular day was located as accurately as possible from surrounding landmarks. Mountain valleys, peaks, reservoirs, and ridges gave a gray scale contrast on the SMS-2 photos that was readily comparable to an ERTS composite photograph of Colorado. In order to locate the South Park area and orient the shapes of the landmarks as they change with the wobble of the satellite orbit, the ERTS photo and the SMS-2 photo with no clouds (and a clear shot at South Park) were kept handy for reference. Although detailed topographic maps of the area were available, the size of the National Forest maps worked best for the accuracy of this study.

The Arkansas River valley to the west of the Mosquito Range and the westernmost edge of South Park are separated by 10 miles at the narrowest part. About one fifth of that separation was detectable over another fifth. In low contrast areas, this detection limit would decrease to about one fourth. So, although the resolution was at least one mile, visual detection was limited to 2 to 2.5 miles. Allowing for other errors, a 3 mile grid (9 square miles) was set-up on a Pike National Forest map of the South Park area (Figure 1). A San Isabel National Forest map would have been useful as it includes the area west of the Mosquito Range, but it was not immediately available. Figure 2 shows the gridded area and some landmarks on a trace

from the ERTS photo.

The grids are numbered with four digits, the first two identifying the 15 rows (01 the northernmost, 15 the southernmost) and the last two identifying the 12 columns (01 the westernmost, 12 the easternmost). So, in Fig. 1, the bold number 5 would be in 0809, the bold 3 in 0409, and the bold 8 in 1112. (The bold numbers happen to be the locations of the mesoscale weather stations.) The locations of the initial cumulus clouds were identified using this grid.

RESULTS

Initial times and locations are assembled in Table 2 and the X's in Fig. 1 show the grid frequencies of the locations. The general comments in Table 2 describe other convective areas, areas of further or rapid development, the quality of the photos, and the days when the park was obscured or partially obscured by early clouds. If a line of clouds had formed, the brightest cloud was considered to be the first. Two or more grid locations on a single day indicate that there were two or more clouds of equal brightness on the examined photo. Although the west side of the park was of the most interest, there were times when convection was clearly dominant in the north or east areas. The comments should clarify the differing situations.

The morning sounding was used to predict the time of the first puff. A knowledge of the normal morning heating rate in South Park, a judgement of moisture adequacy, and a synoptic forecast were used to determine when the surface inversion would be broken and how fast and deep the clouds would grow.

TABLE 2 Time and location of first puffs (1975).

DATE	TIME(GMT)	GRID LOCATION	COMMENTS
7/7	16:00	0405	Cu line along Mos. Range, also Cu north Kenosha Range.
7/8	15:30	0804	Many landmarks obscured by early clouds
7/9	16:00	0303,0703	At 15:45 a Cu shows over 0201, cloudy over Leadville valley
7/10	15:00	0607	Partially obscured by early clouds so first convective element reported
7/11	14:30	not possible	Obscured by early clouds, convection starts on 14:45 photo
7/12	16:30	(0701,0801) (0504,0405)	Two convective elements reported, mostly obscured by early clouds, photo is fuzzy
7/13	15:30	0902	One cloud at 1504 on 14:45 photo that dissipates
7/14	15:15-15:30	0604	Missing 15:15 KB8 photo
7/15	15:15	0704	
7/16	16:00	0704	Some Cu north of Kenoshas at 15:45
7/17	14:30	0803	Partially obscured by early clouds, Cu form over Kenoshas at 15:15
7/18	15:00	0306	Possibly Cu on 14:45 photo but very light
7/19	15:30	0105,0903, 0703	Cu also over south Kenoshas and Tarryall Reservoir (0612)
7/20	case study day		early convection obscured by clouds
7/21	[15:00 15:30	0112] 1104	(of marginal interest) Over Mos. Range by 16:15
7/22	16:00	0506	Many early clouds, Cu also over Mos. Range by 16:15
7/23	14:30	0903	14:45 photo poor quality, 15:15 shows rapid development
7/24	15:00	1103,0811	A line develops just south of Kenoshas
7/25	15:30	1104	A couple less bright Cu near Sheep Mt.

TABLE 2 (con.)

DATE	TIME(GMT)	GRID LOCATION	COMMENTS
7/26	15:30	0712	16:15 shows rapid development in this area, and development beginning north of the park
7/27	16:30	1103	This is a lone cloud, none over park until 21:15
7/28	15:30	0504,0403	
7/29	15:00	0404	Cloudy over Leadville area, ~~cells beginning in far~~ southwest
7/30	15:00	0403	Cells beginning in far southwest
7/31	15:00	0605	Convection reigns by 16:45
8/1	not done		
8/2	not done		
8/3	20:30	1101(very faint)	Best convection is south of Buena Vista and over Kenoshas at 22:45
8/4	16:00	0502	Cu over Thirty-Nine Mile Mt. at 15:45, major cells develop far south end
8/5	17:30	0311,0110	Cu north of Kenosha Pass at 17:15, convection started at north end, over Mos. Range by 18:15
8/6	16:00	0407,0505	16:15 photo is fuzzy
8/7	16:00	0704	Two Cu just north of Copper Mt.

This was operationally important in determining 1) whether or not the day was an experimental day, 2) the best time for NCAR's sailplane to take-off, 3) the possibility of an early morning chaff drop for the doppler radar to follow, and 4) the time to start the photogrammetry cameras. Table 3 contains the first puff forecasts from the morning soundings, observations at the time of launch, and any additional comments from the daily log that were pertinent to this study. Satellite-determined times in MDT are included for comparison.

CONCLUSIONS AND DISCUSSION

At the beginning of this paper, differential heating was sited as a factor influencing convection during SPACE. These conclusions continue along that line. All but five days have initial convection along the eastern slopes of the Mosquito Range or southeast of the Continental Divide (northcentral to northwest border of South Park). It is obvious that the early morning sun strikes these areas first, causing an initial temperature difference to form between these slopes and the environment. This is also supported by the fact that convection was prevalent over the Kenosha Range on most days. This range has a northeast facing slope with no ridges to the east, therefore enhancing its ability to differentially heat since the sunrise was a little north of east during the period studied.

Grid 0703 is reported twice and grid 0704 is reported three times. This hot spot is characterized by the proximity

TABLE 3 Initial times and comments from radiosonde data (in MDT)

DATE	RAOB FORECAST	OBSERVATIONS	LOG BOOK COMMENTS	SAT. TIME
7/7	Not Available (N/A)		N/A	10:00
7/8	9:30, good moisture and instability	7:45, hazy, stratus over north mts.	N/A	9:30
7/9	10:00, very good instab.	7:15, clear, stratus	N/A	10:00
7/10	9:15, good moisture	7:05, fog on foothills hazy, low clouds	10:00, clouds popping all over park, still gen'l cloudiness	9:00
7/11	10:00, upper inversion	8:20, fair, cirrus and middle clouds	Cu deck til 10:30 14:30 small isolated Cu	8:30
7/12	9:30, low CCL	7:00, fair, scattered fog	8:00 low clouds 12:00 scattered Cu	10:30
7/13	9:00, two upper level inversions	7:10, fair and cold, some fog, Cu pancakus on mts.	Rain at 15:30	9:30
7/14	9:00	7:15, fair, clear	9:00 first small Cu	9:15-9:30
7/15	9:15	6:45, fair, some cirrus and cirrocumulus	10:50 Cu starting to close in on park	9:15
7/16	9:30, pretty unstable	7:55, some haze, cirrus, Cu pancakus	N/A	10:00
7/17	8:45, good instab. til inversion at 16K'	7:20, fair, cirrus, some Cu over west mts.	Convection not materializing thru 12:00	8:30
7/18	9:15	6:50, fair, clear, some Cu over mts.	15:00 fair wx Cu	9:00
7/19	8:45, upper inversion at 16.5K' (possibly unreported high clouds)	N/A	Clouds are small	9:30

TABLE 3 (con.)

DATE	RAOB FORECAST	OBSERVATIONS	LOG BOOK COMMENTS	SAT. TIME
7/20	9:45,not good instab. til 14.5 K'	7:10,fair, middle deck of Cu, cirrus	9:00 cameras on 11:00 small showers	----
7/21	10:00	6:35, fair,clear	9:00 cameras on	9:30
7/22	9:30	N/A	12:00 clouds of medium size	10:00
7/23	9:00, two upper inversions	6:35, fair,clear	N/A	8:30
7/24	9:15	6:35, fair,clear	11;00 sailplane up	9:00
7/25	9:45	6:50, fair,stratus	9:41 cameras on 10:30 good iso. Cu	9:30
7/26	9:45	N/A	no comments	9:30
7/27	10:15	6:45, fair,clear	"	10:30
7/28	10:00, good instab.	7:00, fair,stratoCu,Ci	"	9:30
7/29	9:45	7:00, stratoCu	no comments	9:00
7/30	radiosonde was late and puffs had already formed by 9:00			9:00
7/31	9:30	6:45, fair	sonde very stable	9:00
8/1	9:15	N/A	7:30 chaff drop picked up by Cu	----
8/2	9:00	N/A	sonde stable and dry 13:40 fair wx Cu	----
8/3	9:00	6:55, sunny,clear	N/A	14:30
8/4	9:15	8:30, balmy	time(?)-fair wx Cu	10:00

TABLE 3 (con.)

DATE	RAOB FORECASTS	OBSERVATIONS	LOG BOOK COMMENTS	SAT. TIME
8/5	9:15, good instability	6:50, fair,clear	AM very dry, few small Cu	11:30
8/6	9:15, two upper level inversions	7:00, fair, some cirroCu	12:00 sailplane up	10:00
8/7	9:00, capping inversion at 19 K'	N/A	8:20 first puff	10:00

of Sheep Mountain and the valley containing Four Mile Creek (site of the Mountain Met. course two summers ago). Another frequently sited location is the 1103, 1104 area (twice each). Buffalo Peaks are to the southwest, and Buffalo Meadows and Long Park surround this area. The area north of Fairplay is rather active also. Although there is no favored grid location, this part of the park is a broad sloping area up to Mt. Silverheels, Palmer Peak, and Little Baldy Mt. Also, there are many gulches that could act as pockets for moisture. The mechanism most probable for initial convection is the heating of the elevated surfaces to a higher temperature than the surrounding air causing convective currents. This heating breaks through the inversion more quickly being at a higher altitude. Also, some mixing must occur in the lower levels prior to the break, because the CCL of the morning sounding was consistently lower but always close to the true cloud base. The mixing does not have to be very intense, as lower levels with higher moisture content are close to these hot spots. Hence, convection occurs rapidly at these locations, transporting moisture effectively to create the first cumulus clouds in the South Park area.

Some personal observations follow that support these findings. The area southwest of Weston Pass appeared as a valley between the Buffalo Peaks and the Mosquito Range from the radar site (see Fig. 2). This was often the site of the first radar returns with the showers often moving northeast over the radar site. The three or so occasions when hail occured directly above the radar appeared to come from this region also. It is

interesting to note that the four locations where data was taken by the chase van (equipped for raindrop distribution measurements and electric field changes) were situated just downwind from these hot spots (e.g. 180°-270°). The chase van usually locates as close to the strongest echo as possible.

In summary, the first puffs appeared above slopes with the longest time of intense sunlight, and followed fairly closely the predicted times from the morning sounding. Also, it is evident that the strongest echo-producing cells may grow from these first puffs, or at least take advantage of these hot spots. While these results are not earth-shattering, many interesting studies could be done with the data presented. As an introduction along these lines, a descriptive case study of July 20th is presented.

CASE STUDY: JULY 20,1975

This day was chosen for many reasons. The first was the fact that initial convection could not be looked at on this day because of cloud cover, but the day looked too interesting to pass up. Secondly, half-mile resolution pictures that included South Park were available and of good quality. Another important reason was that initial cursory examination revealed some real intense storm cells developing during the day, and upon reviewing the radar log, the 20th turned out to be a day of many hail events.

The sequence of pictures to be discussed begins at 16:45 GMT and ends at 21:49 GMT. It appears that the Colorado-New Mexico

area is under some general dynamic lifting because of the frequency of thunderstorm activity. This is not immediately apparent from the 500 mb pattern. However the map does show light and variable winds in the South Park area, accounting for the variability of direction and of speed with which the reported storm cells move. Early storms are evident along the southern Colorado border and in southeastern Colorado, and convective cells have formed over the Breckenridge-Copper Mt. area. These cells organize and move eastward as a storm center. It loses definition during 18:15 and 18:45, but becomes well defined as an intense center in the 19:15 photo (19:15 is missing). It eventually organizes with a larger system to the north.

During this time, another strong cell develops in the southern Arkansas River valley near Salida. This one grows and moves northeasterly, organizing with a line of convective cells probably originating over the Collegiate Range. This line moves northeasterly over the Mosquito Range, and possibly organizes with the first storm between 18:45 and 19:45, making it so intense and well defined. General cloudiness and some small cumuli move in behind this system. However, the area around Buena Vista has been relatively clear for an hour or so, increasing the instability in that region. The small cumuli, upon moving over this area (19:45-20:15) grow rapidly as separate entities. By 20:45, some rather intense cells have developed, and continue to grow and organize to some extent by 21:49. Although South Park is obscured after this time, the

growth and extent of some of the cells over the park become very impressive. The radar data available on this day could serve as groung truth for investigating storm cells with a possible hail signature. (Note: Around 16:00-17:00 MDT, pea and marble sized hail accumulated in large amounts (drifts) at the radar site.)

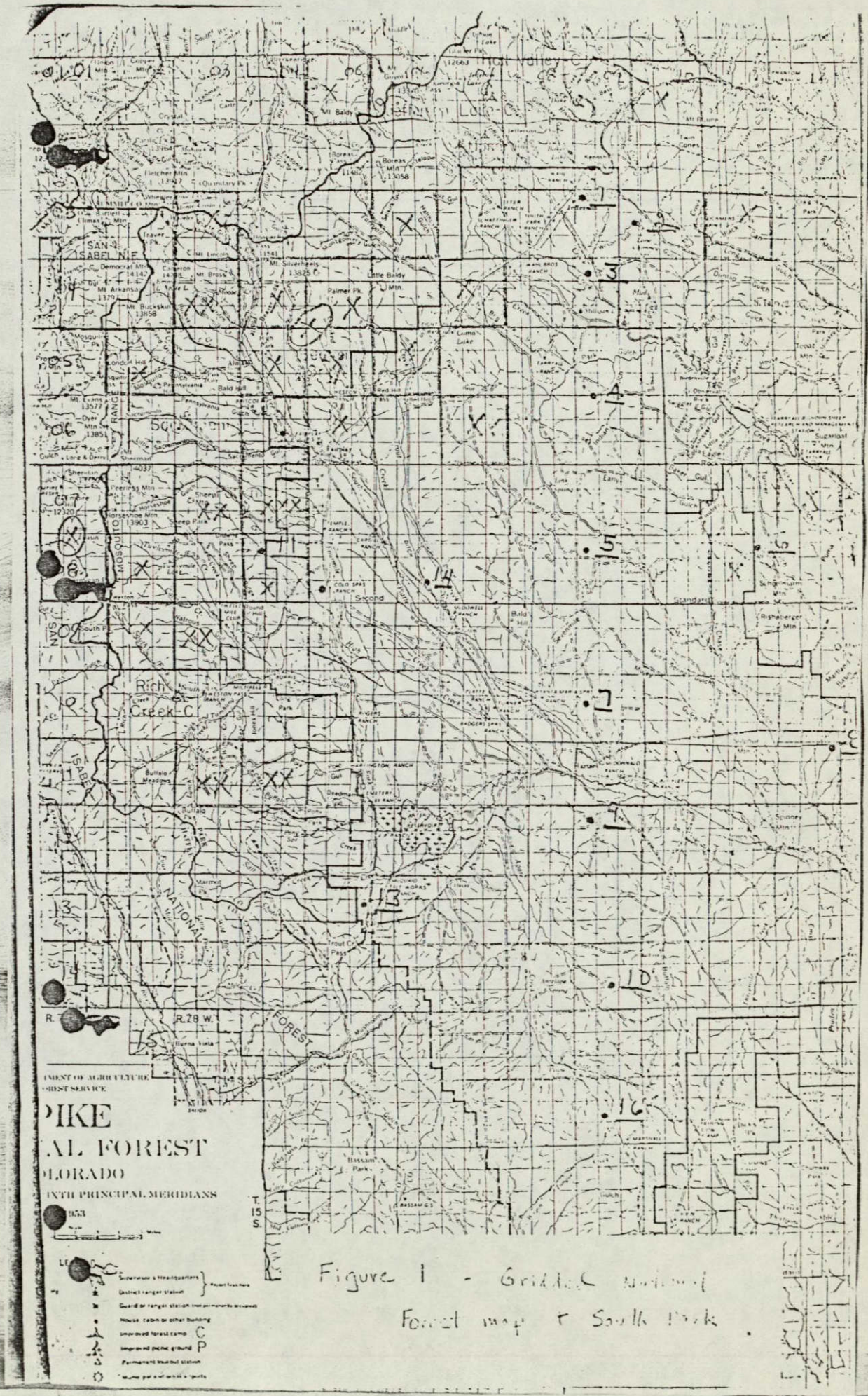

Figure 1 - Gridded National Forest map of South Park.

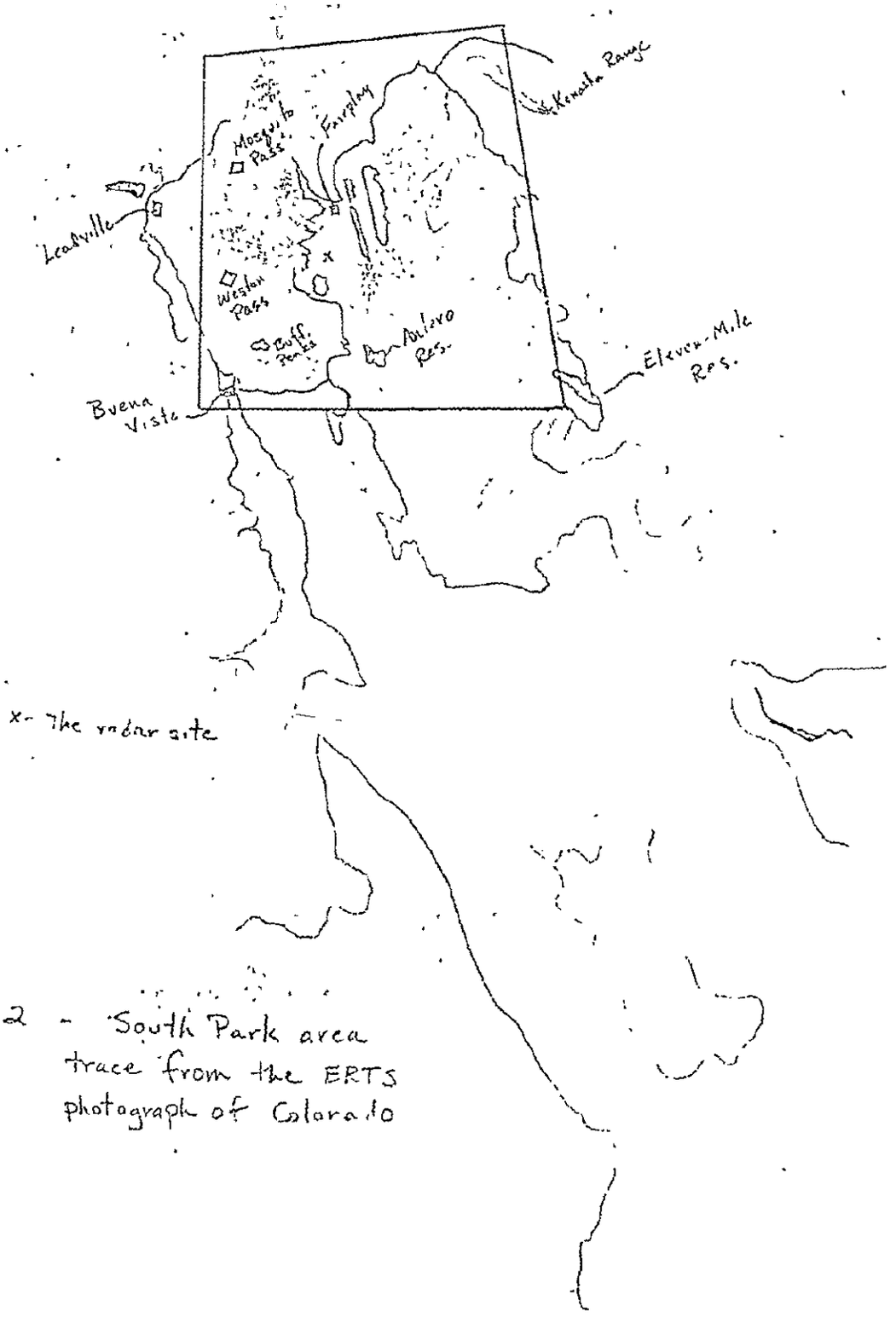

Figure 2 - South Park area trace from the ERTS photograph of Colorado

THE EVOLUTION OF CUMULONIMBUS SYSTEMS IN RELATION TO LOW-LEVEL THERMALLY-DRIVEN MESOSCALE SYSTEMS

William R. Cotton and Raymond L. George

Department of Atmospheric Science
Colorado State University
Fort Collins, Colorado

Roger A. Pielke

Department of Environmental Sciences
University of Virginia
Charlottesville, Virginia

1. INTRODUCTION

The importance of extra-storm scale mesoscale systems to the genesis and propagation of cumulonimbus systems is only recently becoming fully appreciated. A number of workers (Malkus and Riehl, 1964, Matsumoto et al, 1967; Lavoie, 1972; and Bhumralkar, 1973) have found that cumulus activity is strongly correlated with mesoscale and synoptic scale convergence zones. Chang and Orville (1973) found that a two-dimensional cumulus model responded much more vigorously and penetrated to a considerable depth when large-scale convergence was imposed on the boundary of the cumulus model. Furthermore, Cotton, Pielke, and Gannon (1976) showed that a one-dimensional time-dependent cumulus model developed a significantly deeper, longer lasting cloud when the initial sounding was replaced by theoretical soundings predicted with the Pielke (1974) mesoscale model in the vicinity of observed cumulus models.

In addition, Cotton et al (1976) found the sea breeze mesoscale system modified the cumulus scale environment by:

1. Increasing the depth of the planetary boundary layer.
2. Inducing larger surface fluxes of momentum, heat, and moisture.
3. Changing the vertical shear of the horizontal wind in lower levels of the atmosphere.
4. Developing intense, horizontal convergence regions of heat, moisture, momentum, and cloud material.

2. INTERPRETATION OF FLORIDA MODELING AND OBSERVATIONAL EXPERIMENT

Still, the primary role of extra-storm scale mesoscale systems is often viewed simply as an initiator of cumulonimbus convection. Once such systems form, they so perturb the planetary boundary layer by means of intense penetrating downdrafts, that the extra-storm scale mesoscale convergence fields are no longer of prime importance. Recently, Pielke (1974) developed a fully three-dimensional mesoscale model of the Florida sea breeze circulation. The sea breeze was initiated and evolved in response to the boundary layer fluxes of heat and momentum and interacted with the large scale flow. The effects of deep, precipitating cumuli and cumulonimbi on the mesoscale circulation were not considered in the simulation. In spite of this neglect, Pielke found that on synoptically undisturbed days with generally weak flow through the depth of the troposphere, the predicted patterns of convergence agreed favorably with the observed locations of clouds and showers throughout an extensive portion of the day. Contrary to the generally accepted view point mentioned above, the agreement between the locations of predicted convergence zones and locations of echo patterns of extensive thunderstorm complexes improved as the day progressed. Figure 1 illustrates such a correspondence.

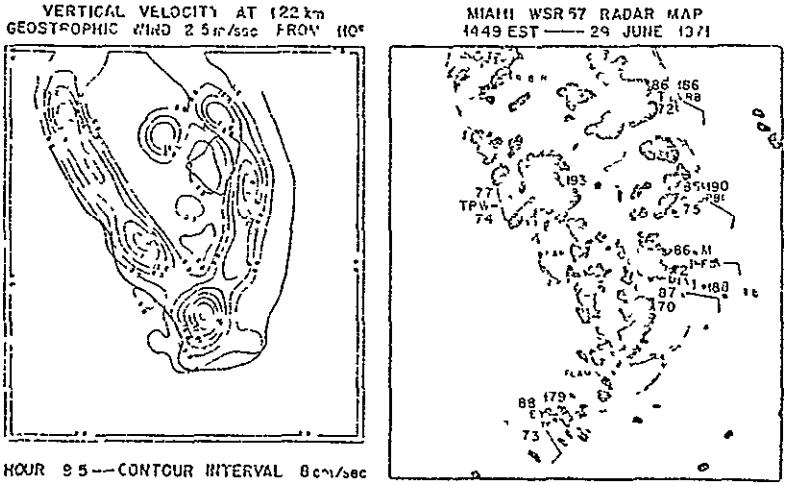

Fig. 1. The model predicted vertical motion field at 1.22 km and the radar echo map at equivalent times for 29 June, 1971.

The interpretation of this result is as follows. Individual cumulus congestus and cumulonimbus clouds can be initiated by small-scale moisture anomalies not necessarily well-defined by a mesoscale model. Once initiated, a cell may survive and propagate by virtue of penetrating downdrafts for periods of 45 minutes to 1 1/2 hours. A complex of cumulonimbus systems, on the other hand, processes so much moisture that they cannot survive for an extensive period (one to three hours) without the enrichment of moisture convergence by extra-storm scale mesoscale systems. This interpretation has been corroborated by the analysis of several case studies, one of which has recently been reported by Cotton and Pielke (1976a,b). In this study, they found that the general complexes of cumulonimbi evolved and migrated across the Florida peninsula in response to the lower tropospheric winds similar to the predictions of the Pielke model. Individual cumulonimbus cells, on the other hand, were observed to propagate in response to deep tropospheric winds 50 to 75 km away from the main centroid of cumulonimbus complexes. In addition, the magnitude of the ratio of eddy transport of moisture at cloud base to the 11 km mean moisture transport was found to be on the order of 2 to 6%. At the same time, it was found that the ratio of eddy kinetic energy to mean kinetic energy ranged from a high of 1700 in the vicinity of cumulus congestus and isolated cumulonimbi to a low of one below extensive cumulonimbus complexes. It is thus seen that thermal scale and cumulonimbus scale eddies make substantial contributions to the kinetic energy budget of the subcloud layer, while the cloud base moisture fluxes are dominated by mesoscale eddies.

3. OBSERVATIONAL AND THEORETICAL STUDIES OF THE COLORADO RIDGE-VALLEY CIRCULATION

We are now in the process of determining whether or now our conclusions from the study of the Florida sea breeze can be generalized to other thermally-driven mesoscale circulations such as the ridge-valley circulation which forms over the Colorado Rockies. As in the case of the sea breeze circulation, the idealized two-dimensional solenoidal field set up by elevated heat sources is fairly well understood. Using a two-dimensional vorticity model, Danks (1969) showed that a prevailing flow with vertical shear produced a pronounced tilt to the circulation cell above the slope so that part of the cell appeared to break off and form a much larger circulation cell out over the plains. Figure 2 illustrates such a circulation cell. In addition, a simulation of the onset of the noctural regime demonstrated a strong enhancement of vertical motion over the plains as the downslope flow carried the upper level westerly momentum downward and outward into the plains. This is shown in Fig. 3.

As we have found in the simulation of the Florida sea breeze, the actual three-dimensional flow is considerably more complex. This is particularly true of the mountain-induced mesoscale flow where the complex topography illustrated in Fig. 4 can initiate intense dynamic interactions with the prevailing

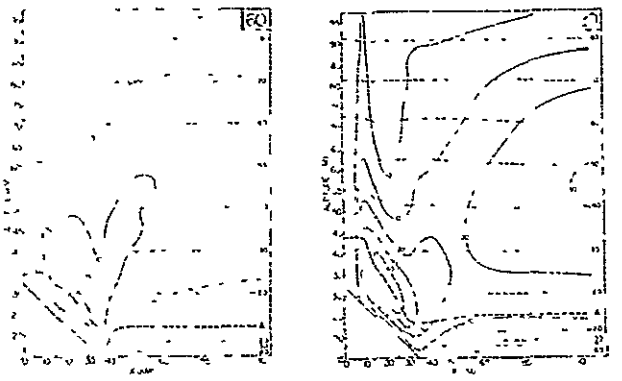

Fig. 2. Evolution of the deviation stream function (solid lines in 10^2 m^2 sec^{-1}) and potential temperature deviation (dashed lines in C deg) fields for Case D. Top of superadiabatic region is shown by heavy dashed line (A).

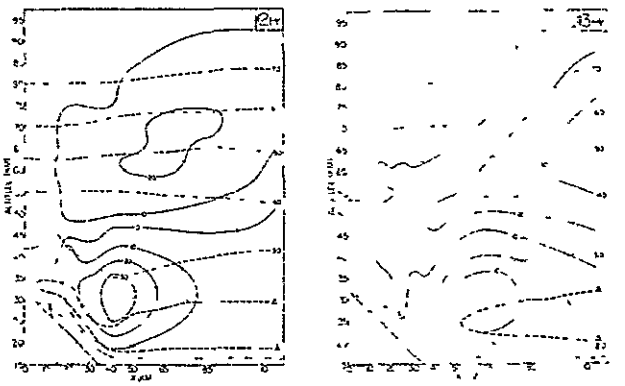

Fig. 3. Evolution of the deviation stream function (solid lines in 10^2 m^2 sec^{-1}) and potential temperature deviation (dashed lines in C deg) fields for Case E. Time is in hours past start of diurnal sine wave.

flow aloft as well as complicated patterns of elevated heating which can drive the upslope flow. To study the spatially and temporally varying pattern of surface temperature, cross sections of surface temperature were measured from aircraft with a Barnes PRT-5 IR radiometer. Figure 5 illustrates an east to west cross section observed at 0900 LST on August 2, 1975, from a point nearly half way between Denver and Colorado Springs, Colorado, over the plains, westward to Leadville, Colorado. The data have been averaged over 11 km intervals and the variance with respect to such an average is shown in Fig. 5c. Not surprisingly, the regions of contrast between the plains and foothills, and mountains and plateau are the regions of maximum temperature variance. What is most surprising, however, is that the South Park elevated plateau heats up considerably faster than any of the surrounding eastward facing slopes or the plains to the east. The magnitude of the difference in temperature between the plateau and the plains to the east reaches its maximum between 0900 and 1100 MST with values greater than 10°C. While the exact reason for the differences in response to solar heating of the relatively horizontal surfaces is not fully understood, it appears to be largely a

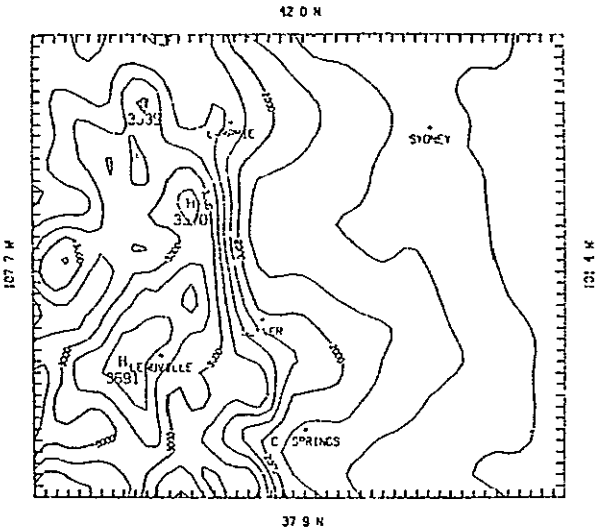

Fig. 4. Smoothed topography (2 and 4Δx trends removed for a 11 km grid) used as input in the Pielke mesoscale model. (contour interval 250 m)

function of differences in thermal inertia of the soil types. The importance of such a temperature difference is even more striking when one realizes that the plateau represents a large-area elevated heat source some 2600 to 4000 feet above the surrounding plains. Thus, it would appear to be a major driving force in the mountain upslope flow.

Another characteristic of the pattern of elevated heating is that the plains to the east rapidly catch up to the elevated plateau exhibiting a surface temperature comparible to the plateau. Shortly after local noon the plateau begins to cool, partly in response to extensive developing cloud cover and precipitation along the higher mountains to the west and partly due to the lower thermal inertia of the plateau soil. During the same period, the plains to the east continue to warm, finally reaching their maximum surface temperature around 1400 LST. Associated with the cooling of the upper level plateau is a reversal in flow from a generally easterly upslope to a prevailing westerly current. The impact of this pattern of elevated heating and associated flow reversal on the genesis of cumulonimbus systems over the western plains will be analyzed by combined numerical experiment with the Pielke model and satellite and radar data analysis.

The SMS-2 satellite photograph at 2145 GMT (1445 LST) illustrated in Fig. 6 shows the extensive cloud cover which shrouds the higher elevations, as well as two preferred regions of convective activity over the western great plains. The regions of cumulonimbus activity are generally located over the Cheyenne ridge to the north and the Palmer ridge to the south. Also of possible importance is the fact that both ridges lie to the east of major plateaus, namely South Park and North Park.

4. SUMMARY AND CONCLUSIONS

It is clear that thermally driven mesoscale systems such as the Florida sea breeze and Colorado ridge/valley circulations play an important role in the genesis, organization and

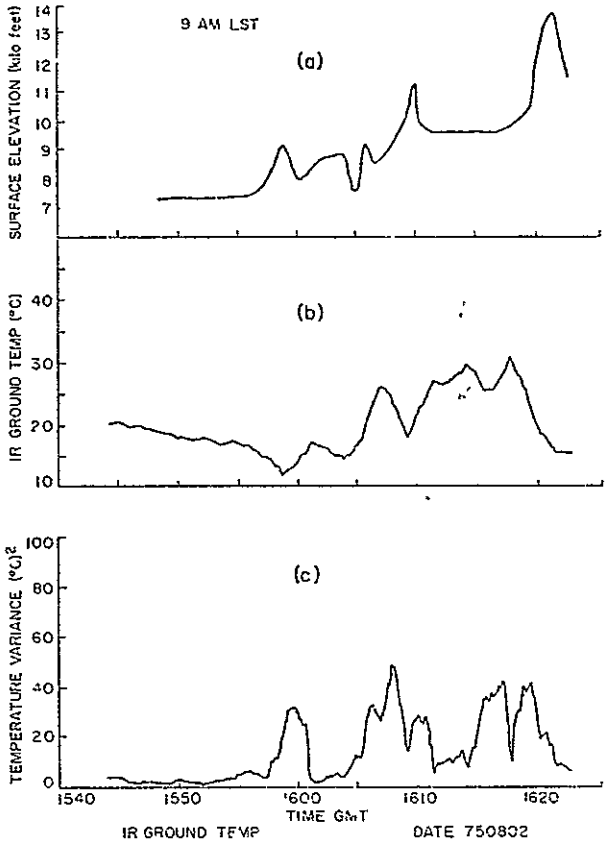

Fig. 5. East-west cross section of IR surface temperature observed at 0900 LST on August 2, 1975. Top represents smoothed elevation of topography. Middle represents 11 km average surface temperature. Bottom represents variance with respect to 11 km smoothed surface temperature.

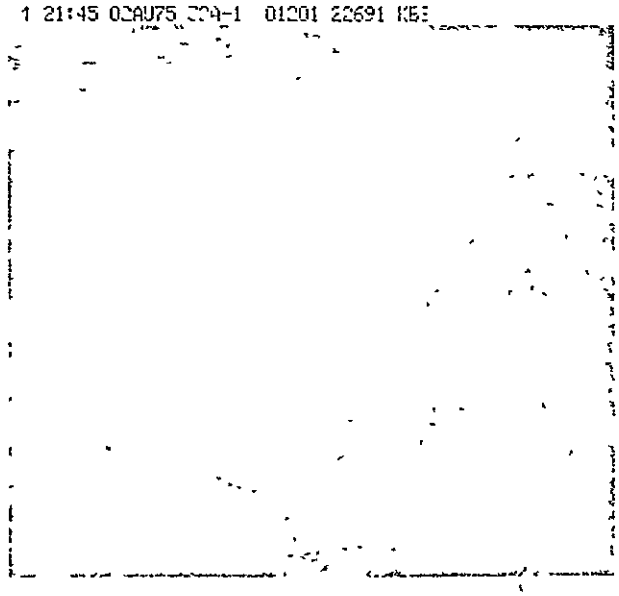

Fig. 6. SMS-2 satellite photograph at 2145 GMT (1445 LST) with 1.85 km resolution.

intensity of cumulonimbus systems. In the case of the Colorado ridge/valley circulation, however, the importance of the circulation to the genesis and propagation of severe storm systems over the western great plains still remains to be demonstrated. The emphasis in the oral presentation will be on the evidence indicating the role of such a circulation in the genesis and propagation of hail producing storms.

5. ACKNOWLEDGEMENTS

A portion of this research was done while Drs. Cotton and Pielke were associated with the Experimental Meteorology Laboratory, NOAA, Coral Gables, Florida. This work was partially supported by National Science Foundation Grants GA-43040X, DES75-17313, and National Aeronautics and Space Administration Grant NSG-5011.

6. REFERENCES

Bhumralkar, C. M., 1973: An observational and theoretical study of atmospheric flow over a heated island. Mon. Wea. Rev., 2, 101, 731-745.

Chang, S., and H. D. Orville, 1973: Large-scale convergence in a numerical cloud model. J. Atmos. Sci., 30, 947-950.

Cotton, W. R., R. A. Pielke, and P. T. Cannon, 1976: Numerical experiments on the influence of the mesoscale circulation on the cumulus scale. J. Atmos. Sci., 33, 2, 252-261.

Cotton, W. R., and R. A. Pielke, 1976a: One day in the life of the Florida sea breeze, Part I: Analysis of mesoscale and synoptic scale observations. Submitted for publication, J. Atmos. Sci.

Cotton, W. R., and R. A. Pielke, 1976b: One day in the life of the Florida sea breeze, Part II: Analysis of sub-cloud fluxes and turbulence spectra. Submitted for publication, J. Atmos. Sci.

Dirks, R. A., 1969: A theoretical investigation of convective patterns in the lee of the Colorado Rockies. Atmospheric Science Paper No. 145, Department of Atmospheric Science, Colorado State University, Fort Collins, Colorado, 122 pp.

Lavoie, R. L., 1972: A mesoscale numerical model of lake-effect storms. J. Atmos. Sci., 1025-1040.

Malkus, J. S., and H. Riehl, 1964: Cloud structure and distributions over the tropical Pacific Ocean. Tellus, 16, 275-287.

Matsumoto, S., K. Nonomiya, and T. Akiyama, 1967: Cumulus activities in relation to the mesoscale convergence field. J. Meteor. Soc. of Japan, Ser. 2, 45, 292-305.

Pielke, R. A., 1974: A three-dimensional numerical model of the sea breezes over South Florida. Mon. Wea. Rev., 102, 115-139.

THE CHARACTERISTICS OF EVOLVING MESOSCALE SYSTEMS OVER MOUNTAINOUS TERRAIN AS REVEALED BY RADAR AND PAM

Raymond L. George and William R. Cotton

Colorado State University
Department of Atmospheric Science
Fort Collins, Colorado 80523

1.0 INTRODUCTION

The 1977 Colorado State University (CSU) South Park Area Cumulus Experiment (SPACE) was a comprehensive summertime field project designed to investigate the structure and evolution of cumulus clouds and convective mesoscale systems over mountainous terrain. Most field measurements were taken in South Park, Colorado, a flat mountain park measuring about 100 km north-south and 50 km east-west, with a mean elevation of 2.8 km MSL. Located about 150 km southwest of Denver, South Park is a natural genesis area for cumulus clouds, with the 4000 – m MSL Mosquito Range directly to the west and smaller ranges on the southwest, northwest, and northeast edges. Within the park, intensive measurements were taken from 10 July 1977 to 13 August 1977, using powered aircraft, the NCAR sailplane, rawinsondes, boundary layer profilers, acoustic sounders, micrometeorological towers, lidar, search radar, triple-Doppler radar, and a square grid of surface meteorological stations, placed at 10 km intervals. In cooperation with the Bureau of Reclamation High Plains Experiment (HIPLEX), an extended area from South Park east to Goodland, Kansas was also covered using search radar, satellite, rawinsondes, and surface meteorological stations. Figure 1 shows the locations of search radars, rawinsonde units, and surface meteorological stations that were used in the combined SPACE/HIPLEX experiment, along with averaged 1000 foot (304.8 m) terrain contours.

The presence of the Rocky Mountains, foothills and South Park immediately west of the Colorado High Plains creates an interesting set of mesoscale-dynamic and thermodynamic influences on the convective precipitation process. The initiation of small cumulus occurs earliest in the day over the Mosquito Range and other high peaks and ridges. This is due to the nighttime drainage of cool, stable air off the slopes, so that the morning solar heating causes the planetary boundary layer (PBL) to deepen to cloud base much more quickly (often by 1000 MDT in South Park) than over the plains to the east which receive the cool drainage air. Strong solar heating on east-facing slopes generates an upslope flow in the lowest layers, creating convergence of mass and moisture above east-facing mountains and ridges. Dirks' (1969) two-dimensional vorticity model over a heated east slope indicated that upper return flow from this upslope circulation would create a zone of subsidence 50 – 100 km east of the mountains, over an area where observed summertime rainfall is in fact less than in either the mountains to the west or the plains to the east.

Thunderstorm activity is also observed to occur earliest near east-facing slopes. Henz (1974) used data from the National Weather Service (NWS) 10 cm search radar (WSR-57) at Limon, Colorado, to show that preferred regions of echo genesis are found near the east-facing slopes of the front range. Cumulonimbus cells from these 'hot spots" often propagate eastward, providing much of the summertime precipitation which falls on the nearby plains. Hourly rainfall data show an eastward shift of the time of maximum precipitation, beginning in the afternoon in the Front Range, midnight in western Kansas, and early morning in eastern Kansas. This supports the hypothesis that early "hot spot" convection is responsible for the formation of or participation in a dynamic meso-wave which propagates eastward.

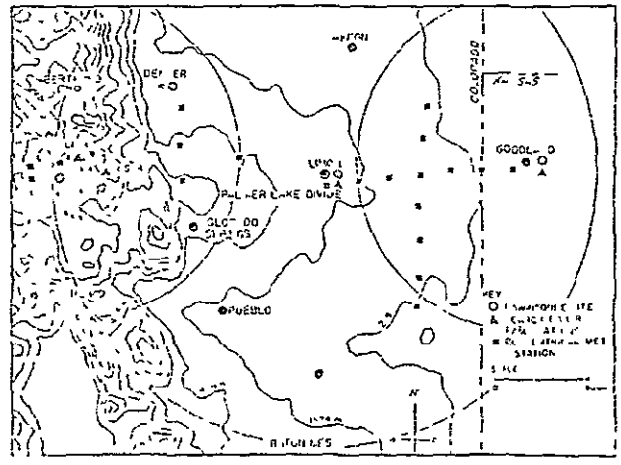

Figure 1 Map of the SPACE/HIPLEX extended coverage area, with computer averaged terrain contours every 1000 feet (304.8 m). The large circles represent radar effective coverage areas.

July 19, 1977 was chosen as the first case for intensive analysis. On this day, strong cumulonimbus cells formed in South Park as well as other parts of the Colorado Rockies and in the plains just east of the foothills, while all convection was suppressed east of Limon, Colorado. Cells tended to move northward with the mean flow, thus not initiating or participating in any kind of eastward-moving mesoscale disturbance. A contrasting case study day is 4 August 1977, in which a strong squall line with high precipitation formed in the eastern part of South Park and propagated eastward through Kansas and Missouri. We will concentrate on the analysis of 19 July 1977 in the written presentation given here. Our oral presentation will include a comparative analysis of these two days.

2. RADAR AND SURFACE EQUIPMENT

The National Center for Atmospheric Research Field Observing Facility (NCAR/FOF) provided the Portable Automatic Mesonet (PAM) and the CP-3 5.5 cm Doppler radar. PAM provided one minute averaged winds, wet and dry bulb temperatures, pressure, and rainfall at 20 locations, shown in Figure 2. Note that three of the locations were at the crest of the Mosquito Range at elevations of over 3.8 km MSL. Data were telemetered to a central site, where they were immediately available for display and were also stored on tape (Cotton and George, 1978).

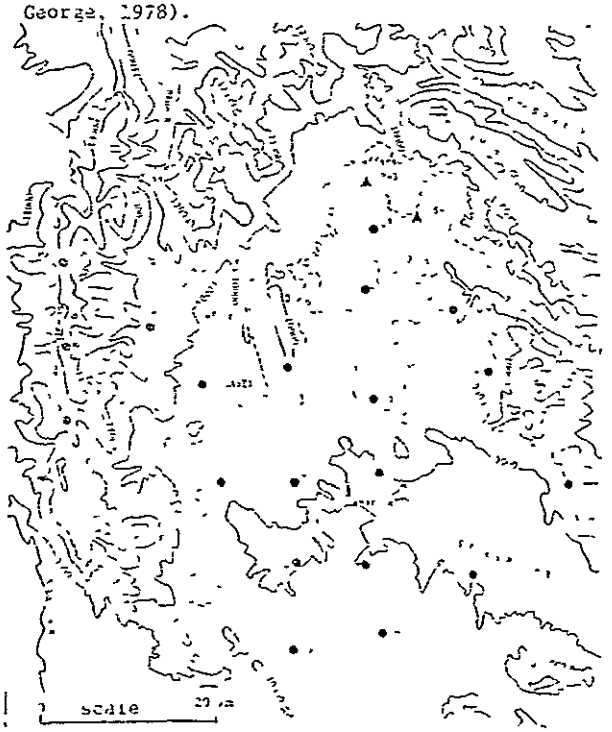

Figure 2 Map of South Park, showing the PAM/CP-3 local coverage area. Figures 3-15 have exactly the same scale and coverage as this map. Actual terrain contours are shown, with solid contours being even 1000's of feet (304.8 m), dashed contours 500's of feet (152.4 m).

Although originally installed for triple Doppler use, the CP-3 radar doubled as a search radar before 1 August 1977, when the CSU FPS-18, 10 cm search radar, came into service. CP-3 would periodically interrupt its Doppler scans to perform full volume scans. CP-3 data for 19 July 1977 are extremely detailed and complete, and of very high quality.

3.0 LARGE SCALE ANALYSIS FOR THE MORNING OF 19 JULY 1977

At 1200 GMT (0600 MDT) on 19 July 1977, a vast subtropical high dominated the weather from the Eastern U. S. west to Colorado. At 500 mb, a branch of this high was centered in eastern Kansas, with resultant southerly flow bringing hot, dry desert air over eastern Colorado. In Wyoming and northwestern Colorado, a baroclinic zone provided southwesterly winds which advected deep Pacific moisture into the Rockies during the day. A weak shortwave in this zone turned the Grand Junction, Colorado 500 mb winds to 260°. Good 500 mb moisture extended from Grand Junction through Wyoming to South Dakota. On the surface, a low was centered in South Dakota, with a surface trough extending southward to cover eastern Colorado. Figure 3 is a surface analysis for 0600 MDT, showing the low pressure trough and associated light winds in eastern Colorado, with stronger winds at the south and east edges of the trough.

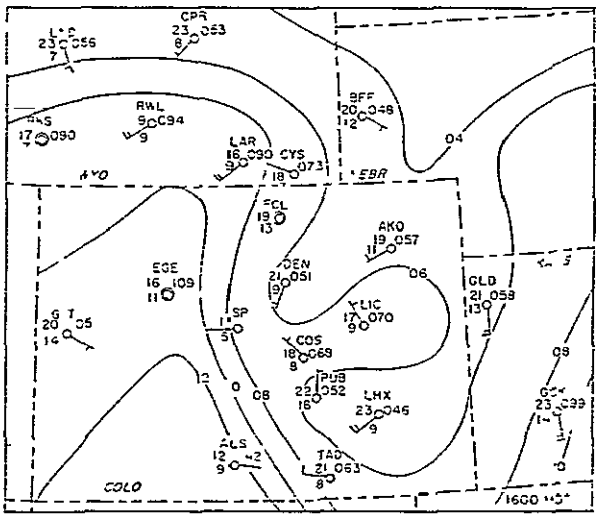

Figure 3. Surface analysis for 0600 MDT (1200 GMT), 19 July 1977, from NWS hourly reports. Pressure contour interval is 2 mb.

An east-west cross-section of 1200 GMT (0600 MDT) rawinsondes is shown in Figure 4. The cross-section extended for 680 km and includes rawinsondes from Grand Junction, South Park and Limon, Colorado, and Goodland, Kansas. Potential temperature θ (°K) and specific humidity q_v (gm kg^{-1}) are contoured, and winds are shown at 40 mb intervals. Both Limon and Goodland had deep dry-adiabatic layers, with low values of q_v (5gm kg^{-1}). This is the result of several days of strong heating with little horizontal moisture

advection or moist convection. The Grand Junction sounding showed the presence of deep Pacific moisture and the effects of deep cumulonimbus activity which occured the previous day and night (as revealed by satellite photographs). Winds in the lowest 80 mb were north or north-easterly at both South Park and Limon, showing the effects of the surface trough over eastern Colorado. Moisture at the 350 mb level over South Park defined the location of a cirrus deck which covered the eastern slopes of the Rockies early in the morning and subsequently dissipated.

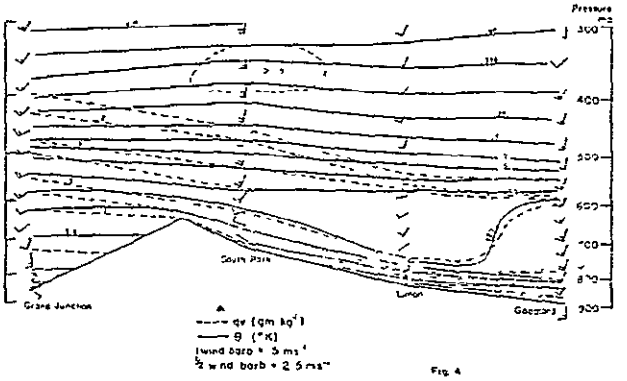

Figure 4 East-west cross-section of 0600 MDT (1200 MDT) 19 July 1977 soundings. Lowest line shows approximate surface elevation.

4 EVOLUTION OF THE PLANETARY BOUNDARY LAYER

Five-minute average surface winds, θ, and q_v observed with PAM are shown in Figure 5. At 0600 MDT (before sunrise), drainage winds pooled the coldest air into the center of South Park. At 0800 MDT and 1000 MDT, light winds were present in the park, with stronger westerly winds on the mountain crest bringing a somewhat higher q_v into the park. The 1000 MDT South Park sounding (Figure 6) showed that the planetary boundary layer already extended up to 600 mb, with θ = 321°K and q_v = 6.5 gm kg^{-1}. No subsidence inversion was present. The cloud condensation level (CCL) was 540 mb, giving a wet-bulb potential temperature θ_w of 22.1°C. This indicates a convective instability of about 1°C at 500 mb, with cloud tops of only 7-8 km. If, however, the mixed-layer q_v was 8 gm kg^{-1} on this sounding (as was available on the 0600 MDT Grand Junction sounding), a θ_w equal to 23.2°C at the CCL of 580 mb, a 500 mb instability of 2.5°C, and cloud tops of at least 12.5 km MSL would be obtained. A time section of the four South Park soundings (Figure 7) shows that the PBL had deepened to 500 mb by 1300 MDT, with θ = 324.5°K and a mixed-layer q_v = 5.5 gm kg^{-1}. The decrease in moisture was due to the entrainment of drier air into the PBL. Limon radar and satellite photographs show that deep convection had begun before noon to the west and northwest of South Park.

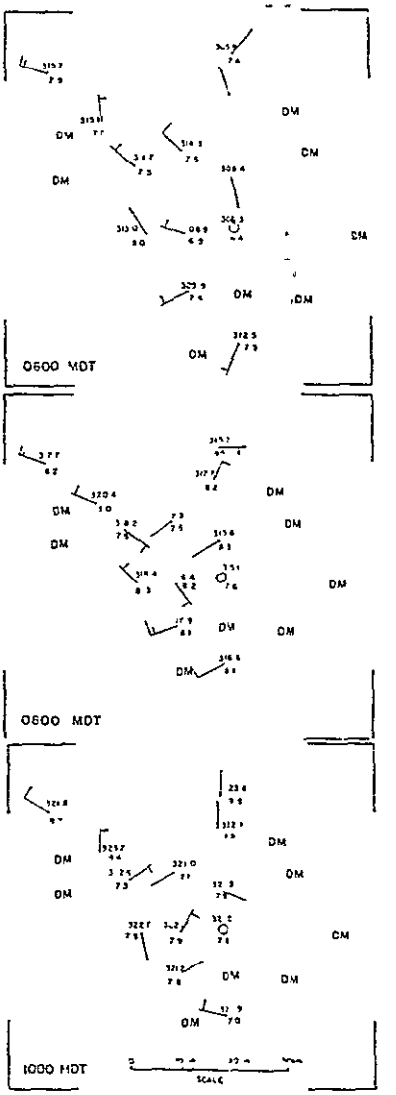

Figure 5 PAM surface data for 0600, 0800, and 1000 MDT, 19 July 1977. DM means data missing. Key on page 9.

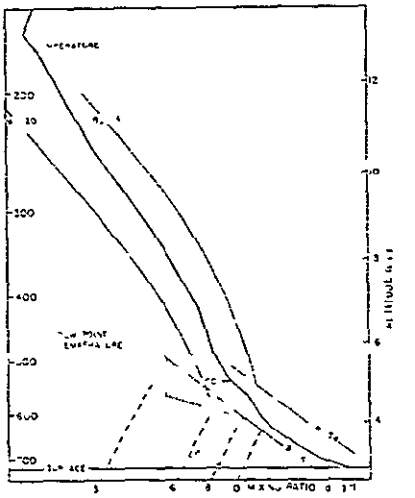

Figure 6. South Park sounding at 1000 MDT, 19 July 1977, skew-T, log-P

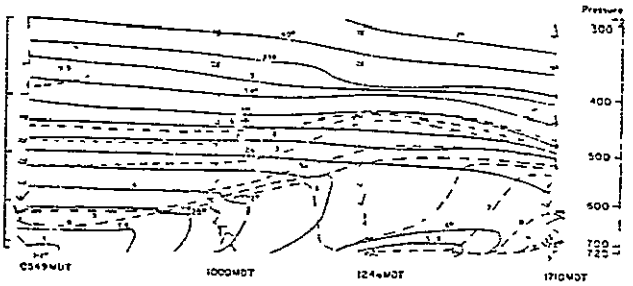

Figure 7. Plot of the four South Park soundings vs time, showing the probable evolution of the planetary boundary layer over South Park during the day. Note the addition of higher values of q_v after 1500 MDT in the PBL. Key on Figure 4.

5. AFTERNOON RADAR AND SURFACE ANALYSIS

At 1239 MDT, the CP-3 radar began recording data. Figures 8-15 are composite CP-3/PAM maps. Echoes are contoured for a scan elevation of 5.5° projected onto a horizontal plane, with only echoes of 30 dBz or greater intensity shown. PAM data and derived parameters are five minute averages about the time of the radar scan. Locations of convergence lines or gust fronts are estimated from single-station time plots by determining the time of wind shifts, temperature drops, etc., and advecting the gust front along with the speed and direction of the winds behind the gust front.

Around 1200 MDT the first precipitating cells formed in South Park along the west and northwest slopes. Figure 8 shows PAM and radar presentations for 1239 MDT. Comparing this figure with Figure 7, we can see that the easterly winds indicated at low levels on the 1246 MDT South Park rawinsonde were confined to a small area of the park that was sheltered from the prevailing westerly and southwesterly winds by the mountains. The balloon was observed to ascend near a cumulonimbus cloud, probably the hook shaped echo north of the base shown in Figure 8. Several convective cells were active in the north end of the park, with one strong precipitation area near CP-3 (at this close range, the scan is only a few hundred meters above ground level). All of these cells were moving toward the north at about 5 ms^{-1}, apparently in response to upper winds.

Small radar echoes continued to form northwest of the base and west of CP-3, in the climatologically most favored echo locations (Huggins, 1975). One cell was observed on radar to intensify greatly as it approached Hoosier Pass from the south (see Figure 2). By 1333 MDT (Figure 9), a line of strong thunderstorms had formed in the Blue River valley north of Hoosier Pass. Range Height Indicator (RHI) scans, which were synthesized from a series of constant elevation, full volume scans (Knupp, et al, 1978) show that these cells had tops of over 12.5 km, whereas the smaller cells within South Park had tops of 7-8 km. This indicates that the increased boundary layer moisture (8 gm kg^{-1}) needed to support deep thunderstorms, as indicated by rawinsonde data, was available just to the northwest of the park. PAM data in Figure 9 indicate that this moisture was being advected across the mountains. The remainder of the park, excluding the north and west edges, continued under strong heating, with surface q_v decreasing to 6-7 gm kg^{-1} as drier air continued to be entrained from above. Limon radar data for 1330 MDT showed that the

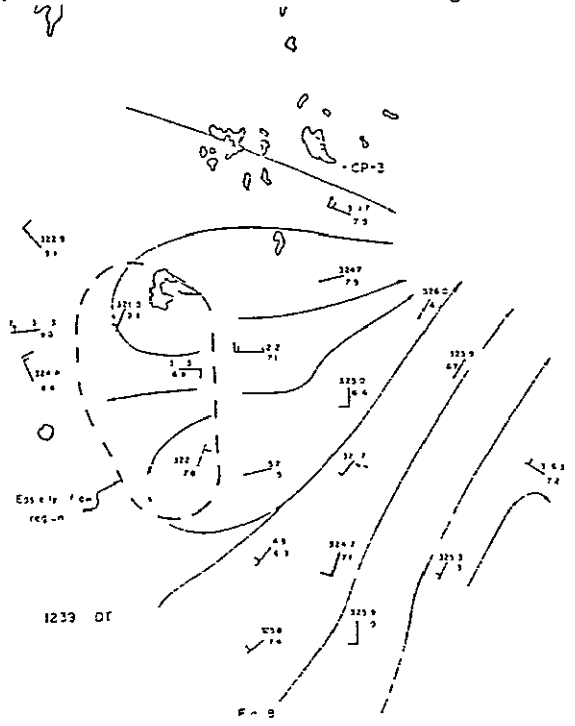

Figure 8. Combined PAM/CP-3 radar plots for 1239 MDT, 19 July 1977. Key to symbols on page 6.

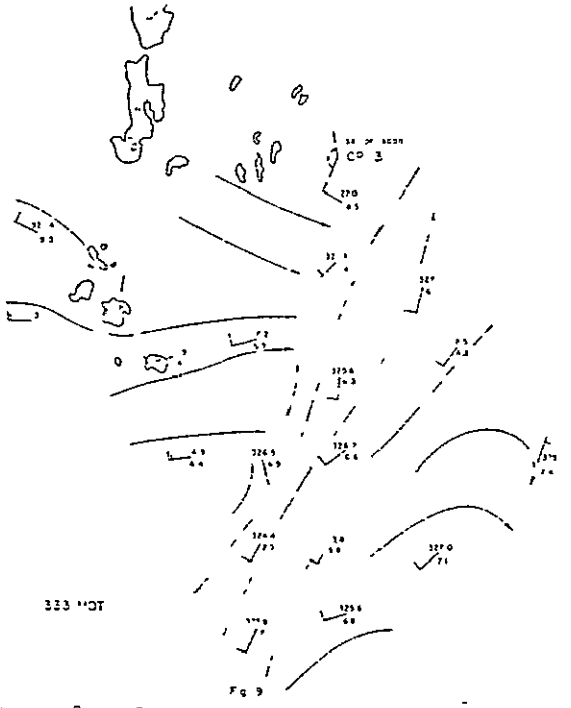

Figure 9. Same as Fig 8, for 1333 MDT, 19 July 1977.

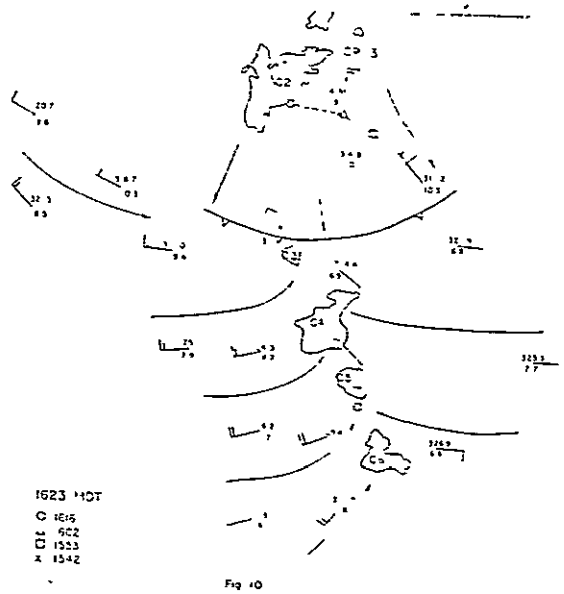

Fig 10

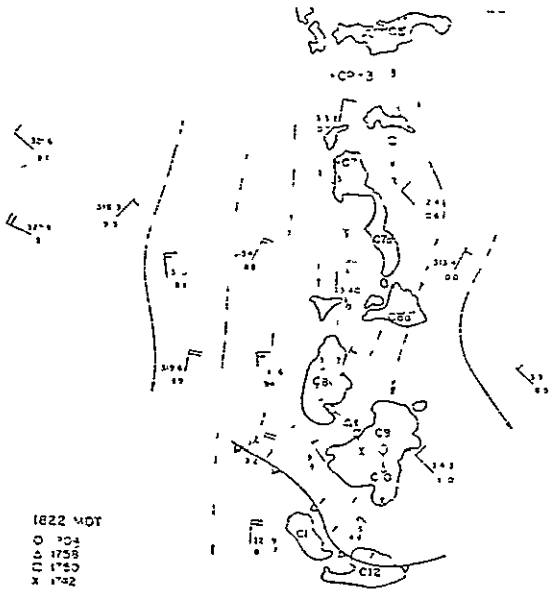

Fig 13

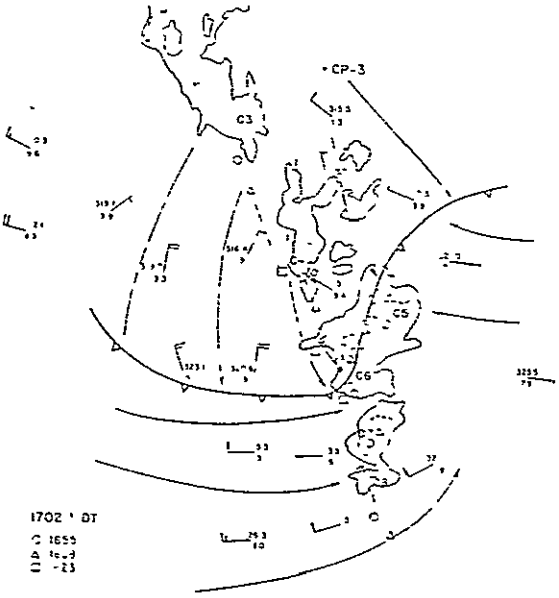

Fig 11

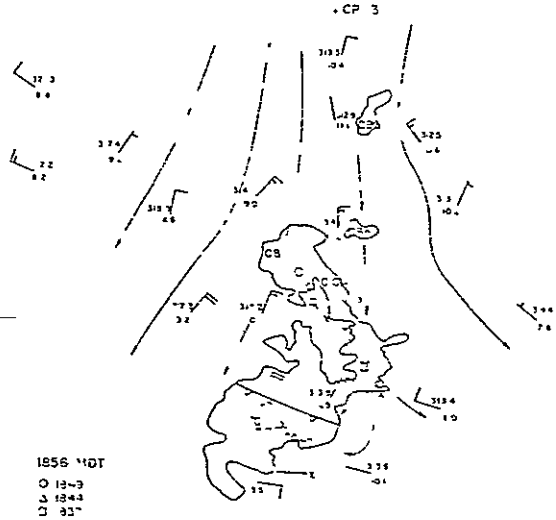

Fig 14

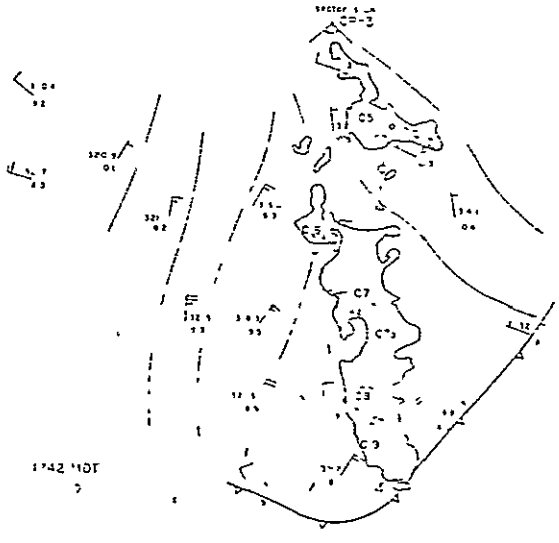

Fig 12

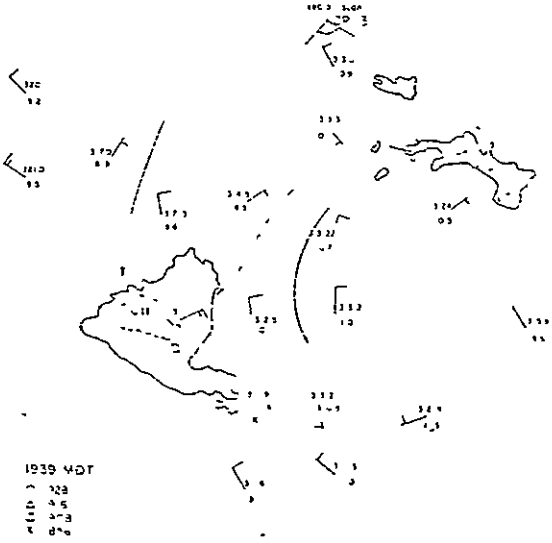

Fig 15

Hoosier Pass storms were part of a larger convective band which extended northeastward for 150 km.

At about 1430 MDT, surface winds in the southeastern part of the park began to shift toward the east. This flow gradually affected the entire eastern edge of the park. The resultant convergence pattern generated numerous small convective cells from 1430-1600 MDT. Surface temperatures remained high, indicating strong heating and increasing instability in the center of South Park. Around 1600 MDT the easterly flow invaded the center of the park, and together with the stronger westerlies in the western portion of the park, formed a convergence line which generated a line of thunderstorms. At this time, two intense cells formed at the north end of the park near Kenosha Pass.

In Figures 10-15, the convective cells are numbered sequentially relative to their probable initiation times. At 1623 MDT (Figure 10), four cells (C3-C6) were visible over the convergence line, with the second of the strong cells (C2) farther north. Note that C2 moved well to the west (left) of the upper winds, while the smaller cell C4 moved from 160°, approximately along the line of convergence. PAM rain gauge data show that station 28 received 1-2 mm of precipitation per minute for at least 15 minutes while cell C2 was overhead. A visual observation of a hail shaft from this cell was reported at about 1600 MDT. A mesoscale cold front had formed south of cell C2, perhaps consisting of outflow from C2 and cells farther north. Wind velocities in the southwest sector had increased to 7-10 ms^{-1}, and considerable cyclonic wind shear existed near the frontal boundary (cell C3).

By 1702 MDT (Figure 11), the meso-cold front had moved about 20 km south on the west side of the convergence line (traveling at 8 ms^{-1}). In succession, cells C4, C5, C6, and C7 had intensified to over 40 dBz

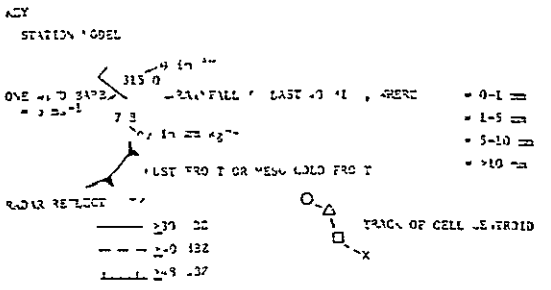

Figures 10-15. Combined PAM/CP-3 radar plots for 1623 MDT through 1939 MDT at 40 minute intervals. Key to symbols above. Arrows are used to suggest possible non-quantitative streamlines

reflectivity as the frontal winds approached. Cells C4 and C5 had partially decayed by 1702 MDT. These cells moved from about 170° at 5 ms^{-1}, with new cells having continuously formed on the south end of the line. Precipitation at rates of up to 100 mm hr^{-1} was measured at the west edge of C6. Note the weak radar return directly over the Continental Divide, with reintensified echoes over the Blue Valley northwest of the park.

At 1742 MDT (Figure 12), surface winds were more or less northerly throughout the PAM network. The latest cell (C9) was also the most intense (over 48 dBz). West of the convergence line, winds were stronger, and values of θ_e (equivalent potential temperature) higher, than that under and east of the line of cells.

By 1822 MDT (Figure 13) the character of the line had begun to change. Cell C8 had split into two parts, with the more intense part (C8) moving at 150° while the smaller cell (C8a) moved almost due north. A gust front, possibly caused by outflow from C8, C9, and C10, was moving into the bases of new cells C11 and C12. Cell C11 grew very quickly into the dominant storm of the day. By 1856 MDT (Figure 14) a hook-shaped echo protruded to the southwest of C11. A surface station under this hook experienced precipitation rates of about 200 mm hr^{-1}, probably including hail. Cell C11 moved at 4 ms^{-1} from 125°, well to the left of the mean winds. Moist outflow from other cells continued to feed this cell from the north. Cell C8 moved from 150°, while other cells in the line moved even farther to the right. Cell C11 continued to move slowly and intensified to at least 56 dBz at 1922 MDT, while the other cells in the line decreased in intensity. By 1939 MDT (Figure 15), cell C11 had begun to decrease in intensity while increasing its speed to 10 ms^{-1}. All the other cells in the line had dissipated, while a new line of cells, oriented east-west but still moving toward the north, had begun in the northeast part of the park. Winds in South Park became lighter and more variable after the passage of C11, with cold, moist air occupying the area. Although no further radar data are available, PAM rainfall data indicates that C11 may have moved over the crest of the mountains at about 2015 MDT.

Total precipitation data for the period 1600-2400 MDT are shown in Figure 16. Note the maxima at the extreme north (from C2), center (from C8), and extreme south (from C11). Rainfall at station 28 may have been higher than shown because it occurred at 1600 MDT, when there were voids in the PAM data.

6. LARGE SCALE ANALYSIS FOR 1300 MDT, 19, JULY 1977

A very complex picture of lower tropospheric flow patterns emerged with the analysis of 1800 MDT (0000 GMT, 20 July 1977) synoptic and large mesoscale data. At 500 mb, southerly flow had resumed through most of Colorado, but the South Park sounding for 1710 MDT still had a 235°

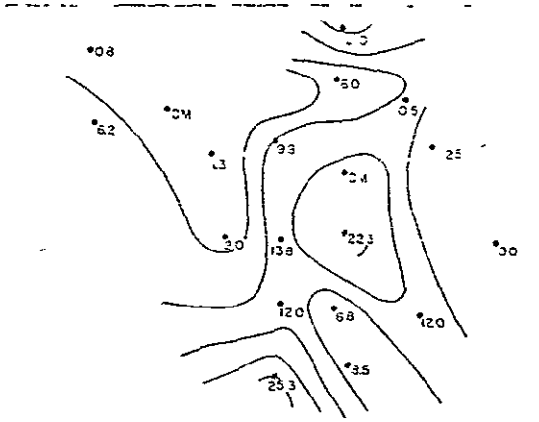

Figure 16. Total rainfall in mm observed at PAM rain gauges, for the time period 1600-2400 MDT, 19 July 1977

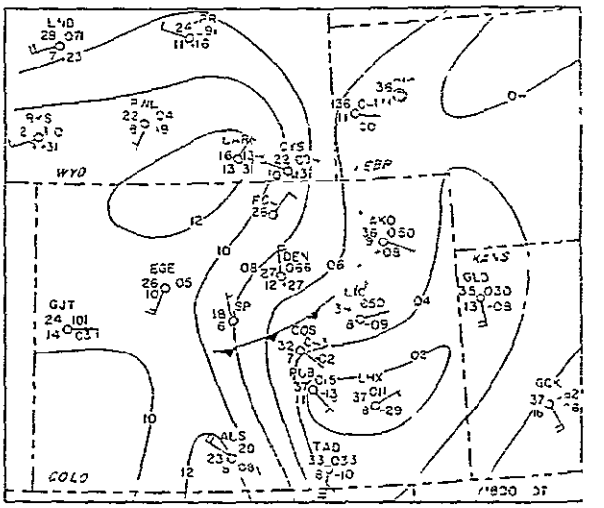

Figure 17. Surface analysis for 1800 MDT, 19 July 1977 (0000 GMT 20 July 1977) from NWS hourly reports. Pressure contour interval is 2 mb

wind at 560 mb (Figure 7), indicating continued advection of Pacific moisture across the mountains. Surface data (Figure 17) showed a strong low pressure center in the plains 200 km southeast of South Park, part of the persistent eastern Colorado surface trough. This low pressure center had deepened during the day, probably in response to both surface heating and a weak short wave which may have passed through the region.

Satellite photographs taken at 1830 MDT show the entire Rocky Mountain region covered with clouds. The deepest storms were located in three north-south bands, each extending from central Colorado into southern Wyoming. The easternmost of these bands extended north-northeastward from South Park to a point north of Cheyenne, Wyoming. This convective band probably marked the easternmost advance of moist Pacific air in the planetary boundary layer. Surface data from 1500 MDT - 2200 MDT show that the first occurrence of strong thunderstorms east of the Rockies was at Cheyenne at 1500 MDT. At this time, Cheyenne winds shifted to northerly, and the temperature dropped about 10°C. This phenomenon then occurred sequentially at each station farther south along the front range. At 1800 MDT, the boundary of this wind shift had passed south of Denver, while the northerly wind shifts observed in South Park had also passed through. In Figure 17, a cold front symbol is used to show the possible location of this air mass boundary.

The Denver sounding for 1800 MDT showed a layer of light north-northeasterly winds extending from the surface (at 840 mb) to about 700 mb. This layer had a potential temperature of about 321°K and an average q_v of about 7.5 gm kg^{-1}. In South Park at 1710 MDT (see Figure 7) there were northerly and northeasterly winds from the surface (719 mb) to about 690 mb, easterlies above that to 600 mb (perhaps an easterly flow regime driven by the southeast Colorado surface low), southwesterlies from 600-520 mb, and southerly winds aloft. This sounding was launched only a few minutes after the northerly surface winds covered the South Park rawinsonde site.

Earlier in the day, at 1333 MDT, South Park radar and PAM data (Figure 9) had shown that the mountain barrier extending to about the 650 mb level (northwest of the Park) had been sufficient to block very moist Pacific air from advecting into the park. This moisture had caused deep thunderstorm activity just outside the park, yet the onset of deep storms in South Park was delayed for at least three more hours. This when combined with evidence from the sounding wind fields at Denver and South Park, indicates that advection of Pacific moisture across the Rocky Mountains took place at very low levels, probably below 700 mb. In southern Wyoming, a gap in the Rocky Mountain barrier allowed such advection to proceed more rapidly into the Cheyenne area.

After 1500 MDT, deep thunderstorms, which had been occurring previously in the mountains west of Denver, invaded the plains along the front range. Persistent northerly flow in the lowest levels was observed at this time in a band about 100 km wide. This was an area of east-west baroclinicity in the lowest levels, while at 500 mb, little height gradient was apparent. Low level air to the west of this zone was cooled by a combination of thermal advection, evaporating thunderstorm downdrafts, and lack of surface heating due to cloudiness. To the east, extreme heating continued in the cloud-free zone. The resultant surface pressure gradient, shown in Figure 17, probably provided the forcing for the northerly winds.

7. CONCLUSION

July 19, 1977 was selected as our first case study day for storm-scale and mesoscale analysis because of its apparent relative simplicity. Extensive analysis of this day revealed a very complex picture of thunderstorm scale, large-mesoscale and synoptic-scale interactions.

Early convection was initiated over the Mosquito Range in the western and northwestern portion of South Park in the moist, Pacific, westerly-flow airmass. As the day progressed, easterly flow, driven in part by the surface low southeast of South Park and in part by the diurnally driven ridge-valley circulation, invaded the Park and set up a north-south oriented convergence line. South Park was apparently the location of the convergence line because it remained cloud free for a major portion of the day and thus became a significant elevated heat source.

Late in the afternoon a cooler airmass began invading the northern end of the Park. At first it appeared to be outflow from a single cell. As time proceeded, however, the northerly flow became quite persistent and coherent across the Park. By 1742 MDT the cool, northerly-flow airmass had invaded the entire PAM network. Because of the temporal coherency and spatial consistency of the northerly-flow airmass, it resembled a synoptic-scale frontal passage. The occurrence of such a frontal passage was conceivable since a weak surface front was analyzed on the morning surface maps along the southern Wyoming border. By 2000 MDT, however, the northerly flow over the PAM network had weakened in intensity and become less consistent, suggesting a diurnal influence.

The difficulty in isolating mesoscale versus synoptic scale influences is that the synoptic-scale baroclinicity was so weak that it cannot be objectively defined. At the same time, the Colorado Rocky Mountain barrier is so large (in its vertical and horizontal extent) that its associated diurnally-driven mesoscale disturbances develop a distinct synoptic-scale character. Thus considerable further analysis and perhaps numerical experimentation is required to isolate the scales having the major controlling influence on this day.

It is interesting to note that the north-south oriented line of convective cells which was preceded by a north-south oriented surface convergence line, retained its general north-south orientative during and subsequent to the passage of a well-defined, larger-scale, generally east-west oriented convergence line. The remarkable strength of the earlier observed mesoscale convergence line is attested to by the fact that this feature was sustained during the passage of a vigorous larger-scale convergence line.

8. ACKNOWLEDGEMENTS

This research has been supported in part by the National Science Foundation under Grant ATM76-83361, by the U. S. Bureau of Reclamation Division of Atmospheric Water Resources under contract number 7-07-83-80006 and by the National Aeronautics and Space Administration under Grant NSG-5011. The Bureau of Reclamation also provided sounding analysis and HIPLEX archived data. The National Center for Atmospheric Research-Field Operating Facility (the National Center for Atmospheric Research is supported by the National Science Foundation) developed the PAM system and CP-3 radar. The excellence of the PAM and CP-3 data is largely due to the hard work performed by FOF field personnel.

9. REFERENCES

Cotton, W.R., and R.L. George, 1978. "A Summer with PAM" preprint volume, Fourth Symposium on Meteorological Observations and Instrumentation, Denver, Colorado, April 10-14.

Dirks, R.A., 1969: A Theoretical Investigation of Convective Patterns in the Lee of the Colorado Rockies, ATS Paper #145, Colorado State University, Fort Collins, Colorado.

Henz, J., 1974: Colorado High Plains Thunderstorm Systems, MS Thesis, Colorado State University, Fort Collins, Colorado.

Huggins, A., 1975: The Precipitation Sequence in Mountain Cumulus, MS Thesis, Colorado State University, Fort Collins, Colorado.

Knupp, K., K. Danielson and W.R. Cotton, 1978: 'A Radar Case Study Analysis of a Heavily Precipitating Quasi-Stationary Convective Storm System', preprint volume, AMS Conference of Cloud Physics and Atmospheric Electricity, Issaquah, Washington, July 31-August 4.

A RADAR CASE STUDY ANALYSIS OF A HEAVILY PRECIPITATING QUASI-STATIONARY CONVECTIVE STORM SYSTEM

K.R. Knupp, K S. Danielson, W.R. Cotton
Department of Atmospheric Science, Colorado State University
Fort Collins, CO 80523

1.0 INTRODUCTION

An integral component of the 1977 South Park Area Cumulus Experiment (SPACE), was the NCAR Field Observing Facility (FOF) CP-3 C-band radar. This Doppler radar system was used to obtain reflectivity and radial velocity data from summertime convective storm systems occurring daily within South Park and adjacent areas. The NCAR/CP-3 radar was part of a triple-Doppler radar array which included the two NOAA Wave Propagation Laboratory (WPL) X-band radars. Fig. 1 illustrates the locations of these radars within South Park.

On 19 July 1977 an intense and long-lived convective storm system was initiated and maintained by phenomenon organized on the mesoscale. The general synoptic-features accompanying the mesoscale system were low vertical wind shear and moisture advection carried by relatively weak southerly flow. George and Cotton (1978), in a companion paper, have investigated the general features and evolution of this mesoscale system. The morphological characteristics of the July 19 radar echos, which is the subject of this paper, will form a basis in selecting cells for subsequent triple-Doppler radar analyses.

Several distinct and intense convective precipitating systems occurred on 19 July 1977 These convective entities had unusually long lifetimes, high reflectivities, and high echo tops when compared with climatological radar data from South Park reported on by Huggins (1975) Two specific intense cells, which differed greatly in echo structures were probable hail producers One of the convective systems was composed of multiple high reflectivity cores, exhibited non-steady-state features, and preceded the formation of convection organized on the mesoscale. The other convective system formed after initial mesoscale organization had taken place. Contrastingly, this system displayed quasi-steady-state echo characteristics.

2.0 GENERAL ECHO CHARACTERISTICS

Initial convective activity on July 19 occurred shortly before noon in the northwestern quadrant of South Park along the eastern slopes of the Mosquito Range By 1530 (all times are MDT) the major area of convection had shifted to the northeastern portions of South Park, where rapidly growing cumulus merged and formed an intense convective system composed of several high reflectivity regions.

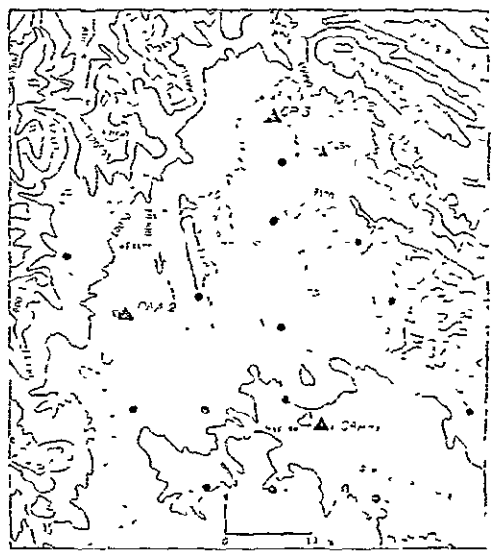

Figure 1. The location of the CP-3 C-band radar and the NOAA X-band radars within South Park. The S-band CSU-4 radar became operational after 3 August 1977 and was used for surveillance purposes. ▲ denotes radar locations, • denotes PMI station locations. Labeled elevation contours are thousands of feet MSL

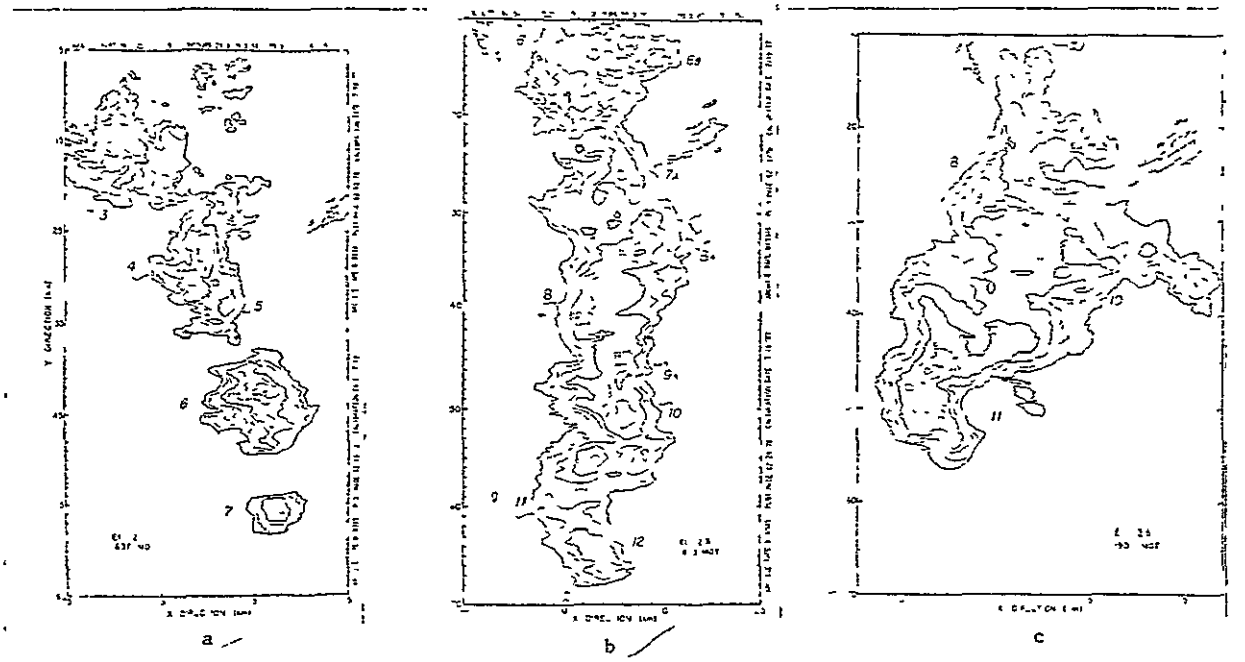

Figure 2. Constant 2.5° elevation radar scans from 1637 MDT (2a), 1803 MDT (2b), and 1907 MDT (2c). Contours are drawn at 5-dBZ intervals beginning at 20 dBZ. The dotted areas represent reflectivity factors greater than or equal to 35 dBZ.

As this system intensified, a broken north-south line of isolated convective echos over eastern South Park extended southward from the intense convective system in the northeast. The developing line at 1637 is shown in Fig. 2a. This line remained in a quasi-stationary position over eastern South Park for the next two hours. By 1804 MDT the echo line had attained a length of ∿100 km and a mean width of 10 -15 km. Fig. 2b clearly shows that by 1804 MDT the most intense convective cells were located at the southern end of the line as opposed to the northern end at earlier times. A typical definable convective cell in this line would form on the southern end of the quasi-stationary echo line and propagate northward through the line with a mean speed of ∿6 ms^{-1}. Two notable exceptions to this scenerio formed and intensified within the line's interior.

Between 1830 and 1900 MDT the convective echo line underwent another transition as a large organized, intense convective system on the line's southern end began to dominate. As this system intensified, cells to the north weakened and the organization of the line, which had been a persistent quasi-stationary feature for ∿2 hrs. rapidly dissipated. The 1906 5.5° elevation scan is shown in Fig 2c. Noteworthy features are the organized appearance of the convective system at the line's southern end and the lack of intense echos (only one appears) to the north. A closer examination of Figs. 2a - 2c reveals a clockwise turning of the line's main axis. This effect may be due to local changes in convergence of the associated mesoscale system. The northwestward propagation of the dominant convective region in Fig. 2c may be a factor in the line's axis change during the latter time periods.

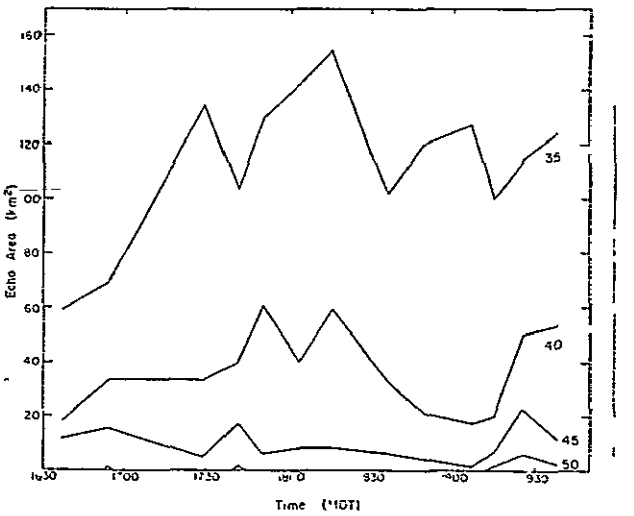

Figure 3. The total echo areas, enclosed by 35, 40, 45, and 50 dBZ contours, as a function of time. The echo areas include only the segment of the echo line south of the CP-3 radar.

A summary of the major convective cells on 19 July is presented in Table 1. These data, when compared with Huggins (1975) data, indicate that cell characteristics, including echo lifetime, maximum echo top, and echo intensity are well above normal for South Park thunderstorms. In his analysis of 1973 South Park radar data, Huggins found that convective echos had mean echo top heights of 9.0 km MSL, with extremes of 13 0 km MSL. As shown in Table 1, echo tops on July 19 often exceeded 12 and 13 km. According to Huggins, mean echo lifetimes of South Park cells were 30-40 minutes, with cells infrequently lasting 80-90 minutes. Table 1 indicates that

TABLE 1. Summary of the major TRW subsystems occuring after 1400 MDT, 19 July 1977.

Subsystem	Time of Echo Appearance (MDT)	Time of Echo Absence (MDT)	Lifetime (Min)	Maximum Top of 20-dBZ Echo (km MSL)	Maximum Intensity (DBZ)
1	?	?	?	?	50+
2	1500-1510	?	>120	>12.0	56
3	1500-1510	?	?	?	50
4	1530	1740	140	13 5	51
5	1600	1900	180	12 0	51
6	1610	1830	140	11 5	47
7	1630	1900	150	13.3	50+
7a	1730	1850	80	12 2	50
8	1645	1945	180	14 1	51
9	1710	1804[1]	-	13.3	51
9a	1720	1740[2]	-	12 8	47
10	1740	1910	90	13.5	51
11	1740	well after 2010	>150	13 7	54
12	1750	1900	80	12.5	45
Average			130	12.8	51

[1] Merged with cell 10

[2] Merged with cell 9

July 19 echo lifetimes often exceeded 140 minutes. Although extensive climatological studies of echo reflectivities are limited for South Park thunderstorms, the maximum intensities appearing in Table 1 appear to be well above normal and approach the echo reflectivities measured within moderately intense NE Colorado thunderstorms. (Foote, et al , 1976.)

Fig 3 presents the time evolution of the total area enclosed by 35, 40, 45 and 50 dBZ echoes after the echo line had attained an organized state. The values plotted in Fig. 3 were obtained from 2.5° constant elevation scans from the portion of the echo line south of the CP-3 radar. One of the noteworthy features appearing in Fig 3 is the relatively constant area of echo intensities for the 1700-1830 time period This constancy reflects the quasi-steady-state properties of the echo line as a whole. However, for the same time period, individual convective cells within the echo line exhibited widely varying echo shapes and intensities The high intensity echo areas reached a maximum near 1930 MDT resulting primarily from the presence of the intense quasi-steady-state convective subsystem described earlier.

The following sections discuss in further detail the individual convective subsystems which exhibited differing echo characteristics. (The term convective subsystem is defined here as a convective entity composed of one or more cells of high reflectivity regions Most of the subsystems listed in Table 1 appeared to be single-celled at a given instant in time.) The three subsystems to be described were the only ones on the 19th whose trajectories were significantly to the left of the mean environmental cloud-level winds (~170°). These subsystems were also quite intense when compared to "average" July 19 convective subsystems.

The first subsystem developed prior to the formation of the mesoscale echo line and displayed multi-cellular and non-steady-state echo features. The second subsystem studied was the most dominant one occurring on 19 July. It attained quasi-steady-state echo characteristics and appeared to communicate with and modify certain mesoscale features. The third subsystem was long-lived, and appeared to exhibit non-steady-state echo characteristics as the result of its interactions with adjacent cells and interactions with the mesoscale

3.0 ANALYSIS OF SPECIFIC ECHOES

3.1 Production of a Multi-Cellular Storm by a Merger Process

Intense reflectivity regions formed in a variety of ways on July 19. One mode of development was through successive mergers of morphologically independent reflectivity regions. The development of a convective subsystem (C2) shows an excellent example of intensification via cell merger. The individual cells which eventually merged to become C2 first became prominent at 1510 before the echo line described in the previous section became organized. PPI data suggest that this subsystem resulted from a two-step merger process. Approximately 8-10 separate reflectivity regions existed initially and underwent mergers in groups of 2 to 3, which resulted in three larger and more intense cell groups. RHI's of the two most intense cells in two of the cell groups at 1532 indicate that the maximum reflectivity core of each lies 3-4 km above the surface. The elevations of these reflectivity maxima at 6-7 km MSL are slightly below but consistent with the median values observed for the South Park region by Huggins (1975) and for NE Colorado by Dye (1976).

The 1542 elevation scan shown in Fig. 4 portrays the cell complex C2 shortly after merger of the three cell groups. These cell groups are now apparent as three maximum reflectivity regions labelled a, b, and c. Also shown in Fig. 4 is the location of C1, a less intense convective subsystem which was prominent before C2. It was noted that another cell group to the south weakened and dissipated as the merger and subsequent intensification of C2 occurred. By 1552 C2 contained one large reflectivity region with a reflectivity factor maximum of 58 dBZ at 3.75 km MSL. It is likely that this reflectivity core contained small hail (or graupel) at this time. The 5.5° elevation scans at 1553 and 1602 indicate that the 40 dBZ echos of C2 had completely merged to form one large echo. Other noteworthy features were the tight echo gradients appearing along the southeastern edge of C2 during its most intense stages (1652-1602). This is contrary to the usual pattern of high reflectivity gradients appearing along the leading edge or inflow area (the northwest quadrant in this case) of intense convective storms. (See Foote and Fankhauser, 1973, for an example.)

During C2's mature stages, the general echo structure was characterized by a 45-55 dBZ reflectivity maximum situated near the surface along the system's southeastern edge, and a secondary, suspended reflectivity maximum located aloft (6 to 8 km MSL) along the western or northwestern edge. At times a third local reflectivity maximum appeared at an intermediate altitude between the other two maxima (see Fig. 5). The average 10-min. time interval between successive PPI scans was too great to track the evolution of these maxima. The location of the major inflow/updraft region along the northwestern quadrant of C2 may explain, by propagation effects, why its trajectory was significantly to the left (~50°) of the mean cloud-level environmental winds during its intense stages.

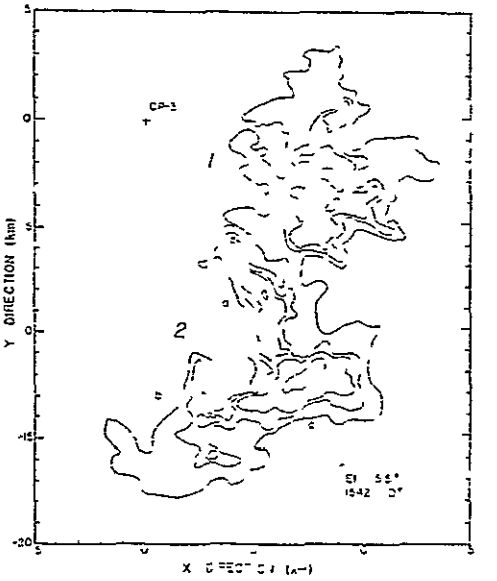

Figure 4. The 1542 MDT 5.5° elevation scan of convective subsystem number 2 (C2) shortly after the merger of three previously separate cell groups. The cell groups, now evident as three reflectivity maxima, are labeled a, b, and c. The reflectivity factor contours are at 25, 35, 40, and 50 dBZ, with dotted regions greater than 40 dBZ. Subsystem 1 is located NE of C2.

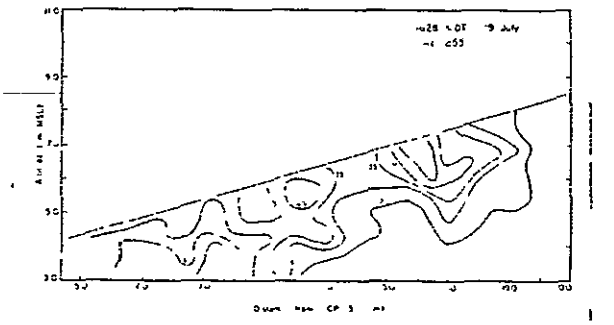

Figure 5. Core RHI of C2 reconstructed from the 1628-30 to the 1632:00 MDT sector scan. Contours are drawn for 20, 30, 35, 40, 45, and 50 dBZ. The dotted areas represent reflectivity factors greater than 40 dBZ. The slanted line depicts the maximum elevation (15.5°) scanned by CP-3.

3.2 Single-Cell Growth in an Environment Modified by Previous Clouds

The subsystem described in this section appeared in a region previously occupied by several relatively passive echos at the southern end of the well-developed echo line described earlier. This passive echo group had moderate radar reflectivity returns for approximately 20-30 minutes before any significant intensification of the echo occurred. The RHI profile at 1814 MDT indicates that this cell (C11) was multi-turreted, with an overranging echo along the northwestern and southern quadrants. A merger phenomenon is not evident in this case. Using surface mesonet data, George and Cotton (1978) suggest that intensification of C11 coincided

with the arrival of outflow air from cells located 10-20 km due north. Examination of the morphology of the cell (C10, Fig. 2b) from which the outflow is hypothesized, indicates that at 1804, this intense subsystem had an extensive overhanging 45-50 dBZ echo along its eastern and southern portions. By 1815 much of the overhanging echo had collapsed and maximum intensities appeared near the surface along the subsystem's southern quadrant. The outflow resulting from this collapse, as inferred from the above descriptive echo evolution, coincides with the gust front detected by the surface mesonet and analyzed by George and Cotton.

The 1837 and 1848 MDT core RHI's show several interesting features of C11's echo morphology in the vertical. Unlike the 1814 RHI of this cell, these later data indicate a single, intense, overhanging echo core. The secondary individual far-side echo appearing on the 1848 RHI in Fig. 7a is associated with the hook-like echo on the southern quadrant of C11. This hook echo, which is shown in the 1848 5.5° elevation scan of Fig. 6a, appears to be a flanking line of towering cumulus emanating from C11's echo core region.

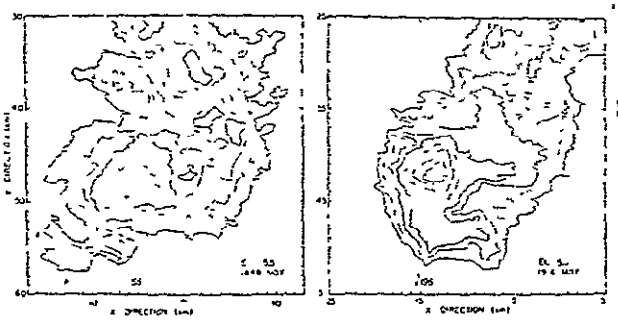

Figure 6. Constant 5.5° elevation scans of convective subsystem number 11 (C11) at 1848 MDT (6a) and at 1918 MDT (6b). Contours are drawn at 5 dB intervals beginning at 20 dBZ. The dotted areas represent reflectivity factors greater than or equal to 40 dBZ. The dashed lines are the horizontal locations of the RHI's appearing in Fig. 7.

Examination of subsequent PPI's and RHI's reveals that this subsystem had the characteristics of a large quasi-steady-state, intense, single-cell storm. Steady-state features of this cell include a fairly persistent PPI hook-echo pattern (Fig. 6), a single, intense reflectivity core often associated with a weak-echo region (WER) to the north or northwest (Fig. 7), and a nearly constant maximum echo top (Fig. 8). The 1928 RHI and 5.5° elevation scan revealed the only exception to the otherwise constant single reflectivity core. These data show a double reflectivity core. The secondary reflectivity core (50 dBZ) appearing at this time was located in an echo overhang in the cell's northwest quadrant. It should be noted that the overhanging echo structures appearing in Fig. 7 are consistent with other spatial and temporal core structures of C11 from 1840 to 1950.

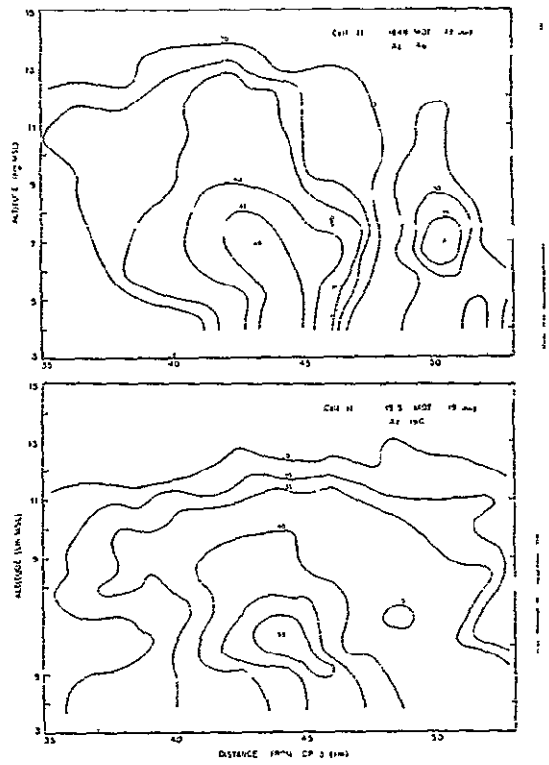

Figure 7. Reconstructed RHI cross sections of C11 from the 1848 MDT (7a) and 1915 MDT (7b) sector scans. The reflectivity factor contours are drawn for 20, 30, 35, 40, 45, and 50 dBZ. The corresponding PPI's appear in Fig. 6. It should be noted that a 4-min. time period was taken to obtain this reflectivity data.

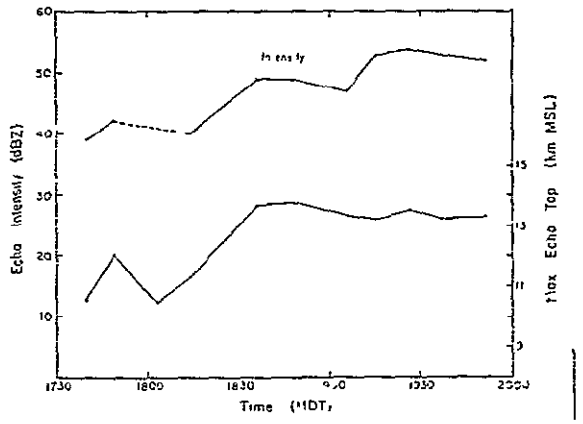

Figure 8. The time evolution of C11's maximum echo intensity in dBZ (top) and maximum 30 dBZ echo top (bottom).

The echo-inferred inflow areas of Cell 11 were initially confined to the southern sectors. The inflow region transferred to the northern and northwestern portions as the cell intensified. At 1837 MDT the major inflow appeared to be divided almost equally between the southern and northwestern portions.

At 1837 a ridge of 13-km 20-dBZ echo tops extended from the south-central portion of Cell 11 to the north-central portion. By 1906 three local 13-km maxima appeared as the major inflow appeared to shift to the northwest quadrant. The 1926 echo-top contours reverted to a single area of 13-km tops. These relatively minor fluctuations (both spatially and temporally) in Cell 11's echo top maxima seem to indicate a slight non-uniformity in cell's updraft and inflow patterns. Despite the relatively minor spatial non-uniformities in echo cores, echo structures, and echo tops, the persistent hook echo and RHI core echo features indicate that Cell 11 was in a steady-state condition for the period 1840 to 1950 MDT.

3.3 A Non-Steady-State, Long-Lived, Interactive Subsystem (C8)

Most convective cells interact to differing degrees with surrounding convective systems. This example provides some clues on the important and complex problems of cell-cell interactions. Many of the physical processes which constitute this interaction have not been well defined. The morphological description in this section presents a highly interactive subsystem as inferred from reflectivity data.

Throughout much of its lifetime convective subsystem number 8 (C8) displayed both vertically and horizontally non-steady-state echo features. The initial echo of C8 first appeared at the southern end of the echo line and moved slowly northward through the line as further echo development occurred to the south. As the subsystem progressed through the echo line, moderate changes in reflectivity maxima, in reflectivity structure, and in echo areas were noted

Sequential RHI cross sections from 1730 - 1837 MDT exemplify the variability in echo structure and inferred flow patterns of this cell. Between 1730 and 1745, the major inflow to Cell 8, as inferred from an overhanging echo structure, shifted from the cell's eastern boundary to its western boundary. C8, which had a width equal to that of the echo line, was located in the south-central portion of the echo line at this time. For the remainder of C8's lifetime, major inflow appeared to stay along the western and northwestern echo boundaries During this same time, the subsystem (C8) itself remained proximal to the western boundary of the echo line. The transition of this inferred inflow region bears a striking resemblence to the inflow transition exhibited by C11. The availability of low-level moisture was probably important in C8's longevity (~3 hrs.), slow average speed of movement (3-4 ms^{-1}), and 20° trajectory deviation to the left of the mean winds.

No significant maximum reflectivity or echo structure changes accompanied C8's inflow transition However, an intense strong cell (C9) did develop near C8 during the 1730-1745 transition period. The 1740 MDT RHI vertical sections of C9 indicate the presence of extensive echo overhang along this echo's eastern edge. Thus, it appears that C8's inflow change was con-current with the appearence of an active cell (C9) which received its moisture from the same general area in which C8 received its low-level moisture. The temporal relationship of these events suggests a causal relationship, the specifics of which cannot be discerned from the analysis of reflectivity data alone

The relative positions of C8 and C9 are shown in the 1740 MDT RHI in Fig 9. By 1751 C8 and the northern portion of C9 appear to have merged Shortly after the C8-C9 merger the cells could not be distinguished from one another.

C8 interacted with two other subsystems, C8a and C10 (see Fig. 2b for locations). C8a first became prominent at 1757 MDT when it appeared as a secondary cell attached to the northeastern quadrant of C8. C8a intensified rapidly to become a separate 47-dBZ echo entity at 1804 MDT (see Fig. 2b) and, for the next 50 minutes, travelled due north with a mean speed of 7.5 ms^{-1}. The difference in the mean propagational velocities of C8 and C8a (150°/3-4 ms^{-1} and 175°/7.5 ms^{-1}, respectively) is quite striking The speed differences, at least, are probably due to east-west gradients in the low-level momentum.

Specifically, the northerly component of low-level momentum west of the echo line was approximately twice as large as that on the eastern side. (See George and Cotton (1978) Fig. 13.) C8, which lay along the line's western border, appeared to be feeding upon the relatively strong low-level moist northerlies, thus acquiring northerly momentum. C8a, on the other hand, appeared to be receiving inflow from the region east of the echo line where the low-level northerly momentum was considerably weaker. This cell, therefore, would have acquired less northerly momentum and consequently exhibited a faster southerly speed. Factors contributing to the different direction of propagation of C8 and C8a have not been resolved.

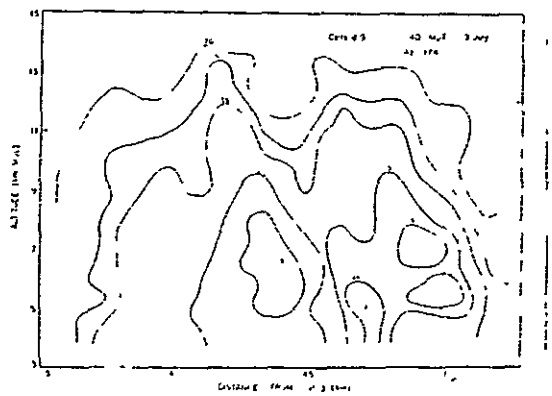

Figure 9. As in Fig. 7, except for C8 and C9 at 1740 MDT. C8 is on the left, centered at 44 km.

4.0 SUMMARY AND DISCUSSION

4.1 Comparison of Results With Other Case Studies

C2's general echo structure, once established, appeared non-steady-state, with the mature stage containing 2-3 reflectivity maxima. One maximum was located along the storm's southeastern region while the other reflectivity maximum was present within the echo overhang along the storm's northwestern segment.

Some of the echo characteristics that C2 exhibited are similar to the multi-cell hailstorms examined by Marwitz (1972b) and Chisholm (1967). In his study, Chisholm found that storm "families" (a family is synonomous with the term convective subsystem used here) were composed of several smaller high-reflectivity cellular echos. Each cell formed in a preferred area of the storm family and moved through the storm family in a direction different from the overall movement of the family. Although the individual cells of C2 could not be accurately tracked, they were multiple and appeared to form in a preferred location along the storm's western or northwestern side. The appearance of multiple cores in C2 implies a storm movement to the left of the mean cloud layer winds by discrete propagation of individual cells.

The echo structure of C11, in contrast to that of C2, appeared to be quasi-steady-state and contained, for the most part, a single reflectivity maximum, an associated weak-echo region, and a hook-like echo. These features are similar to those of supercell storms described by Browning (1964) and Marwitz (1972a). However, several important differences exist between the classical supercell and C11. Most case studies of supercells have found that the storm usually propagates continously to the right of the mean environmental winds. These winds usually exhibit appreciable vertical shear and veering with height, especially in the sub-cloud layer. Cell 11 propagated continuously 30-40° to the left of mean environmental (in-cloud) winds which contained small vertical wind shear and which backed with height. The relatively shallow northerly winds did induce appreciable wind shear (nearly a 180° change in wind direction) in the subcloud layers. C11 had major inflow from northerly low-level winds along its northwestern quadrant and only minor inflow in the vicinity of the hook-like echo. Typical supercell storms generally have substantial inflow from low-level southerly winds within the weak echo region along their southern quadrant. Apparantly, interactions between C11 and the mesoscale were more important in determining C11's echo characteristics than the dynamics of wind shear present in the usual supercell environment.

4.2 Interactions Among Convective Subsystems

It appears that interactions among convective cells of which the line was composed, and interactions between convective cells and the local mesoscale circulations, are important in determining cell characteristics. Marwitz (1972b), using his data and case studies by other investigators concluded that a light wind condition in the subcloud layer is a prominant characteristic of the multi-cell storm environment. Light winds in the subcloud layer were part of C2's environment. During C2's growth and development period, surface winds were generally 5-10 ms^{-1} in the subcloud layer. Conversely, a change in the mesoscale and synoptic-scale features of the subcloud environment surrounding C11 (a quasi-supercell) produced stronger 10 ms^{-1} northerly winds at the surface and greater subcloud wind shear.

Observed interactions among cells included echo mergers and outflow kinematics. Outflow from convective subsystems appeared to be important in new cell production. Initiation of new cells apparently resulted from the outflow of older cells, setting up zones of surface convergence on a more localized scale than the mesoscale. A good example is C11. It appeared that intensification of this subsystem was enhanced by outflow from an adjacent subsystem (C10). Cell mergers appeared to play an important role in the intensification and sustenance of the July 19 convective subsystems. For example, the intensification of C2 appeared to be the result of several cell mergers. Florica studies (Woodley and Sax, 1976; Cunning, et al., 1977) have indicated that cumulus merger events may be important in increasing convergence and cell inflow at lower levels. With the steep vertical moisture gradients present on 19 July, the effect of low-level inflow organization and intensification would appear to be important in drawing a significant increase of water vapor into the convective subsystem. This increase of water vapor influx may then be sufficient for the liquid-water-dependent process of precipitation formation and hailstone growth.

On several occasions the dissipation of weak to moderate cells adjacent to intensifying or intense convective subsystems was noted. For example, between 1538 and 1552 MDT, a moderately weak convective cell 10 km south of C2 rapidly dissipated while C2 rapidly intensified. It was also noted that cells 12 and 13, which formed adjacent to C11, exhibited relatively short echo lifetimes and echo intensities compared to the other subsystems observed on 19 July. Radar observations in central Iowa of small convective showers in the vicinity of more dominating thunderstorms have indicated a similar behavior (H. C. Vaughan, personal communication). Such observations suggest that the circulations induced by a vigorous convective system apparently are sufficient at times to inhibit significant convection in adjacent regions.

5.0 CONCLUDING REMARKS

The cells and convective subsystems occurring on 19 July 1977 contained unusually high echo intensities and echo tops. The echo longevity and high echo intensities are attributed to the presence of the organized mesoscale low-level convergence zone discussed by George and Cotton (1976). Another factor in cell longevity and intensity may have been the north-south orientation of the convective mesoscale line which was parallel to the mean in-cloud southerly winds

This effect "steered" most cells so that they travelled along the echo line in a near-saturated environment modified by previous convection. Erosion and entrainment effects would have been minimized by this type of geometry. Also air at ridge top levels and above was quite moist, again minimizing entrainment effects. There appears to be a feedback mechanism between the mesoscale circulations and the inferred circulations of the convective subsystems. The structure of individual cells or subsystems appeared to be dependent upon the stage of development of the mesoscale system, and the location of the convective entity relative to the mesoscale convective system. Cell's echo structure and inferred circulations appeared to be more organized than those characteristics from the other convective subsystems. This organization was apparently closely related to the organized features of the associated low-level mesoscale convergence field that was observed at that time.

It is hoped that subsequent analysis of storm-scale motions derived from triple-Doppler radar will shed further light on the nature of storm-scale and mesoscale interactions.

6.0 REFERENCES

Browning, K.A., 1964: Airflow and precipitation trajectories within severe local storms which travel to the right of winds. J. Atmos. Sci., 21, 634-639.

Chisholm, A.J., 1967: Small-scale structure of Alberta hailstorms. Out of Alberta Hail Studies 1966, Stormy Weather Group Scientific Rept. MW49, McGill Univ., Montreal, Canada.

Cunning, J., J. Thomas, P. Gannon, 1977. Mesoscale response of the Florida environment to convection on a seeding day - a case study. Preprints, Tenth Conf. on Severe Local Storms, Omaha, Neb., pp. 126-132.

Dye, J.E., C.A. Knight, P.N. Johnson, T.W. Cannon, and V. Toutenhoofd, 1976: Observations of the development of precipitation-sized ice particles in NE Colorado thunderstorms. Proc. Interntl. Cloud Physics Conference, Boulder, Colorado, 1976, 478-483.

Foote, G.B., and J.C. Fankhauser, 1973: Airflow and moisture budget beneath a NE Colorado hailstorm. J. Appl. Meteor., 12, 1330-1352.

Foote, G.B., R.C. Srivastava, J.C. Fankhauser, et al., 1976: Final Rept. - National Hail Research Experiment 1972-74. Vol. IV. National Center for Atmos. Research, Boulder, Colo.

George, R.L. and W.R. Cotton, 1978. The characteristics of evolving mesoscale systems over mountainous terrain as revealed by Radar and PAM. Proc. of Conf. on Cloud Physics and Atmos. Electricity, July 31 - Aug. 4, 1978, Issaquah, Wash.

Huggins, A.W., 1975: The precipitation sequence in mountain cumuli. M.S. Thesis, Colorado State Univ., Fort Collins, Colorado.

Marwitz, J.D., 1972a, b: The structure and motion of severe hailstorms. Parts I and II. J. Appl. Meteor., 11, 166-188.

Woodley, W.L., and R.I. Sax, 1976: The Florida area cumulus experiment, rationale, design, procedures, and future course. NOAA tech. Rept. ERL 354-WMPO-6.

COMPARISON OF SEVERE STORM CLOUD TOP HEIGHTS DERIVED FROM SATELLITE AND RADAR OBSERVATIONS

by

Robert A. Maddox, Andrew J. Negri, and Thomas H. Vonder Haar
Dept. of Atmospheric Science
Colorado State University
Fort Collins, CO 80521

Prepared for

1976 Fall Annual Meeting
American Geophysical Union

1.0 INTRODUCTION

Since the first launch of meteorological satellites, researchers have been utilizing the resultant unique data set in various types of convective cloud studies. For example, Griffith and Woodley (1973) and Reynolds and Vonder Haar (1973) have related cloud visible brightness to radar cloud top heights to develop relationships for remote rainfall measurement. Grant and Vonder Haar (1975) have used satellite data to determine when favorable seeding conditions exist (using IR sensed cloud top temperatures) for orographic precipitation enhancement in the western United States. The detection, study, and prediction of severe convective storms (thunderstorms which produce large hail and/or damaging surface winds and/or tornadoes) is an area of high interest since these types of damaging storms occur frequently over much of the eastern two thirds of the country. The importance of real time detection of large convective storms which are producing abnormally heavy rainfalls was tragically emphasized by the Big Thompson flash flood in Colorado this past summer.

Efforts have been made to use satellite data in a qualitative manner for severe storm identification, mesoscale analysis, and short range "now casting" (see Purdom, 1974; Weiss and Purdom, 1974; and Fujita and Forbes, 1974). Arn (1975) related satellite observed cloud brightness to reported severe storm occurrences, and Shenk and Curran (1973) correlated brightness to observed cloud top heights. Attempts have been made to quantitatively relate satellite measured anvil growth rates to severe storm occurrences (Arn, 1975) and to radar measured echo characteristics (Reynolds and Vonder Haar, 1975 and Negri, et.al. 1976).

Efforts of this type have been limited by the long time period which elapses between images (usually 30 minutes at best). Recently Negri, et.al. (1976) have emphasized the importance of using short interval (5 to 7.5 minute) SMS data in studies of convective clouds and storms. A multi-phased study of severe storms and their environments, emphasizing the use and interpretation of satellite data, is underway at Colorado State University and this paper presents preliminary results which compare satellite sensed cloud top radiative temperature fields to corresponding (in time and space) radar echo characteristics.

2.0 DATA

The SMS-1 satellite collected visible (.5 - .7 μm) and infrared (10.5 - 12.5 μm) data at 5 to 15 minute intervals from 1800 GMT, 24 April to 0200 GMT, 25 April, 1975. Numerous severe storms occurred over a region stretching from southwest Oklahoma to eastern Tennessee during the afternoon and evening hours this day. A destructive, killer tornado struck at Neosho, Missouri and hailstones larger than baseballs pounded the small town of Wewoka, Oklahoma. NASA, Marshall Space Flight Center, was conducting an atmospheric variability experiment on this date and provided CSU with upper air data for the eastern two thirds of the country which was taken at three hour intervals. The area of interest of this study included eastern Oklahoma, northern Arkansas, and much of Missouri. Fig. 1 shows this region, some of the storms considered, along with radar indicated heights (x 10^2 ft. MSL), and the location of the upper air station at Monett, Missouri. Distinctive overshooting towers, or tops, are visible on the storms in northeastern Oklahoma.

Fujita (1972) and Pearl, et.al. (1975) have related the rapid collapse of similar overshooting tops to the occurrence of tornadoes and large hail at the surface. The large storm complex in Missouri is intersecting a WNW to ESE orientated frontal surface and a line of cumulus clouds is visible along this boundary. Qualitative studies by Purdom (1975) have shown this type of intersection to be a favored location for the occurrence of intense severe storms. However, in this particular case the storms in Oklahoma are more intense and dangerous, emphasizing the need for quantitative means of analyzing and interpreting satellite data.

NASA, Goddard Space Flight Center, provided CSU with the SMS-1 VISSR (Visible and Infrared Spin Scan Radiometer) digital data, on magnetic tape, that were used in this study. Radar data used were the hourly reports taken at NWS WSR-57 radar sites at Kansas City, Witchita, Oklahoma City, Little Rock, Monett, and St. Louis. Intensity contoured, PPI scope photographs (at zero degree antenna elevation) from Oklahoma City were compared with the satellite data for the storms in Oklahoma.

3.0 STORM TOP COMPARISONS

The semi-isolated nature of the storms of interest made a direct comparison with the radar reports fairly simple. Radar indicated echo tops at 1935, 0035, and 0135 GMT were compared with nearly simultaneous (maximum difference of nine minutes) IR satellite data. If different radar stations reported slightly different top heights for the same storm the values were averaged. A total of 25 radar heights have been compared with the satellite measured radiative cloud top temperatures. The sample number will be increased when the digital IR data for the remainder of

the afternoon are received and processed - IR data were only available for the three times listed above. Smith and Reynolds (1976) reported on several different methods of estimating cloud top heights for a variety of larger cloud types. They compared top heights obtained using cloud shadows, IR-T (Z) relations and radar. Their results showed a fairly large scatter with a root mean difference for an IR/Radar comparison of 2.53 km. Only large thunderstorms which reached near to, or penetrated, the tropopause were considered in the current study whereas Smith and Reynolds studied clouds which ranged from 6 to 15 km in height. A reliable technique to remotely monitor significant storm tops from satellite would provide a valuable complement to conventional radar data.

To determine cloud height using IR data it is usually assumed that the cloud emits radiation as a blackbody and that the cloud top effective temperature is the same as that of its near environment. Negri, et.al. (1976) have detailed some particular problems involved in applying these assumptions to obtain top heights for small, isolated clouds in a hot, dry environment. However, it is felt that for large storms reaching to the tropopause, these assumptions are acceptable. The primary problems in monitoring this type of storm result from the coarse resolution of the IR data (one IR data pixel at 35N 95W represents the mean blackbody temperature for an area approximately 22 km^2) and also from the nearly isothermal lapse rate above the tropopause.

Fig. 2 is a plot of the 2100 GMT special upper air sounding taken at Monett, Missouri. This temperature profile was considered to be representative of that of the environment of all 25 storms used in the study. The sounding is potentially very unstable with a lifted index of -6 and is similar to what is considered the classic central U.S. tornado

proximity sounding (see Miller, 1972). The coldest environmental temperature present was 209°K (-64°C).

An overshooting tower rapidly becomes much colder than its environment as it overshoots its level of zero buoyancy and penetrates above the tropopause height (note the rapid divergence of the moist adiabat and the environmental temperature above 200 mb in Fig. 2). However, as thunderstorm tops boil above the anvil level they are entraining environmental air whose temperature changes little with height. This effect masks or smoothes out the presence of very cold temperatures within the negatively buoyant top. Fig. 3 is a scatter diagram of the radar indicated cloud top versus the minimum IR temperature measured for that cloud top. The dashed line is an estimated smooth fit of the points and the solid line is the Monett sounding (plotted using the radar height scale). The two curves agree quite well up to the tropopause (approximately 42,000 ft.) but with the radar tops consistently higher than IR tops derived using the environmental sounding. The higher bias of the radar tops is likely due to the coarse resolution of the IR data which doesn't "see" small, high rising turrets. The IR temperature measured for the large, severe storm anvils is indicated on the figure. The anvils were at or very near the tropopause.

The scatter for tops above the tropopause illustrates the problems inherent in inferring cloud top heights for severe storms using only satellite IR data. More quantitative techniques are needed to relate IR top characteristics to storm severity. Adler (1976) has studied areal rates of change for cold cloud top temperatures during the life of the Omaha tornadic storm. His technique will be considered as this study continues at CSU, as will other severe storm characteristics. Some

possibilities include: examination of the time rate of change of the minimum cloud top temperature, development of relationships between extent of penetration above the tropopause and the difference between the IR temperature and that of the tropopause, and development of relationships between both IR and visual characteristics of the storm top to its severity.

4.0 PPI DISPLAYS AND IR TEMPERATURE FIELDS

Figs. 4 and 5 present the Oklahoma City WSR-57 intensity contoured PPI display and the nearly simultaneous cloud top temperature field (contoured in $4^{o}C$ intervals with $-70^{o}C$ the coldest region). The very cold cloud top temperatures correlate well with the radar echo configurations of the large storm complexes at 070^{o}/100 n.m. and 130^{o}/75 n.m. The intense echo cells (cross-sectional areas of approximately 50-100 km^2) detected by the radar within these complexes do not show up within the general IR cold cloud area; however, good agreement was noted between intense echo cells and overshooting tops apparent in the visible data. The problem is again most likely one of resolution and points out the need for detailed studies of simultaneous radar and satellite data. Pearl, et.al. (1975) studied overshooting tops on a number of severe hailstorms. The large overshooting domes had diameters of 10-12 km, or cross-sectional areas of approximately 80 km^2. Only a small part of the area is at the top of the dome and an IR data pixel would have to be centered exactly on the dome to sense the blackbody temperature of the highest 22 km^2,

An interesting feature of this situation is the intense echo SSW of the radar. This storm was dropping large hail at the time of the

photograph, but it does not stand out in the corresponding satellite IR data and would pose a serious problem if it were being monitored only by satellite. The radar and satellite evolution of this "hidden cell" is being studied in detail.

5.0 SUMMARY

This paper has presented some preliminary results and interesting features noted during CSU studies of severe convective storms emphasizing the use of concurrent high space and time resolution radar and satellite data. Comprehensive, detailed studies of the satellite characteristics of severe storms are required if the best use is to be made of the tremendous amount of satellite sensed data which are now available to both the operational meteorologist and the researcher. Methods for quantitative, optimum analysis of these complementary data sets should be developed.

6.0 ACKNOWLEDGEMENTS

The authors wish to thank William Shenk and William Valente of Goddard Space Flight Center for supplying the SMS digital data and also Kelly Hill of Marshall Space Flight Center for making the AVE IV sounding data available to us. David Reynolds and Eric Smith provided scientific assistance. This study was supported by the National Aeronautics and Space Administration under Grant NSG 5011.

7.0 REFERENCES

Adler, R.F., 1976: Thunderstorm monitoring from a geosynchronous satellite. Preprints Seventh Conf. on Aerospace and Aeronautical Meteorology and Symposium on Remote Sensing from Satellites, AMS, Melbourne, FL, 307-311.

Arn, R.A., 1975: Anvil area and brightness characteristics as seen from geosynchronous satellites. M.S. thesis, Colorado State Univ. Fort Collins, CO.

Fujita, T.T., 1972: Tornado occurences related to overshooting cloud-top heights as determined from ATS pictures. SMRP Research Paper 97, University of Chicago, 32 pp.

_____, and G. S. Forbes, 1974: Superoutbreak tornadoes of April 3, 1974 as seen in ATS pictures. Preprints Sixth Conference on Aerospace and Aeronautical Meteorology, El Paso, TX, 165-172.

Grant, L. O., and T. H. Vonder Haar, 1975: Studies of satellite support to weather modification in the western U.S. region. Annual Report NASA Grant NSG-5011, 31 pp.

Griffith, C. G. and W. L. Woodley, 1973: On the variation with height of the top brightness of precipitating convective clouds. J. Appl. Meteor., 12, 1086-1089.

Miller, R. C., 1972: Notes on analysis and severe storm forecasting procedures of the Air Force Global Weather Central. AWSTR 200 (Rev.) 102 pp.

Negri, A. J., D. W. Reynolds, and R. A. Maddox, 1976: Measurements of cumulonimbus clouds using quantitative satellite and radar data. Preprints Seventh Conf. on Aerospace and Aeronautical Meteorology and Symposium on Remote Sensing from Satellites, AMS, Melbourne, FL, 119-124.

Pearl, E. W., W. E. Shenk, and W. Skillman, 1975: Cloud-top parameters - a hail indicator. Preprints Ninth Conf. on Severe Local Storms, AMS, Norman OK, 464-467.

Purdom, J. F. W., 1974: Satellite imagery applied to the mesoscale surface analysis and forecast. Preprints Fifth Conference on Weather Forecasting and Analysis, AMS, St. Louis, MO, pp. 63-68.

_____, 1975: Tornadic thunderstorms and GOES satellite imagery. Paper presented at Ninth Conference on Severe Local Storms, AMS, Norman, OK, 5pp.

Reynolds, D. W. and T. H. Vonder Haar, 1973: A comparison of radar-determined cloud height and reflected solar radiance measured from the geosynchronous satellite ATS-3. J. Appl. Meteor., 12, 1082-1085.

Shenk, W. E. and R. J. Curran, 1973: A multi-spectral method for estimating cirrus cloud top heights. J. Appl. Meteor., 12, 1213-1216.

Smith, E. A., and D. W. Reynolds, 1976: Comparison of cloud top height determinations from three independent sources: Satellite IR measurements, Satellite viewed cloud shadows, Radar. Paper presented at COSPAR Nineteenth Plenary Meeting, Philadelphia, PA, June 1976, 17 pp.

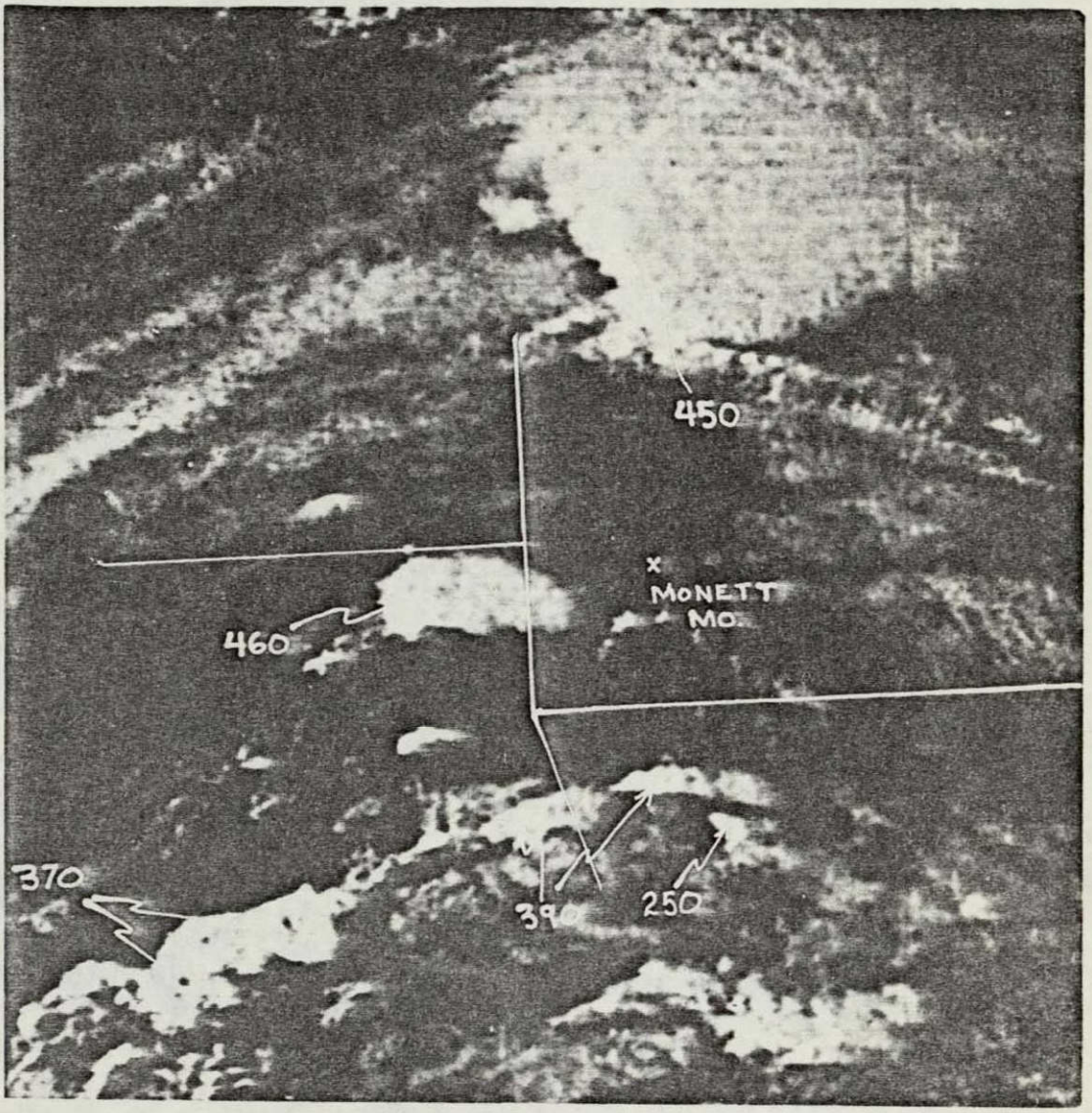

Figure 1. SMS 1 visible photograph of severe storms studied. Radar indicated cloud top heights are shown, as is location of radiosonde station at Monett, Missouri. Time of photograph is 2242 GMT, 24 April 1975.

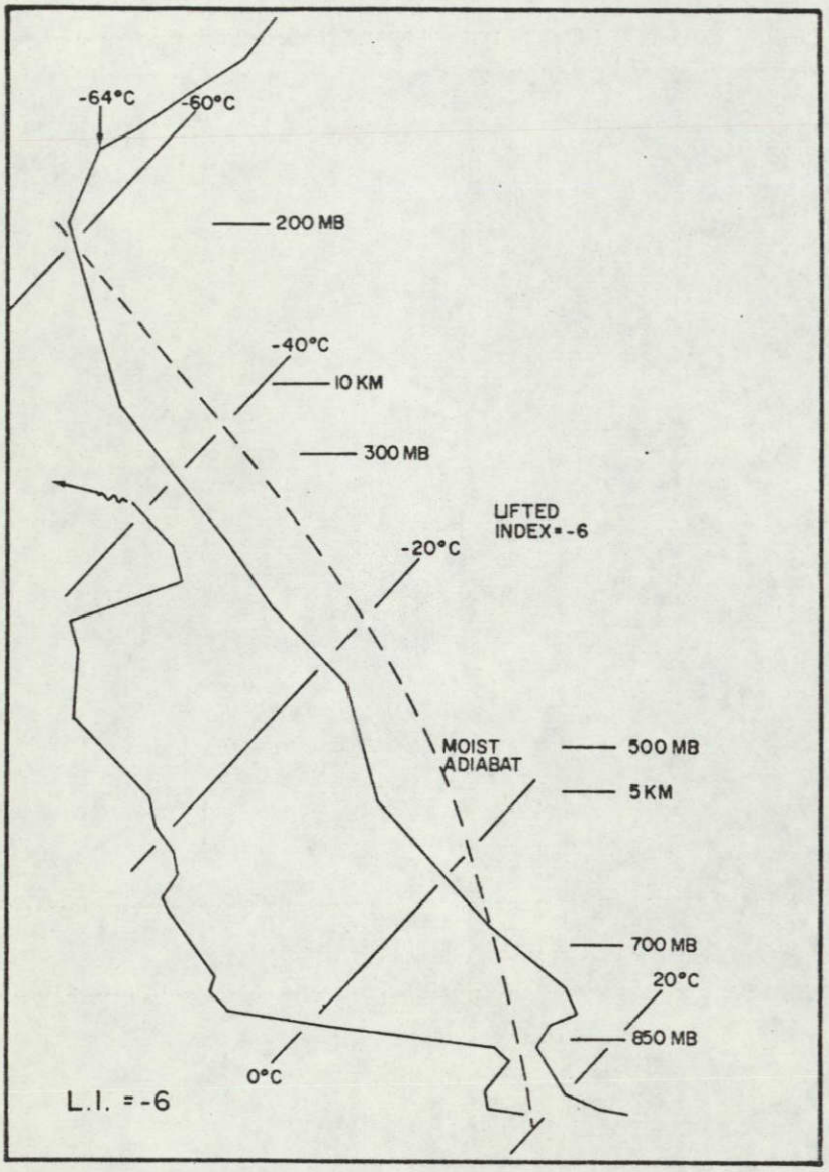

Figure 2. Monett, Missouri sounding at 2100 GMT, 24 April 1975. Of interest are the strong potential instability and the rapid rate at which a parcel following a moist adiabat would become colder than the environment above 200 mb.

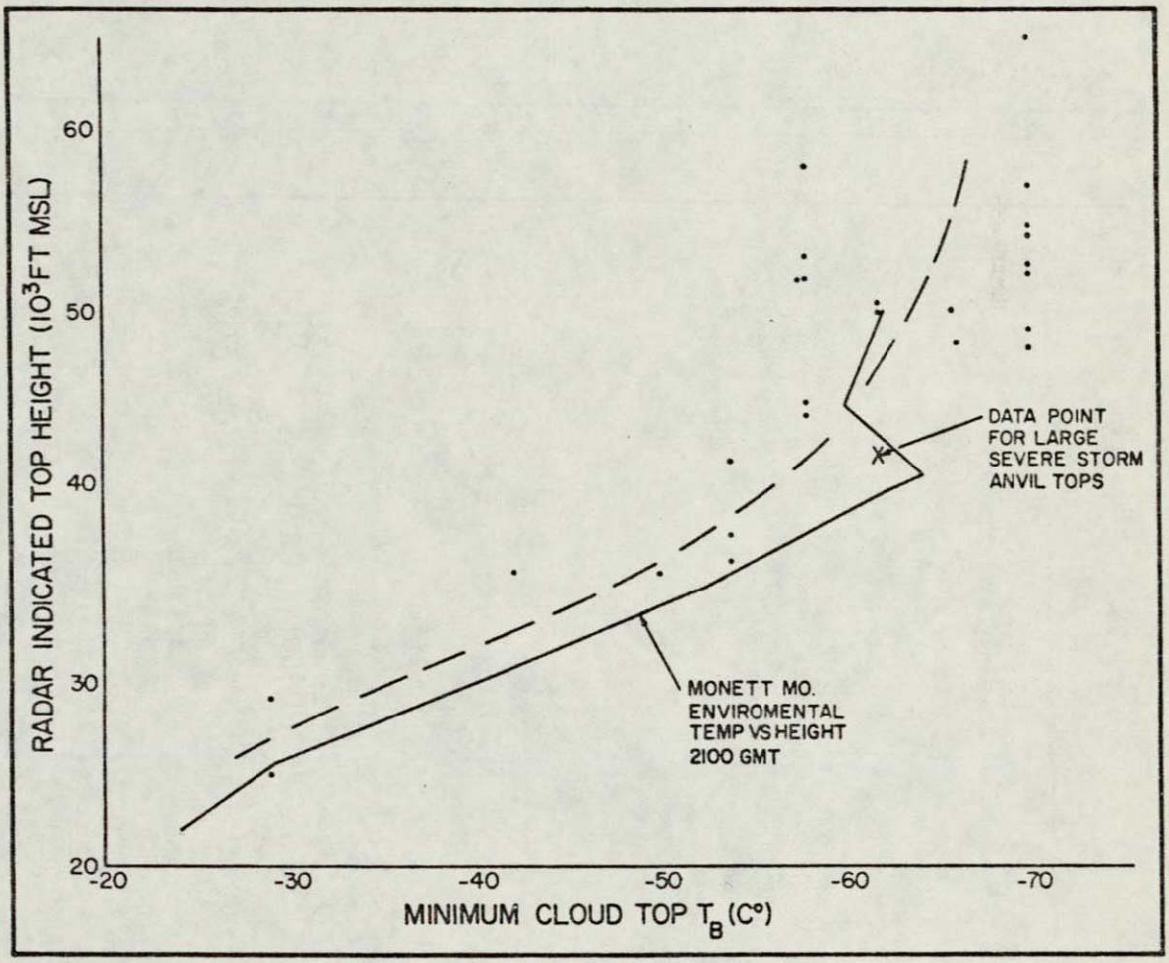

Figure 3. Scatter diagram of radar indicated top height versus satellite sensed coldest IR cloud top temperature. The 2100 GMT Monett sounding is plotted showing environmental temperature as a function of height (for example at 30×10^3 ft. MSL the environmental temperature was approximately $-40^{\circ}C$).

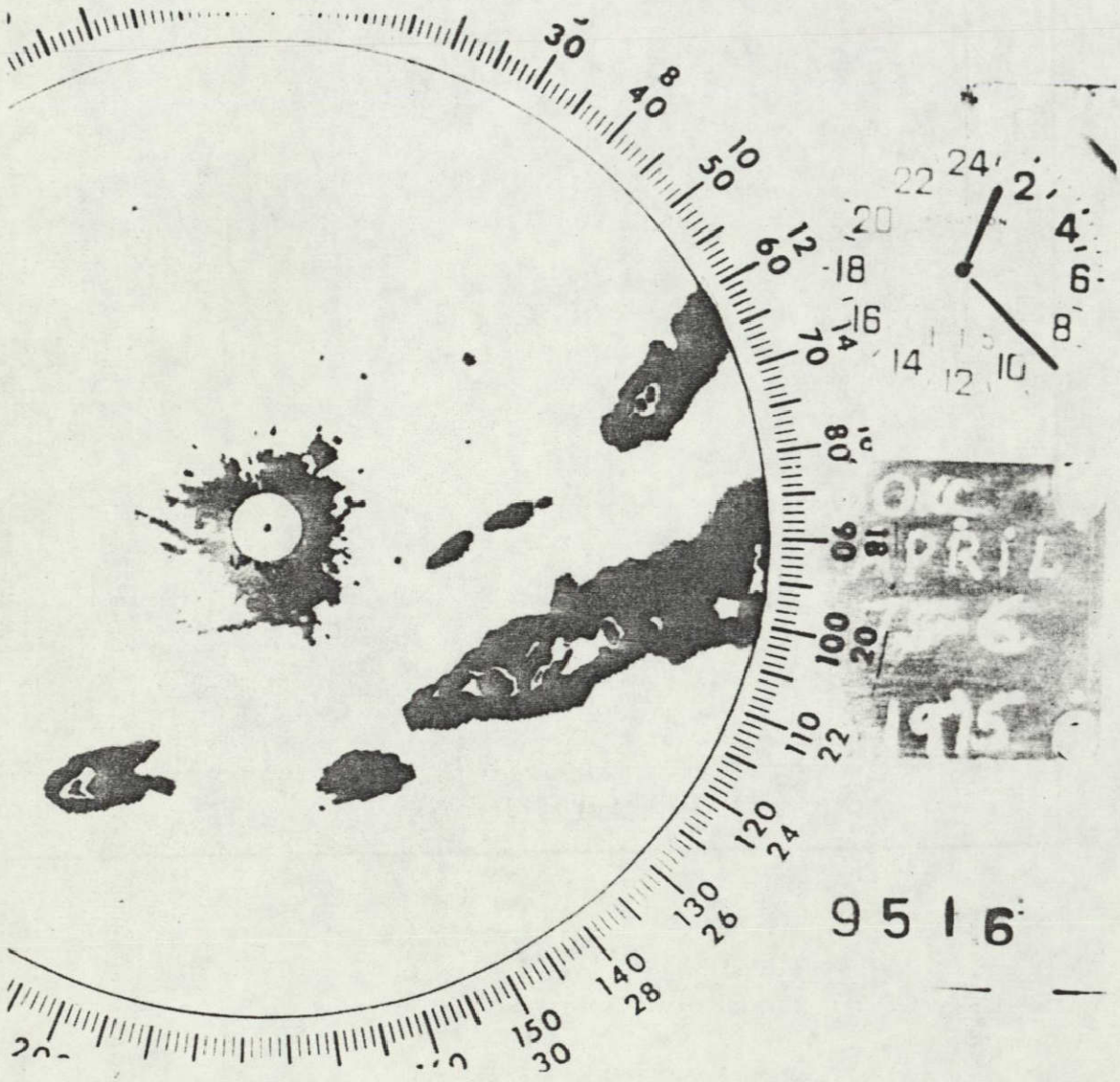

Figure 4. Oklahoma City (OKC) WSR-57 intensity contoured PPI scope picture at 0122 GMT, 25 April 1975.

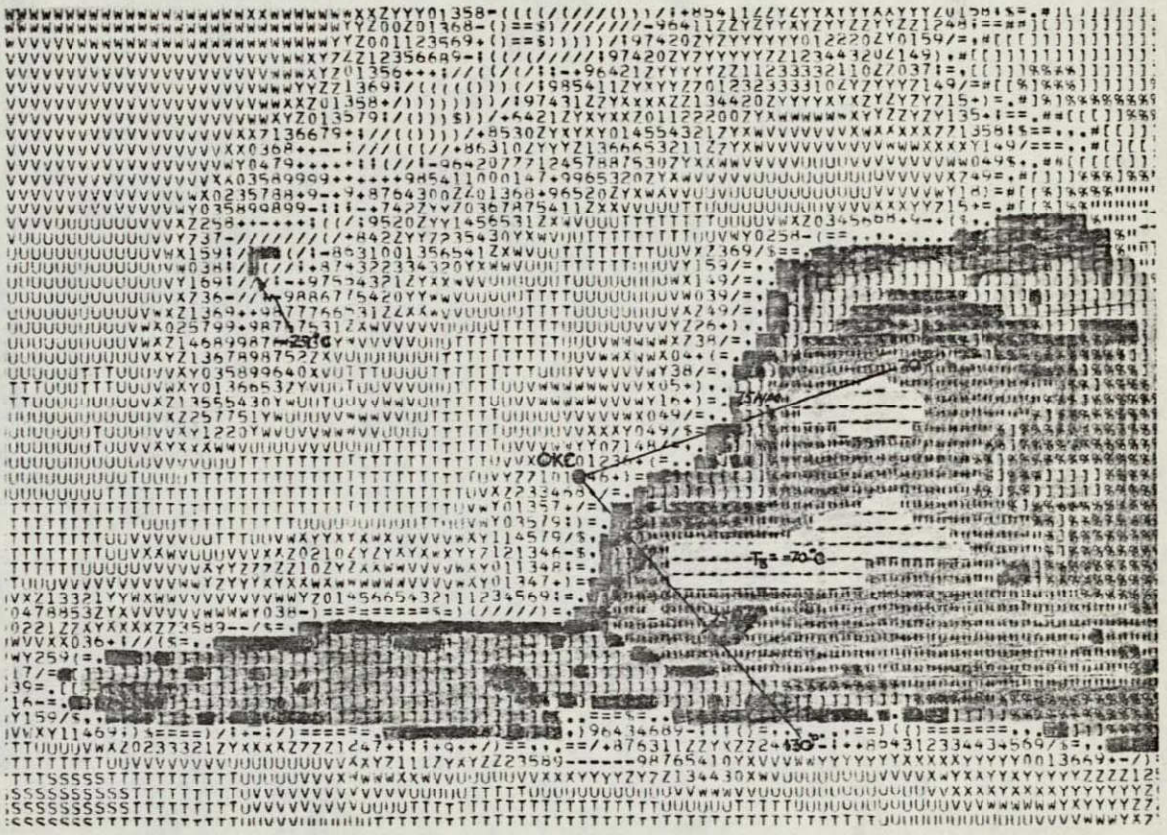

Figure 5. SMS 1 contoured IR black body temperature field at 0120 GMT, 25, April 1975. Location of OKC WSR-57 radar is indicated.

Reprinted from Preprint Volume: Tenth Conference on Severe Local Storms. Oct. 18-21, 1977; Omaha, NE. Published by American Meteorological Society, Boston, Massachusetts.

ANALYSIS OF SATELLITE DERIVED WINDS FOR APRIL 24, 1975

R. A. Maddox,[1] A. J. Negri and T. H. Vonder Haar

Department of Atmospheric Science
Colorado State University
Fort Collins, Colorado 80523

1. INTRODUCTION

High-resolution GOES imagery has been increasingly incorporated in studies of severe convective storms. Most uses of this satellite data have been of a qualitative nature involving image interpretation. (For examples refer to Maddox, 1977; Purdom, 1976; and Weiss and Purdom, 1974.) However, some researchers have begun to use quantitative, digital GOES data in their work. Adler and Fenn (1976) computed growth rates of IR measured cold cloud top area for several severe storms on 6 May 1975 (one of which spawned the Omaha tornado) and compared the changes in growth rate with the timing of severe weather events at the surface. Negri et al. (1976) contrasted visible cloud brightness changes with the evolution of radar echoes for several Great Plains' thunderstorms. They also showed that computed parameters, such as cloud top divergence, may be affected by the time interval separating data used in the computations. Maddox et al. (1976) compared IR inferred storm top heights with radar measured top heights and showed that large scatter existed between radar and satellite heights for severe storms which penetrated the tropopause.

Houghton and Wilson (1975) presented velocity divergence and vertical motion fields computed for a severe convective situation. The winds were derived from tracking clouds on satellite photographs. The resultant fields exhibited horizontal and vertical coherency suggesting that such applications might eventually be of operational utility. During the current study cumulus clouds were tracked to develop low-level wind fields prior to an outbreak of severe thunderstorms. Divergence, moisture convergence, and vorticity fields were then objectively computed. These analyses were compared to similar fields computed using only surface data. Subjective modifications of the data set were made to demonstrate the sensitivity of the results to varying spatial distributions of trackable clouds.

The day chosen for study was 24 April 1975 when several severe thunderstorms developed during late afternoon from north Texas to Missouri. GOES 1 imagery was taken at 5-min intervals beginning at 1200 CST (all times are given in Central Standard Time) and continuing for 8 h. A NASA Atmospheric Variability Experiment (AVE IV) was conducted this day and upper-air soundings were taken at 3-h intervals over a large region east of the Rocky Mountains. (The NASA AVE program has been described in detail by Hill and Turner (1977).) An unusually comprehensive set of data was therefore available for use in the study of the severe storms. Significant storm reports included: hailstones with a diameter of 2.75 in. (7.0 cm) at Wewoka, Oklahoma at 1715; a tornado near Miami, Oklahoma, at 1800; and a destructive tornado at Neosho, Missouri, at 1840.

2. SYNOPTIC SITUATION

At 1500 (Fig. 1) a slow moving cold front stretched from southern Illinois westward to eastern Kansas and then southwestward to the Texas panhandle. South of the front a narrow band

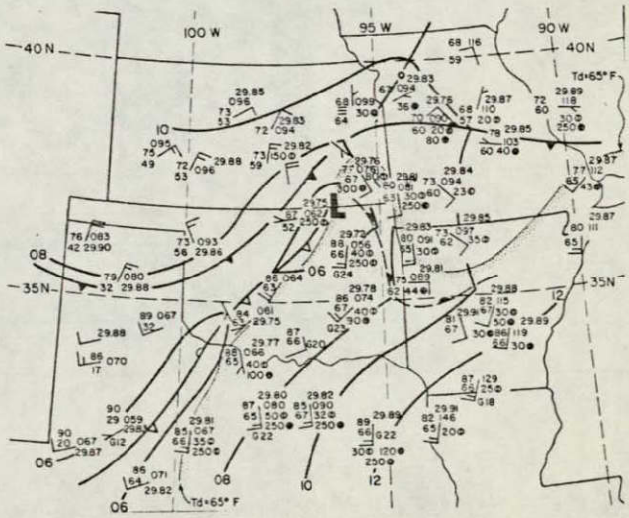

Fig. 1. Surface analysis at 1500 CST. Note the dry line which extends from northern Oklahoma to southwestern Texas. Winds are in kt with full barb = 10 kt.

[1] Also at NOAA-ERL, Boulder, Colorado

of hot, dry air had advanced eastward through north-central Oklahoma into a low pressure area east of Ponca City. The region of lowest pressures was located on the dry line rather than on the frontal wave. The surface pattern resembles that of the sub-synoptic scale surface low documented by Tegtmeier (1974). He found that tornadic storms were most likely to occur within the northeast quadrant of this type low, and this particular case was not an exception. The remnants of a surface boundary, which separated hot, moist air from a region of cool air produced by nocturnal thunderstorms, is depicted as a dissipating warm front. Note that in the narrow warm sector temperatures had climbed into the upper 80's with dewpoint temperatures holding in the uppers 60's.

The 500 mb analysis (Fig. 2) showed that a weak short-wave trough extended from south Kansas into central Texas. The flow field split into two branches to the west over the Great Basin, and this short wave was imbedded within the southerly stream. A stronger short wave, within the northern stream, was moving east-southeastward across the northern Plains. By 0000 on the 25th these two features had moved into phase and merged just west of the central Mississippi Valley. Although severe thunderstorms continued through the night, the most intense storms were those that occurred along the southern short wave during the late afternoon and evening.

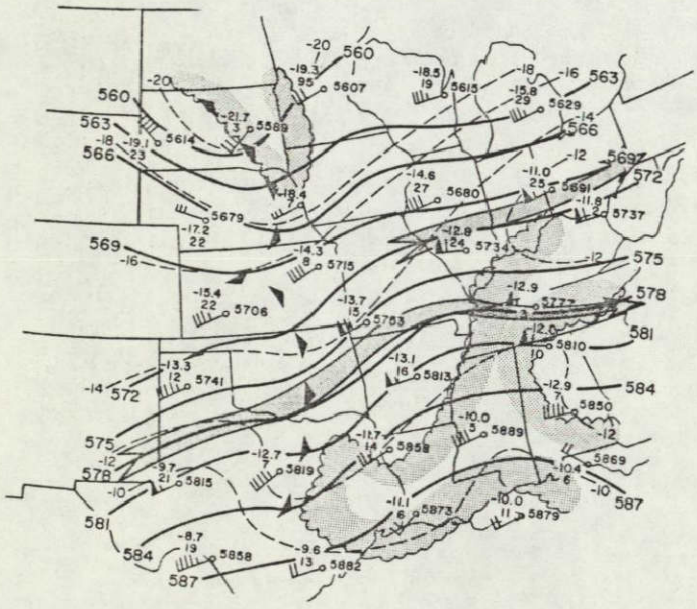

Fig. 2. 1500 CST 500 mb analysis. Triangles show locations of short-wave troughs. Arrows depict axes of maximum wind speeds, full barb = 10 kt, flag = 50 kt. Moist regions with T-Td $\leq$ 6°C are shaded.

Skew T/Log P plots of upper-air soundings taken at Monett, Missouri, and Amarillo, Texas, are shown in Fig. 3. (Release times were 1500 and 1415 respectively.) The Monett plot resembles a Miller (1972) Type I tornado sounding. The lowest 100 mb layer L.I. was -4, and the mean vapor mixing ratio for the same layer was almost 12 g kg^{-1}. However, note that the LFC was almost 200 mb above the LCL with a large negative buoyancy area indicated through the separating layer. Most veering in wind direction occurred below the LCL with west-southwesterly flow extending from 800 through 100 mb. The temperature lapse rate was strongly superadiabatic in the lowest 30 mb.

The Amarillo sonde was released within the hot, dry air mass prior to cold frontal passage. A well mixed, nearly adiabatic layer extended upward from the surface to 600 mb. Although strong westerly flow was present at middle and upper levels, nearly uniform westerly winds of only 10 kt (5 m s^{-1}) existed in the mixed layer. Because of this weak flow the dry line moved only slightly eastward during the afternoon, except over central Oklahoma, where it moved eastward toward the low pressure region.

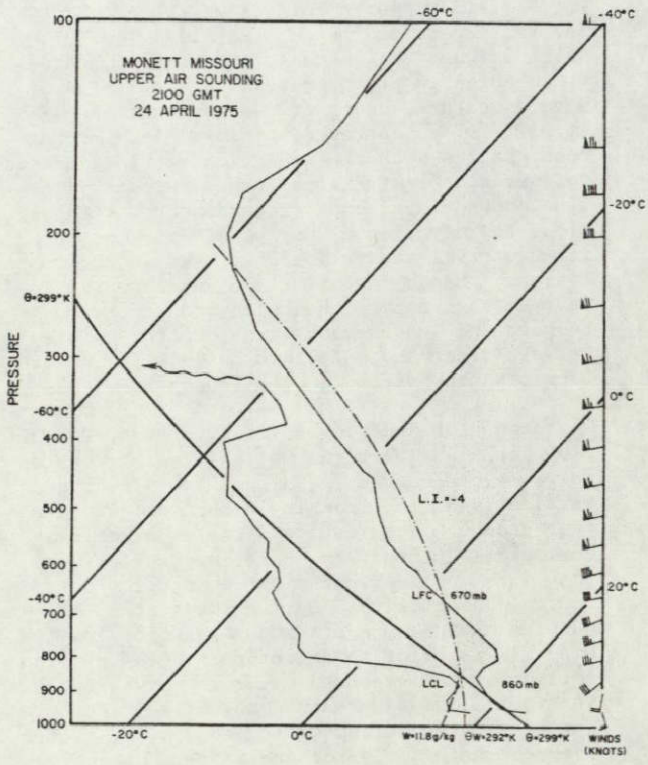

Fig. 3a. A Skew T/Log P plot of 1500 CST Monett, Missouri, upper-air sounding.

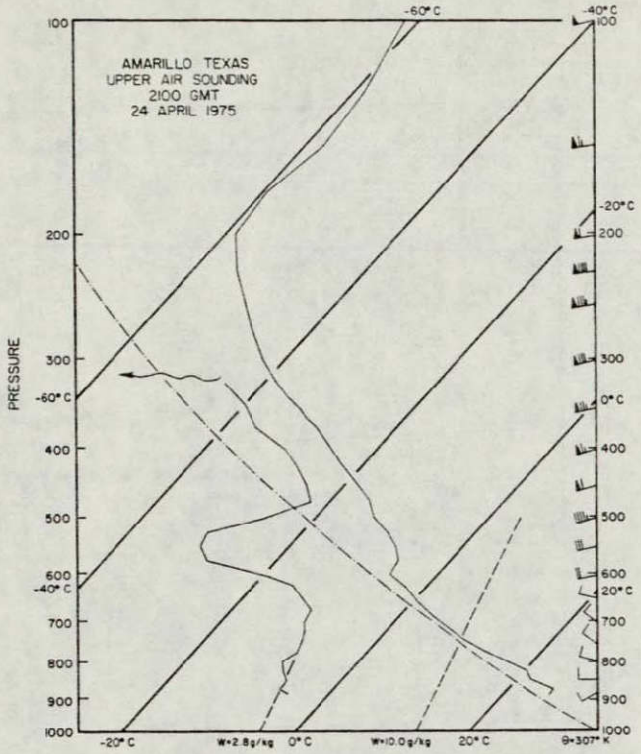

Fig. 3b. Skew T/Log P plot of 1500 CST Amarillo, Texas, upper-air sounding.

Wilson (1976) has computed large scale vertical motion fields (700 mb ω computed with an adjusted kinematic method) using the AVE IV sounding data. His 1500 700 mb ω field is shown in Fig. 4, along with the concurrent surface analysis. Regions where severe thunderstorms developed during the following 2 h are indicated. The large scale vertical motion fields apparently did not play a dominant role in organizing convection on this particular day since the storms developed in regions of diagnosed subsidence, or of only slight upward motion.

The 1702 satellite photograph is shown in Fig. 5 with the 1700 surface analysis superimposed. The three large storms in northern Missouri, northeastern Oklahoma and southern Oklahoma were all severe. The Missouri storm-complex was oriented north to south and intersected the surface front and an associated east-to-west line of convective clouds. Empirical rules (Purdom, 1976) suggest that this storm would be a likely tornado producer. Similarly, the large storm in southern Oklahoma would be considered highly suspect because of its extremely rapid growth rate (refer to Negri et al. (1976) for details), and the obvious flanking lines which extended west-southwestward from the storm complex. However, it was the less spectacular storm (as viewed from satellite) located east-northeast of the sub-synoptic surface low that became tornadic.

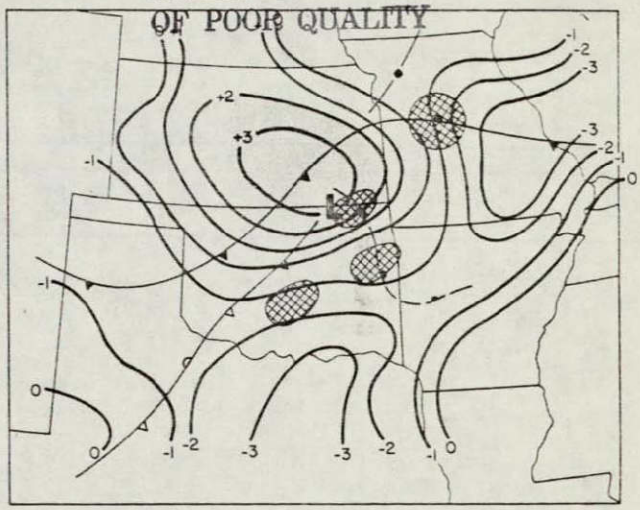

Fig. 4. 1500 CST 700 mb vertical velocity in μbars s^{-1} (from Wilson, 1976). Regions where severe thunderstorms developed during the following 2 h are cross-hatched.

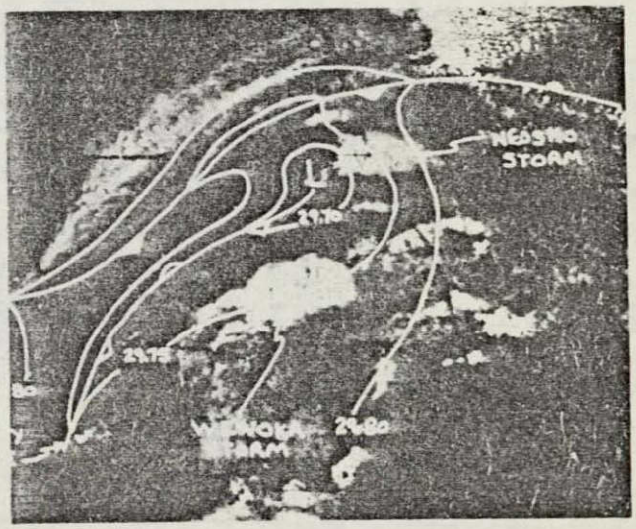

Fig. 5. 1702 CST GOES photograph with 1700 suface analysis.

3. SATELLITE DATA SET

A low-level wind field was developed by tracking cumulus clouds through a four-picture loop which began at 1458 and continued through 1513. The tracking was accomplished on the NASA Atmospheric and Oceanographic Information Processing System (AIOPS). Manual cursor positioning methods were employed. (The AOIPS and cloud tracking techniques are described by Billingsley et al. (1976).) Acceptance of a derived vector was subjective and was primarily based upon obtaining consistent cloud motion through the loop.

The set of 214 wind vectors obtained is shown in Fig. 6. These data were objectively interpolated onto a 0.4 degree grid (approximately 9 degrees square and centered on southwestern Missouri) using a 2-D cubic spline technique which was developed by Fritsch (1971). The resultant wind field is shown in Fig. 7. The spatial distribution of the data points indicated that the validity of the gridded winds would be most questionable over northwestern and southeastern corners of the domain, regions not affected by storms.

Results of previous studies have indicated that cumulus motion represents the cloud-base environmental wind to within 5 degrees and 1 m s^{-1} (Fujita et al., 1975 and Hasler et al. 1975). Hasler et al. also noted that there were no discernable biases to the differences indicating that analysis of a large, closely spaced data sample might minimize the error present.

Several dynamic fields were computed using the wind field shown in Fig. 7. The representativeness of these fields is partially a function of the spatial distribution of trackable cumulus clouds, and this important

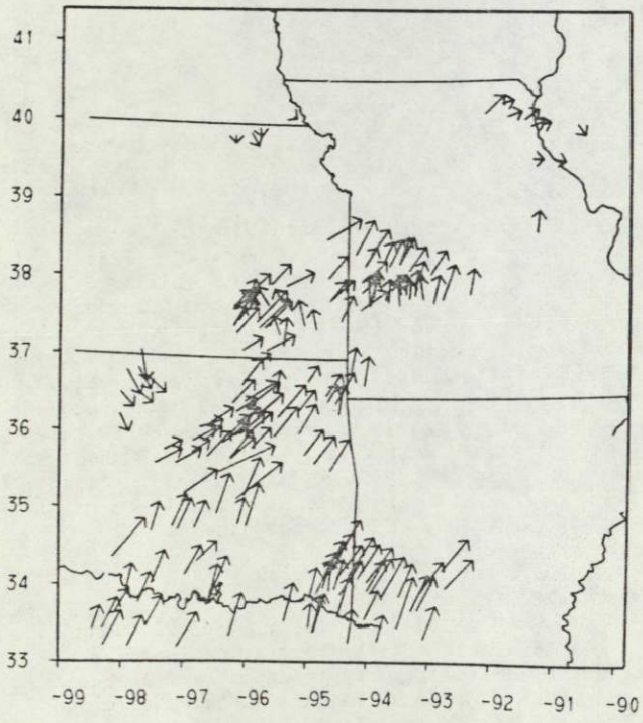

Fig. 6. Set of 214 wind vectors obtained by tracking low-level clouds on the NASA AOIPS. One degree of latitute = 22.2 m s^{-1} and one degree of longitude = 17.8 m s^{-1}.

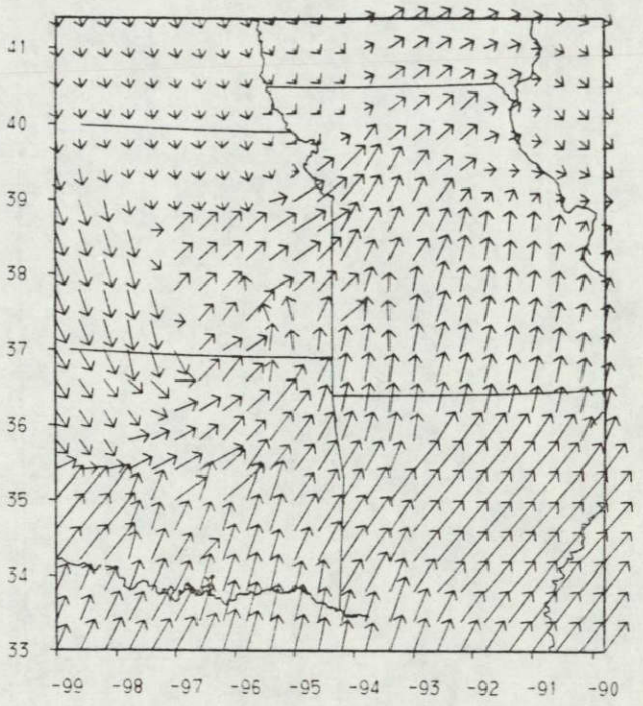

Fig. 7. Objectively gridded field of wind vectors. Scaling is same as in Fig. 6.

limitation is considered in a subsequent section. Location of the wind vectors in z-space is also a significant problem. Schaefer (1973) noted that usually neglected terms which appear when divergence is computed on a nonhorizontal surface can significantly affect the resultant fields. However, in this case it was assumed that the satellite derived winds were on a horizontal surface, even though rawinsonde data indicated that the LCL ranged from 910 to 800 mb across the region where clouds were tracked. Although simplifying assumptions have been made, the results do seem promising.

4. MOISTURE CONVERGENCE FIELDS

Hudson (1971), Newman (1972), and Sasaki (1973) have all shown that severe thunderstorms and squall lines tend to develop in regions where values of moisture convergence are large. Identifiable maxima in the surface moisture convergence field may precede development of intense convection by as much as 2 to 3 h.

Studies by Pearson et al. (1967), Steyaert and Darkow (1973), and Schaefer (1975) have presented results indicating that surface mixing ratios might be combined with the satellite derived low-level wind field to approximate mean mixed layer moisture convergence. Surface mixing

ratios were computed for the 1500 observations using Tetens' empirical formula for vapor pressure and the definition of mixing ratio. The mixing ratios were objectively analyzed onto the same grid as shown in the wind field of Fig. 7. These two fields were used to compute the moisture divergence (V.wV), hence moisture convergence is of negative sign.

The resultant field is presented in Fig. 8. Comparison with Fig. 5 shows that during the following 2 h storms developed in most of the regions characterized by large values of moisture convergence at 1500. The main exception was the lack of activity within the moisture convergence zone in central Kansas. The moisture convergence field calculated using only surface data is shown in Fig. 9. The overall pattern of the two fields is similar; however, significant differences do exist. The most pronounced of these was the band of high moisture convergence values that stretched across south-central Oklahoma in the satellite field. The surface analysis indicated moisture divergence over much of this area. This was an important difference since several severe storms developed across this region.

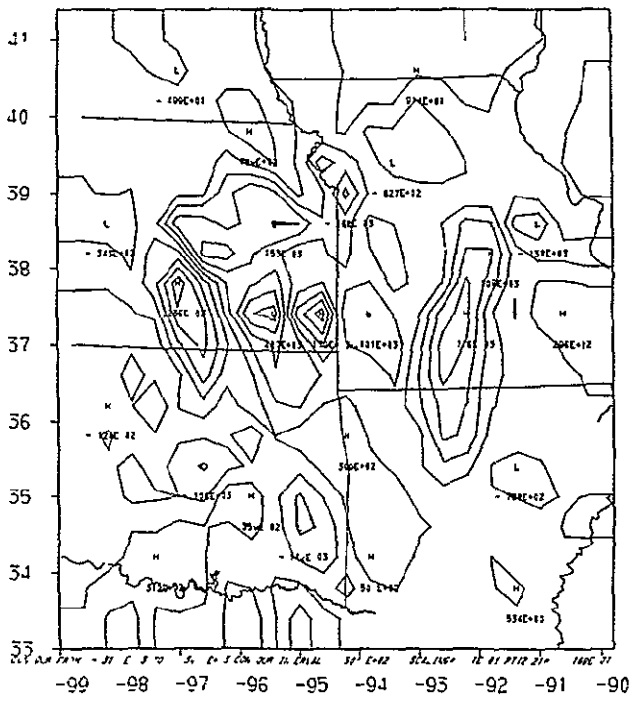

Fig 8. 1500 CST moisture convergence field computed using satellite derived winds. Units are g kg^{-1} s^{-1} x 10^{-5} and contour interval is 5 x 10^{-4} g kg^{-1} s^{-1}.

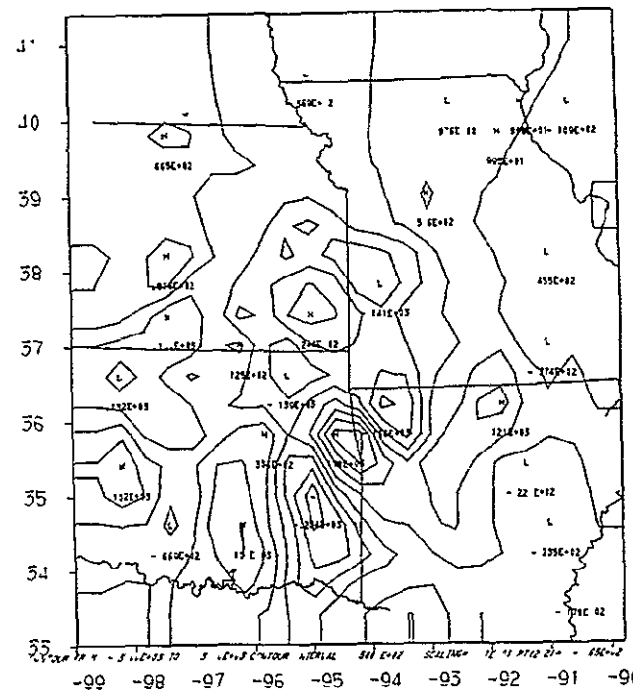

Fig. 9. 1500 CST moisture convergence field computed using observed surface winds Details are same as in Fig. 8.

Maximum values for satellite and surface moisture convergence (~8.5 g kg^{-1} h^{-1}) were similar to values found by Newman (1972) to be associated with severe thunderstorm occurrences. The Neosho tornadic storm began to develop within an hour of the satellite measurements and within the area of highest moisture convergence values. An improved correspondence between maxima and subsequent severe storm genesis were characteristic of the satellite field. This may have been a result of both stronger flow fields at cloud base and an elimination of local influences which affect measurements of surface winds.

5. DATA SENSITIVITY

A modification of the original 214 wind vector set was made to demonstrate that the spatial distribution of trackable cumulus clouds strongly affects the results of calculations of the type considered above. The 24 April tornado case was unusual because strong synoptic scale weather systems and attendant large cloud masses were not present. Eleven of the wind vectors were obtained by tracking individual cumulus within a narrow cloud band that developed to the rear of the surface cold front. These vectors were arbitrarily deleted from the data set.

Calculated relative vorticity fields are shown in Fig. 10 for both the complete and modified data sets. The results differ both in general pattern and also by as much as two orders of magnitude. The data modification was chosen to maximize differences; however, cloud patterns associated with real weather systems are also likely to systematically affect the distribution of trackable clouds, For example, it would be most unusual to find a cumulus cloud field in the air mass behind a dry line, and low-level clouds would often be obscured north of a surface cold front by layers of middle and high clouds.

These limitations emphasize the importance of integrating satellite determined low-level wind fields into a boundary layer model (both diagnostic and prognostic) which incorporates all available conventionally and remotely sensed data. This is especially true when operational applications are considered.

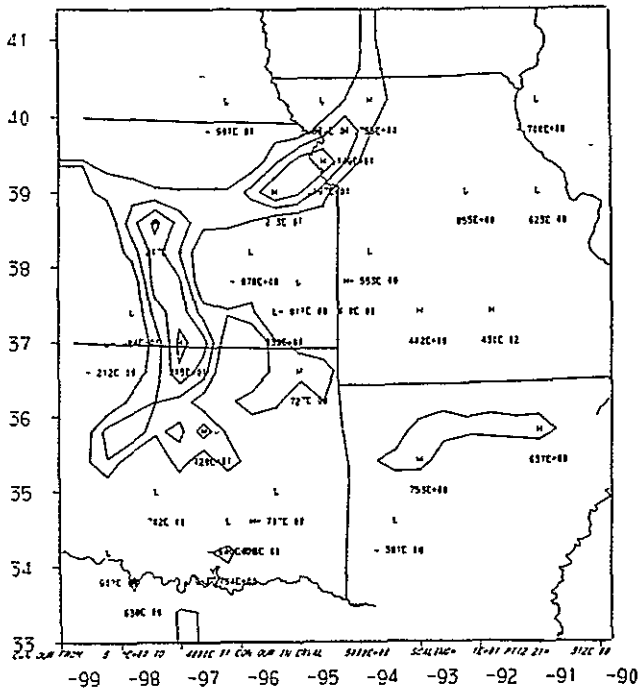

Fig. 10a. 1500 CST relative vorticity computed using satellite derived wind field. Units are $s^{-1} \times 10^{-4}$ and contour interval is 5×10^{-3} s^{-1}.

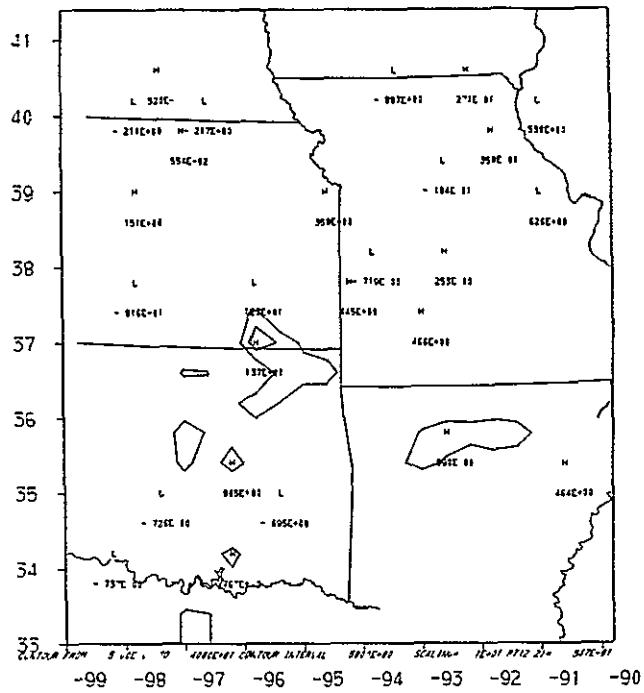

Fig. 10b. 1500 CST relative vorticity computed using the modified satellite derived wind set.

6. SUMMARY

Cumulus clouds were tracked, using short-interval high-resolution GOES satellite imagery, to derive a low-level wind field for a severe thunderstorm situation. The cloud tracking was accomplished during a period prior to storm development. Moisture convergence fields were approximated using these satellite derived winds and surface mixing ratios. Subsequent severe storm development occurred within regions of diagnosed high moisture convergence. Satellite moisture convergence patterns specified convective patterns that developed much better than did the same field computed using only surface observations. These data suggest that useful applications, using satellite wind fields, may be possible in operational severe thunderstorm forecasting.

It was also shown that computed dynamic fields are highly affected by the spatial distribution of trackable clouds. Satellite winds must be accurately located in the vertical before more precise computations can be obtained. Work is underway on development of an optimum objective analysis scheme which would simultaneously analyze satellite winds, surface data, rawinsonde data, and other types of remotely sensed data.

7. ACKNOWLEDGMENTS

R. F. Adler and W. E. Shenk (NASA Meteorology Branch, Goddard Space Flight Center) supplied the data and arranged and coordinated our use of the AOIPS, thereby making this study possible. K. Hill (NASA, Marshall Space Flight Center) kindly provided the AVE IV upper-air data. Ms Marlene Regan skillfully prepared the manuscript. This research was supported by NASA Grant NSG-5011.

8. REFERENCES

Adler, R.F., and D D. Fenn, 1976· Thunderstorm monitoring from a geosynchronous satellite Preprints Senventh Conf on Aerospace and Aeronautical Meterology and Symposium on Remote Sensing from Satellites, AMS, Melbourne, FL, 307-311.

Billingsley, J., A. F. Hasler, T. Mottershead, and J. Chen, 1976: Interactive metorological data analysis. In proceedings of Geosynchronous Meteorological Satellite Data Seminar, NASA Report X-931-76-87, Goddard Space Flight Center, MD, 60-68

Fritsch, J. M., 1971: Objective Analysis of a two-dimensional data field by the cubic spline technique. Mon. Wea. Rev., 99, 379-386.

Fujita, T. T., E W. Pearl, and W. E. Shenk, 1975: Satellite - tracked cumulus velocities. J. Appl. Meteor., 14, 407-413.

Hasler, A. F., W. E. Shenk, and W. C. Skillman, 1975: Wind estimates from cloud motions: preliminary results from phases I, II and III of an in situ aircraft verification experiment. NASA Report X-911-75-302, Goddard Space Flight Center, MD, 12 pp.

Hill, K. and R. E. Turner, 1977: NASA's Atmospheric Variability Experiments (AVE). Bull. Amer. Meteor. Soc., 58, 170-172.

Houghton, D. D. and T. A. Wilson, 1975: Mesocale wind fields for a severe storm situation determined from Synchronous Meteorological Satellite (SMS) cloud observations. Preprints Ninth Conf. on Severe Local Storms, AMS, Norman, OK, 187-192.

Hudson, H. R., 1971: On the relationship between horizontal moisture convergence and convective cloud formation. J. Meteor., 10, 755-762.

Maddox, R. A , 1977 Meso-β scale features observed in surface network and satellite data. To be published, Mon. Wea. Rev., 105, No. 8.

Maddox, R. A., A. J. Negri and T. H Vonder Harr, 1976 Comparison of severe storm cloud top heights derived from satellite and radar observations. Presented at 1976 Fall Meeting American Geophysical Union, San Francisco, CA, 10 pp.

Miller, R. C., 1972· Notes on analysis and severe storm forecasting procedures of the Air Force Global Weather Central. Air Weather Service TR 200 (Rev), 102 pp

Negri, A. J , D. W Reynolds, and R A. Maddox, 1976. Measurements of cumulonimbus clouds using quantitative satellite and radar data. Preprints Seventh Conf. on Aerospace and Aeronautical Meteorology and Symposium on Remote Sensing from Satellites, AMS, Melbourne, FL, 119-124

Newman, W. R., 1972: The relationship between horizontal moisture convergence and severe storm occurrences. M.S. Thesis, The University of Oklahoma, Norman, OK, 54 pp.

Pearson, A. D., J. G. Galway, and R. L. Inman, 1967· Relationship of surface dewpoint and integrated moisture in the planetary boundary layer. Preprints Fifth Conf. on Severe Local Storms, Chicago, IL, 135-139.

Purdom, J. F. W., 1976: Some uses of high-resolution GOES imagery in the mesoscale forecasting of convection and its behavior. Mon. Wea. Rev., 104, 1474-1483.

Sasaki, Y., 1973· Mechanisms of equal-line formation as suggested from variational analysis of hourly surface observations. Preprints Eighth Conf. on Severe Local Storms, AMS, Denver, CO, 300-307.

Schaefer, J. T., 1975: Moisture stratification in the "well-mixed" boundary layer. Preprints Ninth Conf. on Severe Local Storms, AMS, Norman OK, 45-50.

_____ 1973: On the computation of the surface divergence field. J. Appl. Meteor, 12, 546-547.

Steyaert, L. T., and G. L. Darkow, 1973· Diurnal variations in the ability to infer spatial variability in the themodynamic properties of the lowest kilometer from surface data. Preprints Eighth Conf. on Severe Local Storms, AMS, Denver, CO, 238-243.

Tegtmeier, S. A., 1974· The role of the surface, sub-synoptic, low pressure system in severe weather forecasting. M.S. Thesis, The University of Oklahoma, Norman, OK, 66 pp.

Weiss, C. E,, and J. F. W. Purdom, 1974: The effect of early-morning cloudiness on squall-line activity. Mon Wea Rev., 102, 400-402

Wilson, G. S., 1976: Large-scale vertical motion calculations in the AVE IV experiment. Geophysical Research Letters, 3, 735-738.

MOISTURE CONVERGENCE FROM A COMBINED MESOSCALE MOISTURE ANALYSIS AND WIND FIELD FOR 24 APRIL 1975

A.J. Negri, D.W. Hillger, and T.H. Vonder Haar

Department of Atmospheric Science
Colorado State University
Fort Collins, CO 80523

1. INTRODUCTION

The launch of geosynchronous satellites has provided meteorologists with high spatial and temporal resolution data essential in evaluating mesoscale features which may force the development of severe local storms (SELS). At the present time, only radiances from two channels, the 11-12 μm infrared and the 5-7 μm visible are available, so that vertical temperature profiles cannot be obtained. However, Vertical Temperature Profile Radiometer (VTPR) data are available from the polar orbiting NOAA-4 satellite, which uses the 15 μm CO_2 channels for temperature retrieval and the rotational water vapor absorption band to infer precipitable water values (Hillger and Vonder Haar, 1976), however temporal resolution is poor. This paper explores the possibility of combining these two data sets to simulate data that will become available with the launch of the VISSR[1] Atmospheric Sounder (VAS) on the GOES-D in the 1980's. A moisture analysis of 70 km resolution is combined with wind fields derived from tracking low-level cumulus clouds using SMS visible channel data. This combination allows for the computation of moisture convergence in the boundary layer for the pre-storm environment.

Several researchers, including Hudson (1971), Newman (1972) and Sasaki (1973) computed surface moisture convergence and found good agreement between those patterns and reports of severe weather several hours later. Intense moisture convergence (~ 10^{-3} g kg^{-1} s^{-1}) is one condition found favorable for tornadic storm development (Sasaki, 1975).

The day chosen as a case study was 24 April 1975, when several severe thunderstorms developed during the late afternoon from north Texas to Missouri.

This day is well represented in the literature. Whitney (1977) examined the role of the subtropical and polar jets on this day and concluded that upper-level diffluence ahead of the advancing trough enhanced the convective instability north of the sub-tropical jet. Maddox et al (1976) compared satellite sensed radiative temperature fields to corresponding radar echo characteristics in an attempt to quantify the detection of severe storms by satellite. Negri et al (1976) examined growth rates in SMS visible channel data to determine an operationally significant parameter for detection of storm severity. Purdom (1975) examined the low-level inflow into these storms from both an earth relative frame and a thunderstorm relative frame and concluded that a relative low-level southerly flow into a storm is important in that storm's ability to produce a tornado. This paper will follow the latter approach in using low-level cumulus velocities to compute divergence and subsequently moisture divergence.

2. 24 APRIL 1975

2.1 Synoptic Situation

Numerous severe storms occurred in a region stretching from southwest Oklahoma to eastern Tennessee during the afternoon and evening hours this day. A destructive, killer tornado struck at Neosho, Mo. and baseball-sized hail pounded the small town of Wewoka, Ok. Figure 1 is the surface analysis for 1600 GMT, near the time of the NOAA-4 satellite pass. Features to note are:

1) the intense moisture gradient across the dry line in western Oklahoma
2) very moist air in eastern parts of Texas and Oklahoma
3) cold frontal boundary in the Oklahoma panhandle, becoming stationary out towards the northeast
4) squall line from previous days convective activity running through Oklahoma and Arkansas.

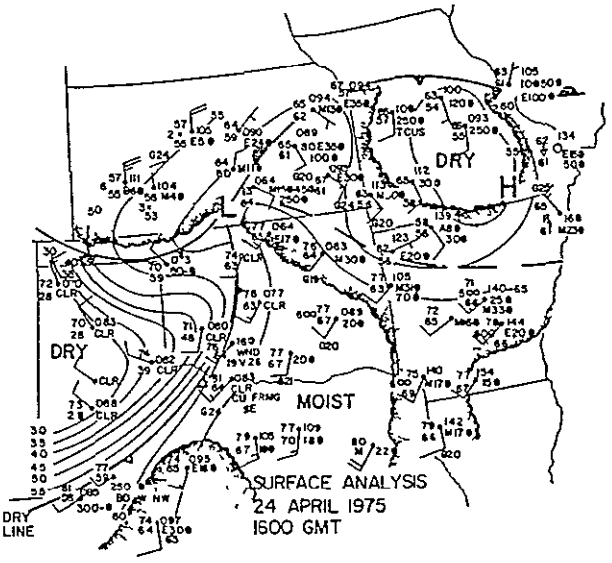

Fig. 1. Surface analysis for 1600 GMT, 24 April 1975.

[1] Visible and Infrared Spin-Scan Radiometer

Figure 2 is the 1500 GMT 500 mb analysis of data collected during NASA's Atmospheric Variability Experiment (AVE) on this date. The weak short wave moving through the midwest increased the instability over the region

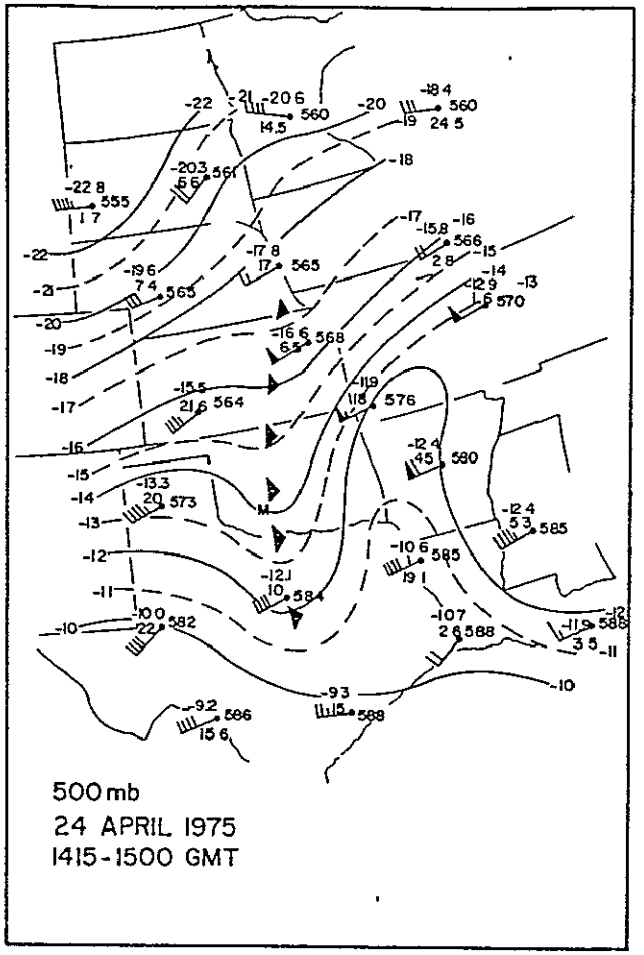

Fig 2. 500 mb analysis for 1500 GMT. Data were collected during NASA's Atmospheric Variability (AVE) experiment.

2.2 Mesoscale Precipitable Water Analysis

High horizontal resolution moisture information was obtained at 1615 GMT on 24 April 1975. This moisture analysis was available in terms of total precipitable water (PW) values at a resolution of about 70 km from the VTPR on NOAA-4. Table 1 shows the spectral characteristics of the VTPR instrument. Clear column temperature profiles were retrieved through use of an iterative temperature retrieval algorithm, (Hillger and Vonder Haar, 1977). As an initial guess profile the retrieval program used a composite temperature and moisture sounding constructed from 1800 GMT AVE radiosonde profiles. The temperature profile was then iterated until the RMS residual between observed and calculated radiances for the CO_2 channels reached some limiting noise value (the instrumental noise level for the VTPR instrument).

NOAA VTPR CHANNELS

CHANNEL NUMBER	WAVELENGTH (microns)	WAVENUMBER (cm^{-1})	APPROXIMATE PEAK LEVEL OF WEIGHTING FUNCTION (millibars)
CO_2 channels (15 micron CO_2 absorption band)			
1 (Q branch)	14.96	668 5	30
2	14 77	677 5	50
3	14 38	695 0	120
4	14 12	708 0	400
5	13 79	725 0	600
6	13 38	747 0	surface
H_2O channel (Rotational water vapor absorption band)			
7	18 69	535 0	700
Window channel (Atmospheric window region)			
8	11.97	833 0	surface

Table 1

Table 1. Spectral characteristics of the Vertical Temperature Profile Radiometer.

After the temperature profiles were retrieved using the six CO_2 channel radiances, a comparison was then made between the observed and calculated radiances for the VTPR H_2O channel The observed H_2O channel radiance is dependent upon both the temperature and moisture structure of the sounding column, whereas the CO_2 channels are in general less dependent on moisture than temperature.

The calculated radiance is an integrated value obtained by applying the radiative transfer equation to the retrieved temperature profile with the initial guess PW amount. If the retrieved temperature profile is sufficiently accurate, then the only difference between observed and calculated radiances should be due to the difference between the observed and initial guess precipitable water amounts. The initial guess PW amount is not changed in the iterative process and does cause some errors in the derived temperature profile which are of smaller magnitude than the PW effect on the H_2O channel. Since the initial guess PW amount is a constant value, the H_2O radiance residual should therefore be proportional to the actual PW amount in the sounding column.

For the area of the satellite pass over the

Great Plains, a correlation between the H_2O radiance residuals and the actual PW values at AVE radiosonde launch sites is shown in Figure 3. The rather high correlation of -.88 shows that much of the moisture distribution on the mesoscale was explained by the radiance residuals. All the values except Fort Sill, Oklahoma (FSI) are within the absolute error bias of $\pm$0.5 cm of H_2O which is considered as a maximum error for this data set.

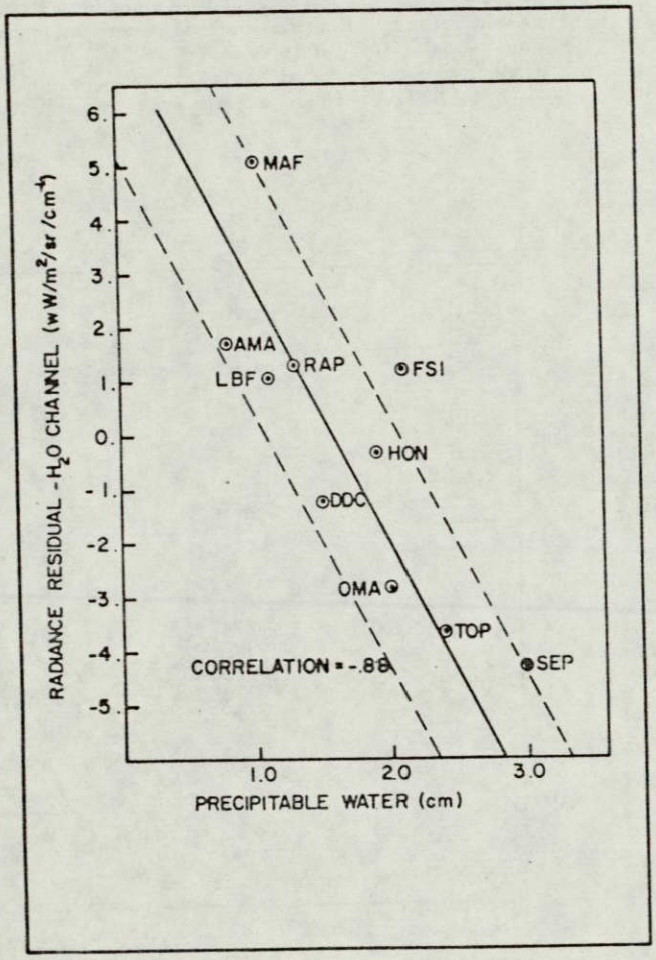

Fig. 3. Observed precipitable water values versus H_2O channel radiance residuals.

A least squares linear fit was made to the individual points to derive PW values at the places other than radiosonde sites which were used for calibration. The resultant PW field is shown in Figure 4 for the satellite pass time. One region in question is in central Kansas where high clouds caused the PW values to be low. The clouds there extended above 500 mb and the values obtained are not reliable. Otherwise, the individual values should be accurate to within $\pm$ 0.5 cm of PW.

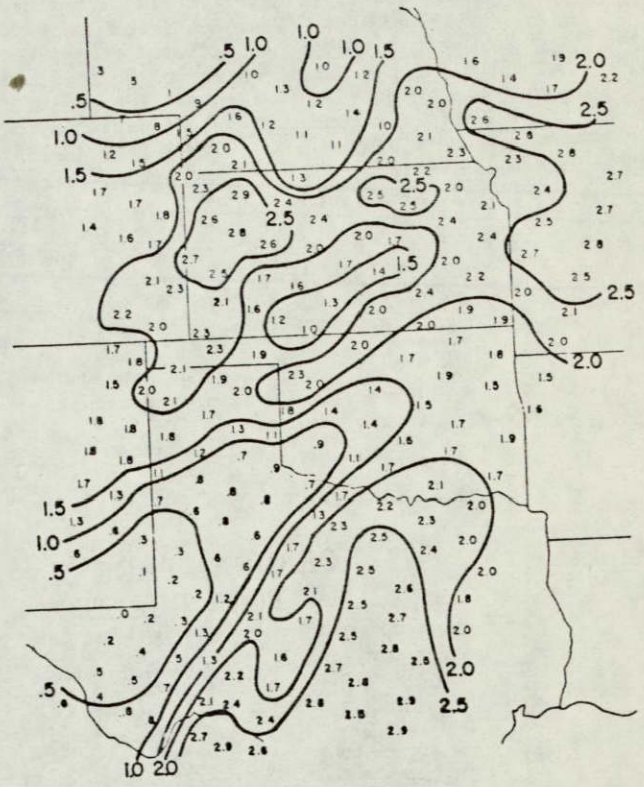

Fig. 4. The precipitable water field (cm) at 1615 GMT.

2.3 Wind Fields

Five minute interval SMS visible channel data were used to track cumulus clouds and derive low-level wind fields from their motion. Winds were tracked on NASA's Atmospheric and Oceanographic Information Processing System (AOIPS) by NASA scientists and the data furnished to CSU. Cloud location is determined by means of a cursor, which is moved about the screen by means of a joystick. Prior navigation of the images to within one picture element (~ 1 km) allows for cloud tracking in an earth relative frame. [A description of the AOIPS and cloud tracking techniques was presented by Billingsley (1976).] Figure 5 is one such satellite image used. Cumulus clouds were tracked in an area approximately 11 degrees on a side centered near Oklahoma City, Oklahoma. Figure 5 shows the original wind field, with a vector of length one degree representing a wind speed of 17.8 ms^{-1} u velocity and 22.2 ms^{-1} v velocity. Hasler, et.al. (1976) showed that for tropical cumulus, excellent agreement existed between cloud motion and the wind at cloud base ($V_{cloud} - V_{wind} \leq 1.3\ ms^{-1}$).

Fujita et.al, (1975) used ATS images to infer environmental winds and concluded that cumulus turrets 0.3 to 2 miles in size appear to be the best targets to infer mean winds in the sub-cloud layer. Accuracy in velocity computation was shown

to be $\pm$ 1 ms^{-1} speed and $\pm$ 5° direction. More recently, Suchman and Martin (1976) explored the accuracy and representativeness of tracer winds in the GATE area. They found that ship winds used as "ground" truth differed from satellite winds by less than 3 ms^{-1}. Using 30 minute interval imagery, they found a reproducibility of 1.3 ms^{-1} for cumulus level winds. Cumulus tracked winds would seem to better indicate boundary layer motion than do the corresponding surface winds because:

1) a 20 minute "average" of mean flow is obtained, and
2) surface winds are influenced by topography and surface stress.

Doswell (1976) recognized the importance of using "filtered" surface data in computations of low-level moisture divergence.

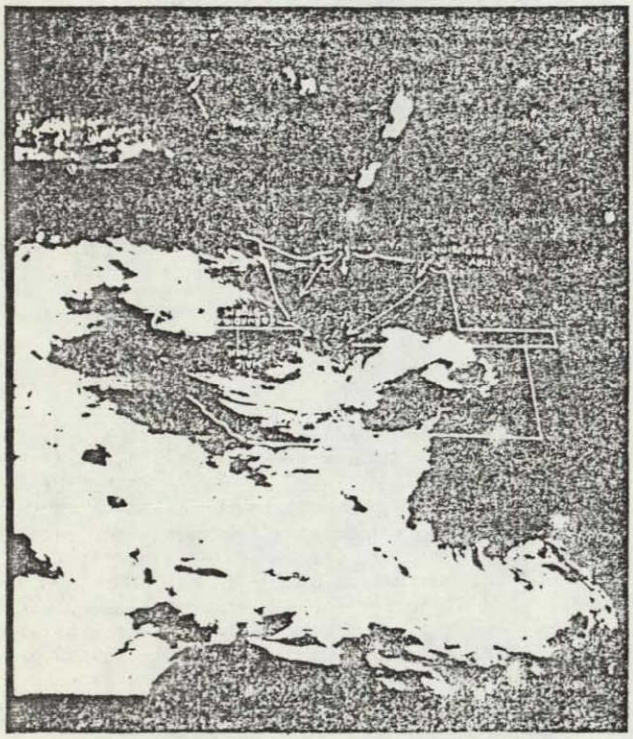

Fig. 5. SMS visible channel image at 1757 GMT.

3. RESULTS

3.1 Dynamic Parameters

The wind field of figure 6 was objectively analyzed using a cubic spline technique developed by Fritsch (1971). Figure 7 shows the objectively analyzed wind field, using a grid interval of 0.5 degrees, with lengths scaled as in figure 5. The divergence field, figure 7, shows the areas of strongest low-level convergence located in central Kansas, southwestern Oklahoma and southern Missouri. Magnitudes of this convergence are 10-20 x 10^{-5} s^{-1}. A final compution is done with the addition of the satellite derived PW fields. The moisture field of figure 8 was objectively analyzed onto the same grid as the winds and the moisture divergence ($\nabla \cdot PW\,V$) was calculated. This field is illustrated in figure 9, and is similiar in structure to the divergence field alone. The maximum moisture convergence was ~30 x 10^{-5} cm H_2O s^{-1} centered in eastern Kansas. Local maxima are also found in southern Missouri, southwestern Oklahoma, central Texas and northern Louisiana. The radar summary at 1835 (Fig. 10) shows some convective activity ooccurring in Kansas, however these storms were not severe.

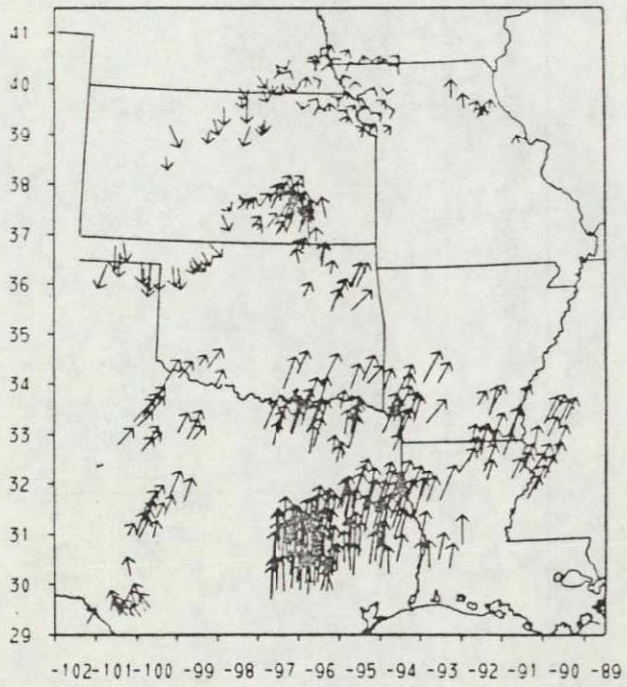

Fig. 6. Original wind field at 1800 GMT from satellite inferred cumulus velocities.

Because of the rather large time discrepancy between the moisture field (1600), the wind field (1800) and the time of initial storm genesis (2200), emphasis has been placed on the description of a technique rather than on demonstrating the possible correlation between moisture convergence patterns and the occurance of severe local storms. Maddox et.al. (1977) coupled 2100 GMT derived winds with corresponding surface mixing ratios on this day to determine possible correlations. The authors are well aware of some of the shortcomings of the technique described. A satellite wind which was

not accurately located in the vertical has been multiplied by an estimation of the total atmospheric water content. The wind fields are sensitive to the density and spatial configuration of the cumulus clouds used to derive them, as well as to the objective analysis scheme used Total PW content is likewise not retrieved perfectly. It is hoped that by the time VAS is launched there will be improved algorithms for determining H_2O content and its vertical distribution

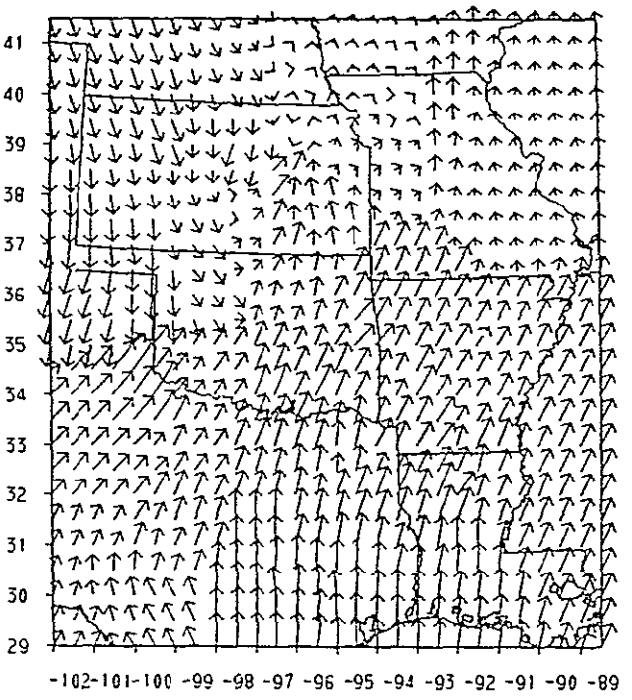

Fig 7. Objectively analyzed wind field at 1800 GMT Grid interval is 0 5 degrees

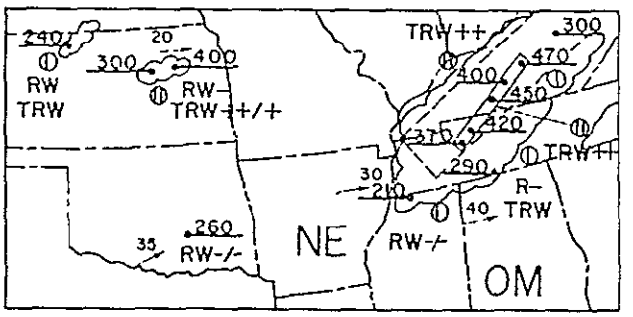

Fig 10. NWS radar depiction chart for 1835 GMT.

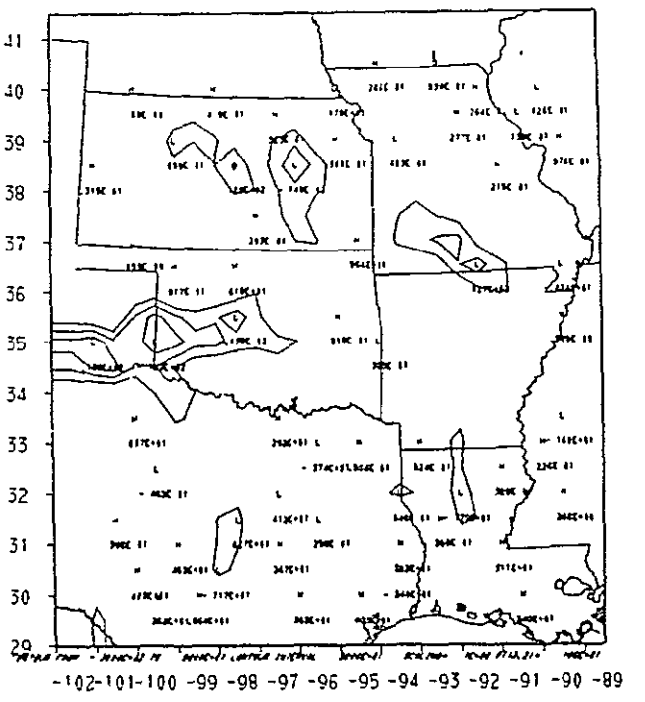

Fig. 8. The 1800 GMT divergence field Units are 10^{-5} s^{-1} and only negative values (convergence) have been contoured.

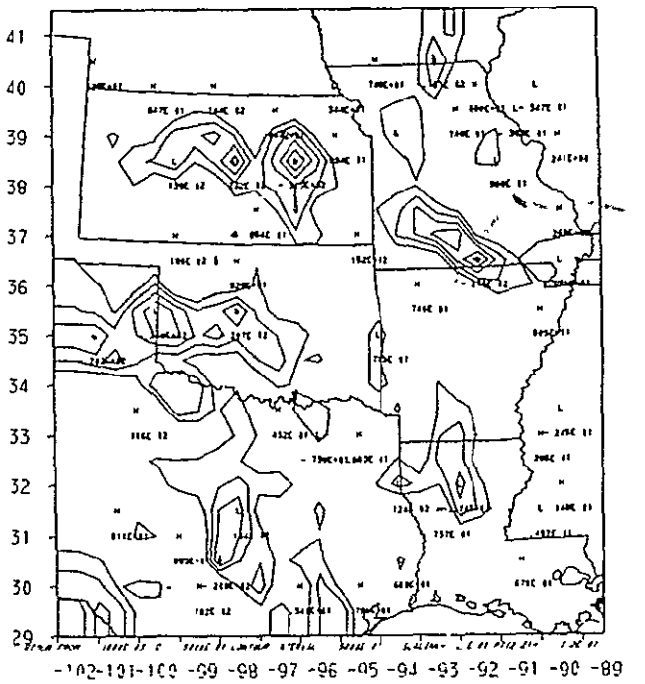

Fig 9. The moisture divergence field. Units are 10^{-5} cm H_2O s^{-1} Only negative values (moisture convergence) have been contoured

4. SUMMARY

The major results and limitations of this preliminary study of combining two types of satellite data included:

1) Using data from satellite sensors only, wind and moisture fields can be constructed and then combined to give mesoscale horizontal moisture flux information.
2) Satellite inferred cumulus velocities provide a usable representation of boundary layer flow, with the limitation of not being exactly located in the vertical Subsequent calculations may be dependent on the number and density of wind vectors and on the type of objective analysis used.
3) While moisture profiles cannot be retrieved perfectly, total precipitable water can be recovered through its large negative correlation with radiance residuals. Most of this PW resides in the boundary layer.
4) Moisture divergence fields reflect important mesoscale forcing mechanisms of severe local storms, notable in the absence of a well defined synoptic pattern.
5) Because of the early NOAA-4 pass time, and a 2 h discontinuity between the wind and moisture fields, no inferences can be made to the correlation of low-level moisture convergence and the occurrence of severe local storms for this case

The proposed VISSR Atmospheric Sounder, with its high spatial and temporal resolution, will provide a vital tool for the implementation and evaluation of this proposed technique.

ACKNOWLEDGEMENTS

The authors would like to thank NASA scientists William Shenk, Robert Adler and Fritz Hasler for deriving the wind vectors and supplying the data to CSU. The advice and creative ideas of Robert Maddox and Dave Reynolds are also appreciated This research was funded under Grant NASA NSG-5011 and NSF ATM 76-21307.

REFERENCES

Billingsley, J.B., 1976. Interactive image processing for meteorological applications at NASA/Goddard Space Flight Center Preprints, Seventh Conf on Aerospace and Aeronautical Meteorology and Symposium on Remote Sensing from Satellites, AMS, Melbourne, FL, 268-275.

Doswell, C.A , 1976· Subsynoptic scale dynamics as revealed by use of filtered surface data. NOAA Tech. Mem. ERL wSSL - 79, 40 pp.

Fritsch, J.M , 1971 Objective analysis of a two dimensional data field by the cubic spline technique. Mon Wea. Rev., 99, 379-386.

Fujita, T.T., E W. Pearl and W.E. Shenk, 1975 Satellite tracked cumulus velocities. J. Appl. Meteor., 32, 407-413

Hasler, A.F., W.E. Shenk, and W.C Skillman, 1976 Wind estimates from cloud motions Phase 1 of an in situ aircraft verification experiment J. Appl. Meteor., 15, 10-15.

Hillger, D.W. and T.H. Vonder Haar, 1976 Mesoscale temperature and moisture fields from satellite infrared soundings. Atmospheric Science Paper No. 249, Dept of Atmospheric Science, Colorado State University, Ft. Collins, CO, 66 pp

_____ 1977 Deriving mesoscale temperature and moisture information from satellite radiance measurements over the United States To be published in J Appl. Meteor.

Hudson, H.R., 1971. On the relationship between moisture convergence and convective cloud formation J. Appl Meteor., 10, 755-762.

Maddox, R A., A.J. Negri and T H. Vonder Haar, 1976: Comparison of severe storm cloud top heights derived from satellite and radar observations. Paper presented at the Fall Annual Meeting, American Geophysical Union, San Francisco, CA, 10pp.

_____, 1977: Analysis of satellite derived winds for 24 April 1975. Preprints, Tenth Conf on Severe Local Storms, AMS, Omaha, NE.

Negri, A.J., D.W. Reynolds and R. A. Maddox, 1976: Measurements of Cumulonimbus clouds using quantiative satellite and radar data Preprints, Seventh Conf. on Aerospace and Aeronautical Meteorology and Symposium on Remote Sensing From Satellites, AMS, Melbourne, FL 119-124.

Newman, W.R., 1972: The relationship between horizontal moisture convergence and severe storm occurrences. Master's thesis, the University of Oklahoma, Norman, OK, 54 pp.

Purdom, J.F.W., 1975: Tornadic thunderstorms and Goes satellite imagery. Paper presented at Ninth Conference on Severe Local Storms, AMS, Norman, OK, 5 pp

Sasaki, Y.K., 1973: Mechanism of squall line formation as suggested by variational analysis of hourly surface observations Preprint, Eighth Conference on Severe Local Storms, AMS, Denver, CO, 8 pp.

_____, 1975 Variational analysis and dynamics of severe local storms Final report submitted to NOAA, U.S. Dept. of Commerce, Boulder, CO

Suchman D., and D W. Martin, 1976: Wind sets from SMS images· An assessment of quality for GATE. J. Appl Meteor , 15, 1265-1278

Whitney, L.F., 1977: Relationship of the subtropical jet stream to severe local storms, Mon. Wea. Rev 105, 398-412